

SCHOOL OF COMPUTATION,
INFORMATION AND TECHNOLOGY -
INFORMATICS

TECHNICAL UNIVERSITY OF MUNICH

Bachelor's Thesis in Informatics

**Optimization and Simulation for
Pre-Earthquake Relief Aid Network
Design under Uncertainty: A Case
Study for Istanbul**

Berke Saylan



SCHOOL OF COMPUTATION,
INFORMATION AND TECHNOLOGY -
INFORMATICS

TECHNICAL UNIVERSITY OF MUNICH

Bachelor's Thesis in Informatics

**Optimization and Simulation for
Pre-Earthquake Relief Aid Network
Design under Uncertainty: A Case
Study for Istanbul**

Author: Berke Saylan
Supervisor: Baturhan Bayraktar
Advisor: Prof. Dr. Rainer Kolisch
Submission Date: 17.11.2024

I confirm that this bachelor's thesis in informatics is my own work and I have documented all sources and material used.

Munich, 17.11.2024

Berke Saylan

Abstract: Relief organizations face significant logistical challenges in post-disaster scenarios, motivating numerous studies on the use of stochastic optimization models for last-mile relief networks. This study addresses the challenge of selecting relief distribution points and determining their supply capacities in an urban area impacted by a major earthquake, accounting for uncertain demand and disruptions in the transportation network. We focus on a case study of Istanbul, specifically the Kadıköy district, where a major earthquake is expected. To simulate realistic disaster scenarios, we gather detailed datasets on building vulnerabilities, population density, and the transportation network. Our model is a modified version of the SLMRND, a two-stage stochastic optimization model designed to maximize accessibility and equity metrics, which we adapt specifically for our simulations to incorporate real-world data. Our scenario generation —designed to simulate varying relief demand and disruptions to the transportation network— relies on informed random selection of collapsed buildings, based on extensive official studies on building vulnerabilities across Istanbul’s neighborhoods. We also introduce Latin Hypercube Sampling (LHS) for building selection to further reduce selection bias, aiming to enhance the realism of our simulations. Rather than solely implementing a single model, our study offers a generalizable experimental framework for integrating diverse datasets into simulations of stochastic optimization models for last-mile relief networks. We demonstrate that while robust modeling is undeniably crucial, incorporating data-driven decision-making through simulations based on real-world data is equally essential for strengthening disaster response strategies. In our simulations, we compare LHS and Monte Carlo sampling methods for collapsed building selection, focusing on their computational efficiency and results in areas such as POD selection, supply distribution, and demand point assignment to PODs. Moreover, we examine the influence of POD locations and capacities on their selection, finding that in urban settings with dense demand points and candidate PODs, capacity plays a more decisive role than location in determining POD selection outcomes. Finally we analyze average outcomes across various simulations to identify which candidate PODs in Kadıköy are consistently selected and allocated significant supplies, providing specific insights into which PODs are likely to play a critical role in a real-world post-earthquake scenario in Istanbul.

Table of Contents

List of Figures	v
List of Tables	viii
1 Introduction	1
1.1 Humanitarian Aid: The Essential Barrier Between Survival and Catastrophe	1
1.2 Last Mile Relief	2
1.3 2023 Türkiye, Syria Earthquakes	3
1.4 The Earthquake Threat Facing Istanbul: Risks and Implications	3
1.5 Contributions of This Study and Methodology	4
1.6 Structure of the Paper	5
2 Literature Review on Post-Disaster Relief Network Design and Optimization	6
2.1 Post-Disaster Humanitarian Relief Network Design	6
2.2 Optimizing Last-Mile Relief Network in Disaster Scenarios	7
2.3 Data-Driven Simulation and Scenario Testing with GIS in Disaster Logistics	8
2.4 Sampling Methods for Scenario Generation in Disaster Simulations	10
2.5 Key Distinctions Between Our Approach and Previous Research	10
2.6 Summary of Key Research in Disaster Relief Network Design	11
3 Problem Definition	13
3.1 Structure of Last-Mile Relief Networks	13
3.2 Challenges in Last-Mile Relief Networks	14
3.2.1 Accessibility	14
3.2.2 Equity	15
3.2.3 Supply Allocation Policies	15
3.2.4 Uncertainties in Post-Disaster	16
3.3 Stochastic Optimization Model	17
4 Istanbul Case Study: Data Preparation and Integration	20
4.1 Scenario Definition for Istanbul Study Case	20
4.1.1 Building Collapse as Scenarios	20
4.1.2 Data-driven Building Selection Methodology	21
4.1.3 Limitations and Assumptions	21

4.2	Neighborhood Data Integration in GIS	22
4.2.1	Using Neighborhood Center Data	22
4.2.2	Using Neighborhood Boundary Polygons in GIS	23
4.3	Building Footprint Data for Istanbul	23
4.4	Population Data for Istanbul	26
4.5	Transportation Network Data for Istanbul	28
4.6	POD and LDC Selection for Kadıköy	29
5	Simulation	32
5.1	Building Selection Algorithms	32
5.1.1	Monte Carlo Based Selection Algorithm	32
5.1.2	Monte Carlo Sampling and Its Bias	32
5.1.3	LHS and Its Reduction of Bias	33
5.1.4	Comparison of Thiessen Polygons in MC and LHS Building Selection	33
5.1.5	Further comparison of MC and LHS in building selection .	35
5.1.6	Role of Sampling Methods in Our Study and Key Assumptions	35
5.2	Simulation Construction	36
5.3	Simulation Model Overview	38
5.3.1	Accessibility Scores	38
5.3.2	Maximum PODs Opened	38
5.3.3	POD Capacity Calculation	39
5.3.4	Scenario Handling and Probabilities	39
5.3.5	Total Available Supplies	40
5.3.6	Other Parameters	40
5.4	Optimization	41
6	Simulation Results and Managerial Insights	42
6.1	Monte Carlo Sampled Building Selection Simulation Results . . .	43
6.1.1	Results of POD Selection	43
6.1.2	Supply Allocation Results for PODs	48
6.1.3	Demand Point Allocation Results for PODs	52
6.2	Latin Hypercube Sampled Building Selection Simulation Results .	54
6.2.1	Results of POD Selection	55
6.2.2	Supply Allocation Results for PODs	58
6.2.3	Demand Point Allocation Results for PODs	62
6.3	Effect of Maximum POD Number on Simulations	63
6.3.1	The POD Consistency Principle: Bigger Capacities Stick Around	64
6.3.2	Short on PODs, High on Deviation: The Effects of Limited Availability of PODs	66

6.3.3 Fewer PODs, More Chaos: Demand Point Allocation Re-	
sults for PODs	68
7 Conclusion	75
7.1 Future Research	76
Bibliography	77

List of Figures

2.1	Table comparison of key research in disaster relief network design and optimization	12
3.1	Example last mile relief network from Noyan et al. (2016)	14
4.1	Building damage estimations for each neighborhood in Kadıköy İBB DEZİM Kadıköy (2020)	22
4.2	Neighborhood boundaries in Kadıköy district	24
4.3	Building data comparison example in Kadıköy: Microsoft Bing Maps (pink) vs OSM (cyan) buildings	25
4.4	Population distribution in Kadıköy at a 100m x 100m grid resolution estimated by Living Atlas Team (2023)	27
4.5	Population data aggregated from 100m x 100m grid cells, with every 5 consecutive cells represented by a single mean center point	28
4.6	A segment of the transportation network dataset for Kadıköy	29
4.7	Example POIs in Kadıköy from OSM Turkey (2024)	30
4.8	Example manual area calculation for PODs	31
4.9	Selected LDC and PODs in Kadıköy	31
5.1	MC and LHS building selection: Thiessen polygon comparison	34
5.2	Comparison of Monte Carlo and LHS building selection: deviation across neighborhoods	35
5.3	LHS Scenario 1: Buffer around destroyed buildings	37
5.4	Example to show how demand is calculated for demand points	38
6.1	Comparison of Monte Carlo simulations: Mean y-solution and the closest y-solution to the aggregated result	44
6.2	Comparison of Monte Carlo simulations: Mean y-solution and the furthest y-solution to the aggregated result	45
6.3	Relationship between POD area and selection probability (mean POD y-value)	47
6.4	Relationship between POD location relative to the POD centroid and selection probability (mean POD y-value)	47
6.5	Monte Carlo Simulations: Mean supply allocation to PODs in Kadıköy .	49
6.6	Relationship between POD area/capacity and mean supply allocation relative to the POD area	49

6.7	Relationship between POD area/capacity and deviation of supply allocation relative to the POD area	51
6.8	Monte Carlo Simulations: Deviation of supply allocations to PODs in Kadıköy	51
6.9	Relationship between POD location relative to the POD centroid and deviation of supply allocation	52
6.10	Monte Carlo Simulations: Demand point assignment to PODs	53
6.11	Monte Carlo Simulations: Demand point assignment to PODs - detailed map	54
6.12	Comparison of LHS simulations: Mean y-solution and the closest y-solution to the aggregated result	56
6.13	Comparison of LHS simulations: Mean y-solution and the furthest y-solution to the aggregated result	56
6.14	Comparison of mean y solutions of LHS and Monte Carlo simulations .	57
6.15	Relationship between POD area and selection probability (mean POD y-value)	58
6.16	Relationship between POD location relative to the POD centroid and selection probability (mean POD y-value)	59
6.17	LHS Simulations: Mean supply allocation to PODs in Kadıköy	60
6.18	Relationship between POD area/capacity and mean supply allocation relative to the POD area	60
6.19	Relationship between POD area/capacity and deviation of supply allocation relative to the POD area	61
6.20	LHS Simulations: Deviation of supply allocations to PODs in Kadıköy .	62
6.21	Relationship between POD location relative to the POD centroid and deviation of supply allocation	62
6.22	LHS Simulations: Demand point assignment to PODs	63
6.23	Feasibility gap numbers of simulations with varying C (max POD) values	64
6.24	Comparison of PODs selected on average between C = 20, 30 and 50 .	66
6.25	Deviation of supply allocation to PODs when C = 170	67
6.26	Deviation of supply allocation to PODs when C = 90	68
6.27	Deviation of supply allocation to PODs when C = 20	68
6.28	Demand point assignments to PODs in Kadıköy when C = 20	70
6.29	Demand point assignments to PODs in Kadıköy when C = 60	70
6.30	Overview on demand point assignments to PODs in Eastern Kadıköy when C = 90	71
6.31	Overview on demand point assignments to PODs in Eastern Kadıköy when C = 120	71
6.32	Overview on demand point assignments to PODs in Eastern Kadıköy when C = 170	72
6.33	Total accessibility for C = 70 to 170 for POD capacity scalar 1.5	73
6.34	Total accessibility for C = 70 to 170 for POD capacity scalar 1.5	73

6.35 Total accessibility for C = 20 to 60 for POD capacity scalar 2.5	74
---	----

List of Tables

1 Introduction

1.1 Humanitarian Aid: The Essential Barrier Between Survival and Catastrophe

Natural disasters continue to affect millions globally, causing widespread loss and disruption. For instance, the 2004 Indian Ocean earthquake and tsunami, one of the deadliest natural disasters in recent history, led to approximately 227,000 fatalities across 14 countries (World Health Organization, 2014), underscoring the urgent need for improved disaster response strategies. Similarly, Disasters Emergency Committee (2013) states that the 2010 Haiti earthquake left over 1.5 million people homeless and caused catastrophic destruction to infrastructure, illustrating the importance of immediate humanitarian intervention.

Humanitarian aid is a critical response that emerges in the face of widespread crises, such as famine, epidemics, and natural disasters, which leave millions of individuals vulnerable and in desperate need of assistance. The crucial role of humanitarian aid especially in disaster scenarios, where the swift delivery of aid can significantly decrease suffering and save lives, is further underscored by the standards and ethical principles outlined in the Sphere Project (2011).

Large-scale disasters necessitate equally large-scale and carefully planned humanitarian aid operations. In their study, Holguín-Veras et al. (2007) analyze humanitarian aid response failures in the aftermath of Hurricane Katrina in 2005. Key issues identified include significant logistical deficiencies, lack of coordination among agencies (such as FEMA, federal, state, and local first responders), inefficiencies in resource pre-positioning, and procurement challenges. These reports underscore the need for a robust logistical framework to effectively address emerging operational challenges in disaster response. Kovacs and Spens (2007) emphasize the logistical complexities inherent in disaster response, noting that disrupted infrastructure, urgent needs, and unpredictable demand require adaptive and agile logistics. In these scenarios, the rapid delivery of essential services and supplies is crucial for meeting the immediate needs of affected communities. Effective supply chain management thus becomes pivotal, often making the difference between life and death in many situations.

1.2 Last Mile Relief

Last-mile relief operations are crucial in the humanitarian supply chain, representing the final step in delivering essential aid from distribution centers to disaster-affected communities. This phase involves unique challenges such as restricted access, complex urban environments, and the need for rapid response, which can significantly hinder effective aid delivery and necessitate adaptive logistics solutions.

This study focuses on optimizing last-mile logistics by designing a relief network with three key components: Local Distribution Centers (LDCs), Points of Distribution (PODs) and demand points, with the network modeled as a two-echelon supply chain. LDCs serve as central hubs, such as large warehouses, where aid is prepared and dispatched to PODs, which are typically set up in accessible public areas like schools or parks. PODs then distribute aid to multiple demand points, representing affected populations, ranging from specific neighborhoods to larger community groups in need. A key challenge in this network is efficiently selecting PODs and allocating supplies from LDCs to PODs, and from PODs to demand points. As noted by Balcik et al. (2008), uninformed POD selection and improper resource allocation can result in shortages, leaving vulnerable populations without essential aid.

Our model, based on the SLMRND model from Noyan et al. (2016), incorporates two key objectives: *accessibility* and *equity*, both of which are crucial to the decision-making process. Accessibility measures the efficiency of relief supply delivery, focusing on minimizing time rather than distance due to disruptions in transportation networks during post-disaster conditions. It is evaluated in two ways: 1) the accessibility of PODs from LDCs, and 2) the accessibility of PODs from demand points. To promote fairness, we also consider equity, which we define as the balanced allocation of resources. In our model, equity is achieved by minimizing the *maximum proportion of unsatisfied demand (MPUD)* across PODs, ensuring that all populations receive a fair share of the available aid.

While candidate PODs are deterministic, demand for aid and disruptions in the transportation network are highly uncertain in post-disaster conditions. To address this, we use a stochastic optimization framework that simulates building collapses to generate various scenarios, capturing fluctuations in demand and network disruptions. By incorporating these uncertainties, our model optimizes the relief network across multiple scenarios, ensuring resilience and robustness against real-world variability.

1.3 2023 Türkiye, Syria Earthquakes

The 2023 Kahramanmaraş earthquakes serve as a recent example of the critical importance of efficient humanitarian aid and logistical coordination in disaster response. Affecting over 15 million people across southern Turkey and northern Syria, the twin earthquakes caused devastating damage, resulting in extensive casualties, widespread homelessness, and severe infrastructure destruction (Disasters Emergency Committee (DEC), 2023; AFAD, 2023).

Having close friends and acquaintances impacted by this disaster, we observed the immense significance of timely and well-organized humanitarian efforts in alleviating suffering. In response to this crisis, an unprecedented outpouring of national and international support was mobilized, with over 90 countries and multiple organizations sending aid (Anadolu Agency, 2023; IHH, 2023). However, various logistical challenges limited the effectiveness of aid delivery, particularly in the critical last mile phase. On social media, citizens documented these difficulties, sharing videos that revealed uncoordinated convoys and repeated deliveries to the same locations, while other affected areas remained underserved. These coordination lapses highlighted critical gaps in distribution planning, as aid convoys often failed to account for accessibility constraints, leading to route congestion and delays that hindered the timely arrival of assistance to communities in the remote, less accessible areas.

These issues underscore the importance of effective supply chain planning in disaster scenarios, particularly in the design and management of last-mile relief networks. Such networks require precise selection of distribution points and calculated assignment of resources to distribution points to maximize coverage and prioritize accessibility and equity in the distribution strategy. Without well-structured last-mile relief networks that account for demand point assignment and resource allocation, large-scale mobilization can still fall short of addressing critical needs equitably and efficiently.

1.4 The Earthquake Threat Facing Istanbul: Risks and Implications

Istanbul, the most populous and economically significant city in Turkey, is at substantial risk from an impending earthquake due to its location along the North Anatolian Fault. Research indicates that a magnitude 7.5 earthquake represents a credible worst-case scenario for the region Erdik et al. (2003) and as past earthquakes in the Marmara region have also demonstrated, a major earthquake in this area could cause catastrophic damage. In a study assessing potential earthquake losses for Istanbul, Ansal et al. (2009) estimate the extent of likely damage based on deterministic scenarios, emphasizing the urgent need for disaster preparedness and mitigation strategies to safeguard the city's residents and infrastructure.

These projections align with findings from local risk assessments, which suggest extensive physical and economic impacts, particularly in densely populated districts (Kandilli Observatory, 2023; İBB DEZİM Kadıköy, 2020). This looming earthquake threat and its potential consequences provide strong motivation to focus disaster preparedness efforts on Istanbul, where effective last-mile logistics and resource allocation strategies will be critical to a robust humanitarian response.

1.5 Contributions of This Study and Methodology

Given the magnitude of the threat posed by the anticipated Istanbul earthquake, this study is focused on proactive planning for the city, particularly in the Kadıköy district. Although the analysis and simulations are confined to this specific area, the insights and methodologies developed here are intended to be applicable throughout the broader context of Istanbul. Our research emphasizes optimizing last-mile relief networks through the strategic positioning of distribution points and effective resource allocation. This approach seeks to maximize both accessibility and equity metrics, which are essential for effective and fair distribution of aid in the chaotic conditions following a disaster.

The simulation of models and scenario generation within the stochastic optimization of relief networks has not been as extensively studied as the optimization modeling itself. Consequently, rather than introducing a new stochastic optimization model for last-mile relief networks, our primary goal is to create a robust simulation framework. This framework enables the effective testing of existing stochastic optimization models while utilizing diverse datasets relevant to Istanbul. Importantly, the simulation framework we develop can be adapted to evaluate other stochastic optimization models.

We are simulating a well-established stochastic optimization model within the Kadıköy context, assessing key aspects such as the selection of aid distribution points and the amount of resources allocated to them. This evaluation aims to bridge theoretical constructs with real-world data to provide practical insights. Our focus includes assessing the practical applicability of the model, examining how the presence or absence of specific data influences the simulation outcomes, and analyzing the effect of various parameters on the realism of the results. Additionally, we will identify areas for improvement in future research efforts, particularly concerning the accuracy of modeling and simulation.

A critical element of our methodology involves leveraging ArcGIS tools to access realistic datasets pertaining to the network, buildings, population, and infrastructure. The Network Analyst tool within ArcGIS facilitate logistics calculations that

accurately reflect practical conditions, thereby reinforcing the realism and applicability of our simulation framework.

Another significant contribution of this study is the preparation of datasets. We utilize a unique combination of various datasets sourced from official repositories, as detailed in the dataset preparation section, to increase the realism of our simulations. This necessitates extensive pre-processing to ensure integration among the datasets. In this work, we will thoroughly clarify the rationale and methodology behind the combination of these specific datasets. The datasets curated for this research will not only serve our immediate purposes but will also be beneficial for future researches into last-mile relief networks and other logistical studies.

1.6 Structure of the Paper

The paper is structured as follows. In Section 2, we review prior research on post-disaster humanitarian relief and last-mile relief networks. Section 3 discusses the structure, objective metrics, and uncertainties in last-mile relief networks, while introducing the two-stage stochastic optimization model. Section 4 outlines the data preparation and integration process for the simulations, covering scenario definitions, transportation infrastructure, and the population and building datasets in Istanbul. In Section 5, we describe the key steps in our simulation, including the use of the ArcGIS environment, and compare the Monte Carlo and LHS methods in terms of their handling of randomness in our simulations. Section 6 presents the results of the simulations and provides managerial insights based on the findings. Finally, the conclusion in Section 7 summarizes the study's findings and suggests potential directions for future research.

2 Literature Review on Post-Disaster Relief Network Design and Optimization

2.1 Post-Disaster Humanitarian Relief Network Design

Many studies on post-disaster humanitarian operations emphasize early response stages or general approaches to relief network design. The survey by Anaya-Arenas et al. (2014) provides a systematic review of relief aid network design, categorizing the literature by key characteristics such as uncertainty modeling (deterministic, stochastic, robust optimization), sampling techniques (e.g., Monte Carlo, Latin Hypercube), and measures of *accessibility* and *equity*. Balcik et al. (2016) provide an in-depth review of inventory management within humanitarian supply chains, with a focus on strategies for both pre- and post-disaster scenarios. Their work categorizes existing research based on the disaster management cycle, addressing key inventory decisions such as determining the quantity, location, and timing of stock-piles. Other studies, such as Day (2014), analyze how supply networks need to adapt during large-scale disasters, highlighting the importance of managing changing demands, resource limitations, and uncertainties in real time.

To address these uncertainties, researchers have developed stochastic optimization models that enhance network resilience. For instance, Noyan (2012) introduces a risk-averse two-stage stochastic programming model to improve facility location and inventory management under uncertain demand and damage scenarios. This model contributes to disaster preparedness and response planning by balancing risk management with computational efficiency. Building on this approach, Özgün Elçi and Nilay Noyan (2018) focus on pre-disaster relief network design, highlighting the importance of pre-positioning supplies at multiple facilities. Their risk-averse two-stage stochastic framework optimizes facility location and inventory decisions before a disaster, emphasizing the need for risk-averse models to handle uncertainty and avoid poor performance in rare events.

Further expanding on resilient and adaptive logistics frameworks, Afshar and Haghani (2012) propose a comprehensive mathematical model structured in alignment with FEMA's logistics framework. Their model integrates commodity flow, vehicle routing, facility location, and capacity constraints to optimize resource allocation through

a centralized, multi-layered network. Their study uses numerical experiments to demonstrate the model's ability to handle large-scale operations and capture essential operational details. Another study in this field, Daneshvar et al. (2023), introduces a two-stage stochastic model with a three-layer network for designing and operating post-disaster humanitarian supply chain networks. Their model addresses demand and capacity uncertainty while accounting for the residual impact of unmet demand over time, offering critical insights for effective short-term recovery planning.

Two-stage stochastic programming models are often used to develop disaster preparedness plans, but their complexity increases with uncertainty and interdependent decisions. Ece Sanci and Mark S. Daskin (2021) introduce an integer L-shaped algorithm to address the integrated location and network restoration problem, focusing on optimizing the locations of emergency response facilities and restoration resources under uncertainty. Their algorithm demonstrates greater computational efficiency compared to CPLEX, with solution time increasing linearly as the number of disaster scenarios grows. Focusing on a different aspect of disaster preparedness, Mahdi Mostajabdeh and Salman (2019) develop a stochastic programming model for selecting shelter locations, aiming to minimize both the mean distance to shelters and inequity in resource allocation under uncertainty. They introduce a Genetic Algorithm (GA) to solve larger instances of the problem efficiently, achieving small optimality gaps in less time compared to conventional methods.

2.2 Optimizing Last-Mile Relief Network in Disaster Scenarios

As demonstrated by events such as Hurricane Katrina and the Kahramanmaraş Earthquakes, optimizing the last-mile relief network is critical to ensuring the effectiveness of humanitarian operations. Despite the availability of substantial resources, the lack of clear criteria for selecting distribution points and allocating aid often hampers relief efforts. Horner and Downs (2008) highlight this issue, emphasizing that transportation networks play a vital role in determining accessibility, a factor frequently overlooked in relief planning. Their study focuses on optimizing the location of distribution points in hurricane-affected areas to enhance access to relief supplies. By using integer programming, they identify ideal Points of Distribution (PODs) and allocate them to Local Distribution Centers (LDCs) in a way that minimizes distribution costs. In a subsequent study, Horner and Downs (2010) extend this model by incorporating the quantities of relief supplies allocated to each POD.

Similarly, Noyan et al. (2016) focus on last-mile logistics optimization, with an emphasis on balancing equity and accessibility in POD selection and supply allocation

for post-disaster scenarios. Their model considers both demand and network uncertainties. In another approach, Zhang et al. (2020) propose a robust optimization model for last-mile relief network design. Their model determines the locations of PODs and demand nodes while addressing uncertainties in post-disaster scenarios by using two uncertain sets to manage objective and chance constraints. They validate their model by applying it to the Wenchuan earthquake, demonstrating its effectiveness in uncertain conditions.

In the context of optimizing last-mile relief delivery, Dukkanici et al. (2023) introduce an innovative solution to the relief distribution problem, incorporating drones and trucks for post-disaster logistics under uncertainty. Their model accounts for factors such as drone range, time-bound constraints, and demand estimation based on earthquake scenarios, presenting a two-stage stochastic programming approach.

2.3 Data-Driven Simulation and Scenario Testing with GIS in Disaster Logistics

Kovács et al. (2017) emphasize the critical role of decision support systems in planning logistics and networks within post-disaster contexts. They highlight advancements in modeling and simulation techniques that improve predictions of network accessibility following disasters, underscoring the importance of integrating data-driven approaches into humanitarian logistics. While the literature offers many models for optimizing last-mile relief networks using stochastic optimization, most focus on resilience through random scenario generation, with fewer studies adopting data-driven approaches to realistically test the practical applicability of these models.

Some research however, such as Noyan et al. (2016), introduce real-life data-driven simulations to bridge the gap between theoretical models and practical needs. In their study on the 2011 Van Earthquake, they model a network with one Local Distribution Center (LDC) and 94 demand points, using Google Maps for settlement coordinates and travel times to account for real road networks and constraints. Demand estimates in each cluster are based on damage intensity levels calculated from distance to the fault line and earthquake magnitude, using a formula from Erdik and Eren (1983). Additionally, population demographics—such as proportions of elderly, children, disabled individuals, and women with children—are sourced from Turkey’s national address-based registration system (TUIK), enabling the researchers to assign mobility scores that reflect accessibility needs within each settlement, where higher scores indicate lower mobility. This comprehensive data-driven approach allows for more realistic assessments of demand and accessibility in disaster simulations.

In their study on post-disaster vehicle routing, Puca Huachi Vaz Penna and Prins

(2018) use real-world data from the 2010 Port-au-Prince earthquake to create highly realistic, scenario-based simulations. They utilize Geo-Eye satellite images taken the day after the earthquake, processed by SERTIT, to map 16,660 nodes and 19,866 edges, with demand points estimated based on temporary shelters. Roads are categorized by width, blockage level, and vehicle compatibility, enabling a detailed simulation of routing constraints. This realistic scenario testing allows their optimization model to address true-to-life uncertainties, improving its effectiveness for last-mile relief distribution in disaster situations. Likewise Aghababaei et al. (2020) provide detailed, data-driven simulation framework for assessing transportation impacts in the aftermath of a potential Alpine Fault earthquake in New Zealand, offering another realistic approach for optimizing last-mile relief logistics. Their study employs a mesoscopic simulation model to predict disruptions in road network performance following an earthquake, analyzing key metrics such as mean travel time and total travel time to assess network resilience. For last-mile relief logistics, these real-life data-driven simulations are essential, as they offer valuable insights into accessibility challenges that may emerge post-earthquake.

In the context of post-earthquake logistics, using real-world GIS and road network data is essential for generating realistic scenarios that enhance the accuracy of simulations. Horner and Downs (2008) highlight how GIS and spatial optimization can systematically organize disaster relief efforts, underscoring the value of geographic precision in relief logistics. Likewise, Hooshangi and Alesheikh (2018) leverage real-world data within a GIS environment to simulate urban search and rescue (USAR) operations in Tehran's District 3. Their agent-based model incorporates building vulnerabilities, road networks, and casualty distributions, resulting in a detailed simulation that closely mirrors actual disaster scenarios. By integrating dynamic task allocation, their model effectively captures real-life challenges and provides critical insights into USAR efficiency and decision-making under uncertainty.

Choukolaei et al. (2022) present a simulation-based approach for decision-making in earthquake crisis management, focusing on the prioritization of relief centers and goods allocation. Their model assesses the impact of earthquakes on urban infrastructure through network simulations, prioritizing shelter locations such as stadiums, universities, and sports centers. The study utilizes GIS-based decision-making methods like TOPSIS and PROMETHEE to optimize the allocation of relief goods, providing a valuable tool for improving post-earthquake logistics and shelter planning. Feizizadeh et al. (2023) present another approach that leverages GIS data and simulations for post-disaster logistics by developing a game-based GIS method to simulate earthquake rescue operations for Tabriz City. Their innovative, rescue-scenario-based game-driven simulation demonstrates how gaming-inspired techniques can enhance crisis management and improve rescue team performance, highlighting the value of interactive and accessible tools for strengthening disaster preparedness.

In this study, we adopt a similar approach by utilizing various GIS datasets, prior research and data on Istanbul's infrastructure, seismic vulnerabilities. For instance, reports like Kandilli Observatory (2023) and studies such as İBB DEZİM Kadıköy (2020) provide essential data on Istanbul's urban layout and projected impact zones in the event of a major earthquake. By integrating these datasets, we aim to create realistic, scenario-based simulations that account for Istanbul's unique structural and logistical challenges.

2.4 Sampling Methods for Scenario Generation in Disaster Simulations

Utilizing real-life datasets and GIS data is crucial for creating realistic simulations to optimize logistics in post-disaster environments. However, large-scale disasters often involve complex uncertainties that no dataset can fully capture. In such cases, sampling-based simulations become essential to account for these unknowns and test logistical models under varied scenarios. To minimize bias, it is critical to employ structured scenario generation methods. For example, Löhndorf (2016) evaluates various scenario generation techniques for stochastic optimization, highlighting Latin Hypercube Sampling (LHS) as a powerful approach for improving scenario accuracy. Kaut and Wallace (2003) also analyze methods for stochastic programming, noting the robustness of LHS in addressing uncertainties effectively. Additionally, Freimer and Linderoth (2012) examine how different sampling methods, impact bias and variance in stochastic programs, underscoring its value in reducing distortions. That's why in this study, we also use Latin Hypercube Sampling (LHS) alongside Monte Carlo sampling to examine how LHS might increase the realism of our scenarios by ensuring more evenly distributed building damage across the study area.

2.5 Key Distinctions Between Our Approach and Previous Research

Building upon prior research, particularly the work of Noyan et al. (2016), our study also aims to optimize the last-mile segment of the relief network, focusing on effective selection of PODs and strategic allocation of supplies. By prioritizing these elements, we aim to improve accessibility and ensure that relief supplies are distributed efficiently and equitably in post-disaster scenarios. While Noyan et al. (2016) emphasize detailed disaster scenario modeling and explore trade-offs among *TD*, *PD*, and *Hybrid* policies within their model, our approach instead prioritizes the development of a robust, adaptable simulation framework. This framework is

designed to be generalizable, enabling simulations and testing of various stochastic optimization models for last-mile relief networks in future research. Rather than introducing a new optimization model, we refine and implement a modified version of the Hybrid policy based on the SLMRND model from Noyan et al. (2016).

Noyan et al. (2016) work with larger areas, such as districts in Van, clustering demand nodes into networks of 30 or 60 nodes using p-median models and running 50-100 scenarios to test the performance of different model approaches. In contrast, our study operates at a much finer granularity, emphasizing real-world applicability and simulation of a single model. We work with a network of 950 nodes and 10-20 scenarios, optimizing the last-mile relief network at the neighborhood level. In our model, demand points represent localized areas, such as small streets or blocks within a neighborhood. This approach allows more detailed and realistic simulations, aiming to capture the finer nuances of local demand fluctuations and disruptions in the post-earthquake network conditions.

Our approach to scenario generation is a key methodological difference. While Noyan et al. (2016) use damage intensity based on proximity to the fault line, we base our disruptions and demand for aid directly on building collapse scenarios. To better capture uncertainty and reduce bias in these simulations, we also introduce Latin Hypercube Sampling (LHS) alongside real-world data for scenario generation.

2.6 Summary of Key Research in Disaster Relief Network Design

In this section, Table 2.1 presents a concise overview of key studies that contribute to the field of post-disaster relief network design. Each study is summarized by its main objectives, the disaster context addressed, modeling approaches used and the data sources applied to enhance model realism and applicability. This table provides a comparative basis for understanding different methodologies and data-driven approaches in various studies aiming to optimize last-mile humanitarian logistics.

Study	Key Objective	Target Area/ Disaster	Modeling Approach	Data Usage
Horner (2008)	Optimize location of PODs to improve accessibility and reduce distribution costs	Hurricane Katrina	Integer programming model for locating PODs and linking them to LDCs	GIS and spatial optimization data for determining transportation networks and aid demand locations in hurricane-impacted areas, data from Hurricane Katrina
Noyan (2012)	Improve facility location and inventory management by balancing risk in uncertain demand and damage scenarios	General	Risk-averse two-stage stochastic programming for facility location and inventory under uncertainty	Theoretical data to simulate demand and damage under different risk scenarios, enhancing computational efficiency
Noyan (2016)	Balance equity and accessibility in POD selection and supply allocation, compare PD, TD and Hybrid policies	Van (Turkey) Earthquake	Two-stage stochastic optimization model balancing accessibility and equity under uncertainty	Road and point data from Google Maps, demand intensity estimates based on fault line proximity, demographic data in Van, data from Van Earthquake in 2011
Penna (2018)	Design a realistic, scenario-based model for post-disaster vehicle routing with optimized relief aid distribution	Port-au-Prince (Haiti) Earthquake	Metaheuristic optimization method, specifically Hybrid heuristic with set partitioning for complex VRP in post-disaster scenarios	Geo-Eye Satellite images processed by SERTIT for road networks and demand points, node and edge data on road blockage, demand estimates based on temporary shelter data, historical data from Haiti Earthquake
Aghababaei (2018)	Simulate transportation impacts post-earthquake to predict network resilience and optimize relief logistics	New Zealand, Alpine Fault	Mesoscopic simulation model to predict travel times and network disruptions	Real-life road performance data using network resilience metrics, geological data on Alpine Fault and historical earthquake data
Our Study	Optimize POD selection and supply allocation using real-world data to create minimally biased scenarios, supported by extensive simulation	Istanbul, Turkey	Two-stage stochastic optimization model balancing accessibility and equity under uncertainty	GIS-based population, road and building data for Istanbul, building collapse scenarios based on official building damage estimate reports by IMM, LHS for scenario generation

Figure 2.1: Table comparison of key research in disaster relief network design and optimization

3 Problem Definition

In this study, we focus on optimizing last-mile logistics for relief networks, specifically addressing the complexities that arise when distributing aid to affected populations in an urban environment after a disaster. Our problem definition and stochastic optimization model is based on the research and model in Noyan et al. (2016), also referred to as SLMRND model.

3.1 Structure of Last-Mile Relief Networks

Last mile networks consist of three main elements: Local Distribution Centers (LDCs), Points of Distribution (PODs), and demand points. In a last-mile relief network, it is common to have only one or a few LDCs, as these are large distribution hubs, such as disaster response warehouses, airports, or major transport stations located in or near the disaster-affected city. These LDCs receive humanitarian aid supplies from various national sources and international organizations, serving as centralized points for further distribution.

From these large distribution facilities, supplies are sent to PODs, which are strategically located across the affected area. PODs serve as temporary distribution sites where aid is provided directly to the affected population. They may be set up in public areas such as schools, sports facilities, parks or other easily accessible locations with big enough free space, depending on the local context and availability of resources. Taking metrics such as capacity and accessibility into account, a POD can serve one or multiple demand locations (such as neighborhoods, villages, buildings, or aggregated local populations) scattered across the affected area.

The structure and connections within a last-mile relief network are illustrated in Figure 3.1. This figure, taken from Noyan et al. (2016), provides an example layout where supplies flow from an LDC to multiple PODs, each of which serves nearby demand points. The arrangement demonstrates the hierarchical organization of last-mile logistics, where a limited number of centrally located LDCs distribute resources to PODs that are accessible to dispersed demand points across the affected region.

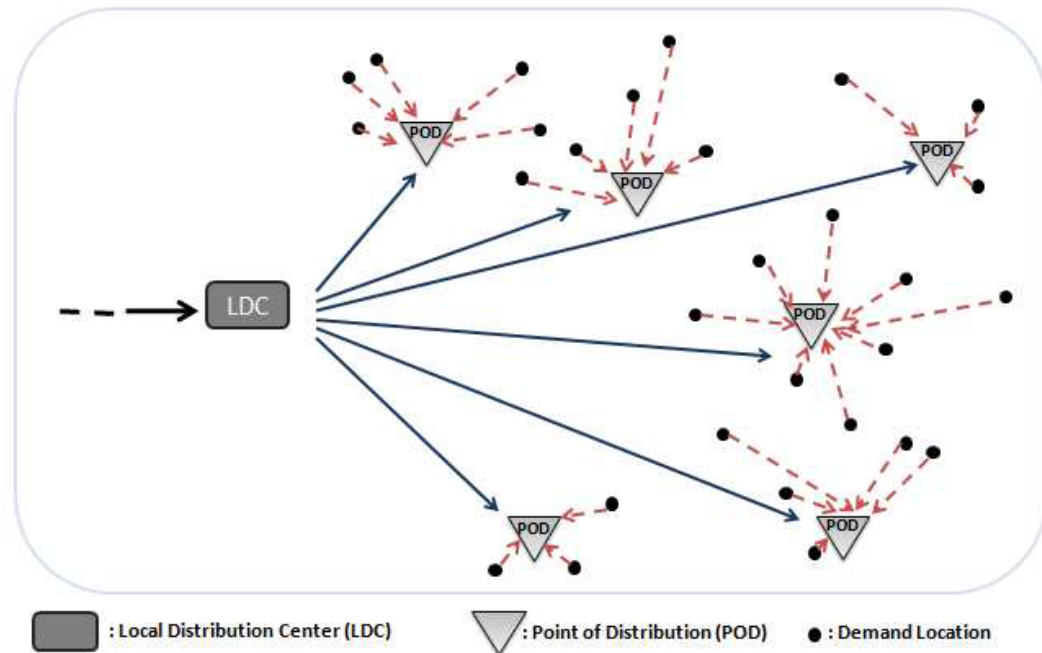


Figure 3.1: Example last mile relief network from Noyan et al. (2016)

3.2 Challenges in Last-Mile Relief Networks

The last mile in relief logistics under uncertainty conditions poses unique challenges, key issues are listed below.

3.2.1 Accessibility

In supply chain management, *accessibility* refers to the ease with which various resources such as products, information, and services can be reached and utilized, where the goal is to reduce the time and cost associated with the transportation process. In the context of a last mile relief network, however, accessibility specifically refers to the ability to efficiently deliver relief supplies such as food, medicine or other essentials to people in need. Since human lives are at stake, the accessibility metric in the last mile relief optimization does not account for cost and is based on time rather than distance. This is because, in post-disaster conditions, transportation networks are often disrupted; therefore, short distances do not always guarantee the quick delivery of aid supplies.

In last mile relief networks, supplies are typically delivered from LDCs to PODs by trucks, while people in the affected regions travel to the PODs to receive relief supplies. In some instances, vehicles may also transport supplies directly from PODs to beneficiaries. Therefore, when developing accessibility metrics, the last mile relief network can be broken down into two key areas of focus: 1) the accessibility

of the PODs from the LDC, and 2) the accessibility of the PODs from the demand locations. These two aspects are essential for ensuring that aid reaches affected populations efficiently, minimizing delays and optimizing the distribution process.

Many studies, including Noyan et al. (2016), highlight that in post-disaster settings, accessibility is influenced by both physical factors (e.g., infrastructure damage) and demographic/socio-economic factors (e.g., limited mobility among vulnerable populations, lower-income groups facing challenges in accessing relief aid), with the latter particularly impacting access from Points of Distribution (PODs) to demand points. However, in our model and simulations, we focus exclusively on physical factors, incorporating only transportation time to calculate accessibility.

3.2.2 Equity

The *equity* metric can be divided into several components: 1) *equitable accessibility*, which minimizes physical, demographic, or financial barriers to relief aid; 2) *equitable allocation of supplies* to PODs from LDC; 3) *equitable (fair) distribution of supplies* to individuals at PODs. In the SLMRND model from Noyan et al. (2016), a coverage set is defined for each demand location, consisting of candidate PODs where accessibility from the demand location meets a specified minimum threshold. Equitable accessibility is promoted by establishing this *minimum accessibility* threshold, ensuring that each demand location can be served by a POD that meets this basic accessibility requirement. Furthermore, the model promotes balanced supply distribution by calculating the *maximum proportion of unsatisfied demand (MPUD)*, which represents the highest percentage of demand not met across all PODs in each scenario. This approach helps ensure equity in supply allocation.

Our model and simulation analysis focus exclusively on achieving equitable supply allocation at the POD level, ensuring that the MPUD metric is satisfied. We assume that individual distribution decisions at PODs are managed by relief personnel during operations, therefore, our model prioritizes a balanced allocation across PODs based on their capacity constraints. While equitable accessibility could have been included in our model, doing so would require a carefully chosen minimum accessibility threshold. As also discussed in Section 5 and in Noyan et al. (2016), this parameter is highly sensitive and often results in infeasible solutions with most values, necessitating extensive research. Therefore, incorporating this parameter is considered beyond the scope of this study.

3.2.3 Supply Allocation Policies

Various supply allocation policies can be employed in designing a last-mile relief network, and the strategic choice of these policies significantly affects the efficiency

and effectiveness of relief operations. For simplicity in our model, like the SLM-RND model from Noyan et al. (2016), we assume a single, comprehensive supply package, even though in reality, the demand for different types of supplies such as medical aid, food, and shelter would vary based on specific needs in affected areas. This approach helps streamline the model, but it also introduces some limitations in accurately representing diverse supply requirements. Future extensions of this model could incorporate multiple types of supply packages such as shelter, water, food, medicine etc. to better align with the varied needs that may emerge in post-disaster scenarios, ultimately enhancing the model's realism and applicability to real-world relief efforts.

Various policies can be established for supply distribution, each tailored to address specific priorities:

- *Proportional Demand Allocation Policy (PD Policy)*: Supplies are allocated proportionally to PODs based on demand, with the aim of distributing shortages evenly across all PODs.
- *Target/Threshold Demand Allocation Policy (TD Policy)*: Supplies are distributed to each POD such that shortage amounts do not exceed a predefined upper limit. This policy allows for greater flexibility and can enhance accessibility.
- *Hybrid Allocation Policy*: Combining elements of both the *PD* and *TD* policies, the *Hybrid* approach seeks to optimize both *accessibility* and *equity*. This policy permits controlled deviations from strict proportionality, addressing the trade-off between ensuring equity and minimizing response times.

Since our model builds upon the SLMRND model, it employs the Hybrid Policy. However, as discussed in Chapter 6, limitations in the available input data and simulations result in our model gravitating towards the TD Policy.

3.2.4 Uncertainties in Post-Disaster

The inherent uncertainty of post-disaster conditions rules out the use of deterministic optimization for designing last-mile relief networks. Numerous factors can impact relief operations, but our model focuses on two primary uncertainty parameters: demand fluctuations and road network reliability. First, given that exact demand levels are highly unpredictable after a disaster, our model incorporates multiple demand scenarios to enhance robustness against real-world demand variability. Second, the model accounts for uncertainties in the transportation network, such as potential road damage or blockages, by using scenario-based modeling to simulate various network conditions. Using stochastic optimization, our model's objective function integrates parameters from each scenario, yielding a solution that balances all conditions. This approach optimizes the relief network across various potential post-disaster scenarios, enhancing reliability of findings.

3.3 Stochastic Optimization Model

Our stochastic optimization model builds upon the SLMRND model from Noyan et al. (2016), with adaptations to better align with the real-world, applied simulation focus of our study. Like the original model, it employs a two-stage stochastic programming framework, which addresses the uncertainties of post-disaster environments and the need for rapid relief distribution. In the first stage, decisions on the locations and capacities of PODs are made before uncertainties in demand and accessibility scores are resolved. In the second stage, once the uncertain parameters are observed, supply allocations and demand point assignments to PODs are determined, incorporating also the predetermined first-stage decisions.

Sets and Indices:

I : set of all points (includes LDC, candidate PODs and demand points)

J : set of all candidate POD locations (includes LDC)

S : set of scenarios

Parameters:

p^s : probability of scenario $s \in S$

d_i^s : humanitarian aid demand at the point $i \in I$ under scenario $s \in S$

$\nu_{0,j}^s$: accessibility score from the LDC to candidate POD $j \in J$ under $s \in S$

$\nu_{i,j}^s$: accessibility score to candidate POD $j \in J$ from node $i \in I$ under $s \in S$

O_{\max}^s : maximum humanitarian aid supply under $s \in S$

K_j : maximum supply capacity of POD $j \in J$

ϵ : penalty parameter for deviation from the *relaxed PD* policy

ρ : maximum allowed shortage ratio from the POD total demand at each POD

Decision Variables:

$y_j \in \{0, 1\}$: 1 if POD $j \in J$ is open, 0 otherwise

$R_j \geq 0$: supply capacity allocated to POD $j \in J$

$x_{i,j}^s \in \{0, 1\}$: 1 if POD $j \in J$ serves point $i \in I$ under $s \in S$, 0 otherwise

$r_j^s \geq 0$: total supply delivery to POD $j \in J$ in scenario $s \in S$

$\beta_j^s \geq 0$: slack variable for demand proportionality for POD $j \in J$ under $s \in S$

Auxiliary Variables:

$$\begin{aligned}
 o^s &= \min \left(O_{\max}^s, \sum_{i \in I} d_i^s \right) : \text{total demand satisfied under } s \in S \\
 TD_j^s &= \sum_{i \in I} x_{i,j}^s d_i^s : \text{total demand assigned to POD } j \in J \text{ under } s \in S \\
 PD_j^s &= \begin{cases} \frac{o^s}{\sum_{i \in I} d_i^s} \cdot TD_j^s & \text{if } \sum_{i \in I} d_i^s > 0 \\ 0 & \text{otherwise.} \end{cases} \\
 &: \text{proportional demand served by POD } j \in J \text{ under } s \in S
 \end{aligned}$$

Objective Function:

Maximize the accessibility and equity:

$$\text{maximize } \sum_{s \in S} p^s \cdot \left(\sum_{j \in J} v_{0,j}^s y_j + \sum_{i \in I} \sum_{j \in J} v_{i,j}^s x_{i,j}^s - \epsilon \sum_{j \in J} \beta_j^s \right)$$

Constraints:

1. Maximum number of PODs that can operate:

$$\sum_{j \in J} y_j \leq C$$

2. Maximum allowed supply capacity of opened PODs:

$$R_j \leq K_j \cdot y_j \quad \forall j \in J$$

3. Delivered capacity limits for PODs:

$$r_j^s \leq R_j \quad \forall j \in J, \forall s \in S$$

4. Total demand served in each scenario:

$$\sum_{j \in J} r_j^s = o^s \quad \forall s \in S$$

5. Each demand point is served by exactly one POD:

$$\sum_{j \in J} x_{i,j}^s = 1 \quad \forall i \in I, \forall s \in S$$

6. Only operating (opened) PODs can serve demand points:

$$x_{i,j}^s \leq y_j \quad \forall i \in I, \forall j \in J, \forall s \in S$$

7. Each POD serves itself if opened:

$$x_{j,j}^s \geq y_j \quad \forall j \in J, \forall s \in S$$

8. Proportional demand upper bound:

$$r_j^s \leq PD_j^s + \beta_j^s \quad \forall j \in J, \forall s \in S$$

9. Proportional demand consistency with total demand:

$$PD_j^s + \beta_j^s \leq TD_j^s \quad \forall j \in J, \forall s \in S$$

10. Maximum allowed shortage at each POD from total demand of the POD:

$$TD_j^s - r_j^s \leq \rho \cdot TD_j^s \quad \forall j \in J, \forall s \in S$$

11. Non-negativity constraints:

$$r_{s,j} \geq 0 \quad \forall j \in J, \forall s \in S$$

$$\beta_{s,j} \geq 0 \quad \forall j \in J, \forall s \in S$$

$$R_j \geq 0 \quad \forall j \in J$$

4 Istanbul Case Study: Data Preparation and Integration

One of the primary contributions of this study is the identification and processing of datasets to build a realistic simulation framework for optimizing post-disaster and more specifically post-earthquake last-mile relief network systems in urban environments. In this section, the data pre-processing and geospatial analysis steps are detailed and explained, which serve to generate input parameters and scenarios for simulating the stochastic optimization model introduced in Section 3. Even though most of the datasets we will utilize in this study cover the data for whole Istanbul metropolitan area, in our simulations we will only explore the Kadıköy district in Istanbul, as with the means we have at hand it is technically infeasible to do a city-wide scaled logistics optimization. However, the simulation framework developed here, along with the datasets prepared for the broader Istanbul area, can support more extensive and large-scaled optimization studies in future research.

4.1 Scenario Definition for Istanbul Study Case

Defining scenarios for our Istanbul study case is a crucial step in simulating the stochastic optimization model introduced in Section 3. By constructing these scenarios, we can explore various outcomes and analyze how network logistics and demand for relief aid might respond under different conditions.

4.1.1 Building Collapse as Scenarios

In this study, scenarios are generated by selecting buildings in Kadıköy through an informed random process, designating the selected buildings as collapsed for each scenario. Varying collapse densities across different areas in each simulation varies the local demand for aid supplies, which is used to create distinct demand scenarios. Additionally, in real world post-earthquake conditions, debris from collapsed buildings would block nearby roads, which serves as the foundation for modeling different transportation network conditions and corresponding network accessibility scenarios in post-earthquake Kadıköy.

4.1.2 Data-driven Building Selection Methodology

Since it is impossible to predict exactly which buildings will collapse, the selection process relies on the İBB DEZİM Kadıköy (2020) dataset, which provides estimates of the number of buildings in Kadıköy neighborhoods likely to experience various levels of damage in the event of a 7.5 magnitude earthquake. Figure 4.1 illustrates this dataset, with each row representing a neighborhood and columns indicating the number of buildings experiencing different levels of damage (very heavy, heavy, moderate, and light). Although the dataset does not predict exactly which buildings will collapse, it provides a realistic approximation for this study. By making the assumption that buildings with very heavy and heavy damage are most likely to collapse in the event of an earthquake, we use the sum of these estimated numbers to determine the total number of buildings to be selected for collapse in each neighborhood for every simulation. This approach reflects the neighborhood-specific damage levels accurately, reducing bias compared to a random citywide selection method.

This dataset for Kadıköy is based on an extensive study by the Istanbul Metropolitan Municipality (IMM), which estimates potential earthquake-related losses across Istanbul's districts (İBB DEZİM, 2019). While it is outside the scope of this study to verify the accuracy of these estimates, the dataset from the IMM remains the most reliable and detailed open-source resource for post-earthquake damage assessment in the city. It will therefore be used for scenario generation in our simulations. It is important to note that this dataset does not fully reflect the current conditions in Istanbul. For instance, in the Fikirtepe neighborhood, the dataset indicates a high number of buildings classified as being at risk of (very) heavy damage in the event of an earthquake. However, recent extensive urban renewal projects in the Fikirtepe region would significantly alter these results, as many older structures have been replaced with newer, more resilient buildings. This discrepancy highlights the need to account for updated urban development data, which however is not publicly available.

4.1.3 Limitations and Assumptions

It is important to note that while this method is effective in generating realistic scenarios, it has certain limitations. The dataset provides aggregated damage levels across neighborhoods rather than detailed information on individual building conditions. So there remains some bias, as the selection of collapsed buildings within each neighborhood is still done randomly. In Section 5 a new methodology is introduced, which aims to reduce such bias. Additionally, this study assumes that buildings categorized as very heavily or heavily damaged are most likely to collapse. However, this assumption may not fully reflect reality, as the IMM study does not establish a direct correlation between assessed damage severity and likeli-

Neighborhood Name	Very Heavy Damage	Heavy Damage	Moderate Damage	Light Damage
MAHALLE ADI	ÇOK AĞIR HASARLI	AĞIR HASARLI	ORTA HASARLI	HAFIF HASARLI
19 MAYIS	3	8	42	204
ACIBADEM	9	20	113	367
BOSTANCI	8	20	96	345
CADDEBOSTAN	6	15	74	260
CAFERAĞA	17	38	196	648
DÜMLUPINAR	13	33	152	248
EĞİTİM	18	49	221	396
ERENKÖY	5	12	53	232
FENERBAHÇE	5	15	81	256
FENERYOLU	4	10	49	198
FİKİRTEPE	17	43	207	316
GÖZTEPE	6	14	66	292
HASANPAŞA	18	40	182	405
KOŞUYOLU	6	23	116	280
KOZYATAĞI	3	8	39	208
MERDİVENKÖY	17	42	191	434
OSMANAĞA	16	33	167	481
RASİMPAŞA	18	41	189	518
SAHRAYICEDİT	4	9	46	204
SUADIYE	5	12	68	265
ZÜHTÜPAŞA	11	20	78	160
TOPLAM	209	505	2.426	6.717

Figure 4.1: Building damage estimations for each neighborhood in Kadıköy İBB DEZİM Kadıköy (2020)

hood of collapse. Thus, a building expected to sustain only moderate damage in a 7.5 magnitude earthquake could still collapse, while another predicted to experience very heavy damage might remain standing despite the extent of damage.

4.2 Neighborhood Data Integration in GIS

4.2.1 Using Neighborhood Center Data

The dataset by IBB Muhtarlık (2024) contains comprehensive information regarding the neighborhood centers (muhtarlık), including their district, neighborhood, location, and address details. In this context, the term ‘neighborhood centers’ refers to the government administrative buildings located within each neighborhood in Turkey. This dataset is crucial, because the dataset from previous subsection doesn’t provide us any geographical information on neighborhoods, however this one pro-

vides the longitude and latitude of neighborhood centers. These two datasets are joined using R-programming based on the neighborhood, district information of each entry as keys, as there are neighborhoods with the same name in different districts in Istanbul. After the join of these datasets, some pre-processing is necessary in R to have tidy data, which can be used in future researches:

1. The encoding is set to UTF-8 to handle Turkish characters properly. However, still discrepancies between the neighborhood names in the datasets are present due to variations in the usage of Turkish characters (e.g., "İ" vs "I"). This causes some neighborhoods to not match correctly during the merge process, this is solved with manual correction.
2. Some neighborhoods do not have the respective neighborhood administrative center information, leading to gaps in the merged dataset, for these neighborhoods the geographical centers are selected as artificial neighborhood centers.
3. Duplicate entries emerge primarily due to variations in Turkish character usage, leading to multiple entries of the same neighborhood, these are fixed.
4. Some observations contained missing values (NAs) in critical columns like 'mahalle_ad', which are filtered out to ensure accurate analysis.

4.2.2 Using Neighborhood Boundary Polygons in GIS

İzzet Kılıç (2020) provides essential neighborhood boundaries for Istanbul in GIS polygon format, allowing precise geospatial representation of each neighborhood. This dataset is critical for accurately executing the random building selection process discussed in Section 4.1.2, as it enables us to select buildings within the precise geographical boundaries of each neighborhood.

With the neighborhood center locations from Section 4.2.1 integrated, we can now perform a geospatial join in ArcGIS to link neighborhood boundaries with corresponding building damage data, resulting in a comprehensive dataset ready for earthquake scenario modeling in ArcGIS. Figure 4.2 illustrates this simulation-ready dataset, where each polygon entry represents a neighborhood in Kadıköy, including longitude and latitude columns for neighborhood center coordinates and building damage data columns from the dataset shown in Figure 4.1.

4.3 Building Footprint Data for Istanbul

Accurate building data for Istanbul is essential in this study, due to the scenario generation methodology outlined in Section 4.1. Two of the leading global open sources for building datasets are Microsoft Bing Maps (2023) and Humanitarian OpenStreetMap (2024). The Bing Maps Building Footprints dataset was created by

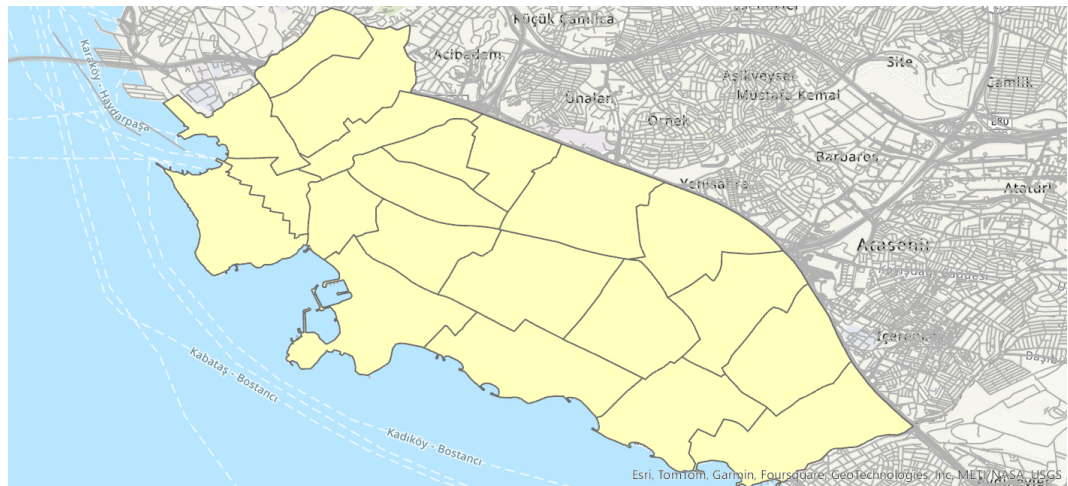


Figure 4.2: Neighborhood boundaries in Kadıköy district

applying deep learning algorithms to satellite imagery, automatically detecting and outlining building footprints across multiple countries. The resulting dataset, provides accurate building polygon data in GIS-ready formats for large-scale mapping. The OSM Turkey Buildings dataset, on the other hand, relies less on automation, as it combines volunteer mapping contributions with aerial imagery analysis to offer community-verified building footprints across Turkey for humanitarian applications. Both datasets however, may lack complete coverage or contain inaccuracies in certain areas. The Bing Maps dataset may miss smaller buildings or misclassify non-building features, as it relies heavily on automated detection methods. The OSM dataset relies on voluntary crowdsourced contributions from users worldwide, which can lead to inconsistencies in quality due to varying levels of contributor expertise and it may lack recent updates, particularly in rapidly developing areas. Despite these limitations, both datasets still offer a valuable foundation for building data in Istanbul.

To determine which dataset better represents the actual buildings in the Kadıköy district, it is essential to compare their coverage specifically within Kadıköy. According to İBB DEZİM Kadıköy (2020), the district contains 25120 buildings. The Bing Maps building dataset includes 16734 buildings, while the OSM dataset covers 19967 buildings in Kadıköy. This initially suggests that the OSM dataset might be more suitable due to its higher building count. However, a closer examination reveals that the OSM dataset lacks accurate building data in certain major areas within Kadıköy.

This difference is illustrated in Figure 4.3, where the pink polygons represent buildings from the Bing Maps dataset, and the cyan polygons represent buildings from the OSM dataset. Due to the representation format in ArcGIS, the cyan polygons appear with priority in overlapping areas, making the pink polygons visible only where the OSM dataset lacks coverage. Particularly in the areas highlighted by

rectangles, it is evident that the OSM dataset is significantly incomplete compared to the Microsoft dataset. Therefore, for this study, we use the Microsoft Bing Maps (2023) as our primary building dataset for the Kadıköy district.



Figure 4.3: Building data comparison example in Kadıköy:
Microsoft Bing Maps (pink) vs OSM (cyan) buildings

To obtain building data for Istanbul from the Microsoft dataset, first the entire building dataset for Turkey has to be filtered from the entire global data using the code provided by Bing Maps Team (2023) on their GitHub repository. Then using Bing Maps Quadkey Locator (2024), the specific quadkeys corresponding to the Istanbul area has to be identified, which are: 120323222, 120323223, 120323232, 120323233, 122101000, 122101001, 122101010, 122101011.

From the whole downloaded Microsoft Turkey Building Footprints dataset, the data files matching these quadkeys is imported, which contain Istanbul's and neighboring cities' building footprints. Then the "Calculate Geometry Attributes" tool in ArcGIS can be used to add the longitude and latitude of the central point of each building polygon as new columns, transforming the building polygon feature class into a point feature class. The final step in preparing the building dataset for simulations involves performing a geospatial join in ArcGIS, which spatially associates each building point with the corresponding neighborhood it falls within in Istanbul. This join ensures that each building is linked to its neighborhood and district, allowing us to implement the building selection process as described in Section 4.1.2. The result is a table of points, where each observation represents a building and includes attributes such as longitude and latitude, neighborhood and district information etc.

4.4 Population Data for Istanbul

For generating demand scenarios in our simulations, we incorporate not only the collapsing buildings in each area but also a more deterministic component: the population density. One reason for this is that our study focuses on a single type of aid supply. In real-world scenarios, however, areas with a higher density of collapsing buildings would likely require different types of aid compared to less affected areas. For example, areas with extensive destruction would have a greater need for immediate medical assistance, while areas with fewer collapses might primarily require food and shelter due to a likely lower rate of injuries. Since our model does not differentiate between types of aid needs and, in the aftermath of a major earthquake, people in all areas would require some form of assistance regardless of the level of destruction, we base demand scenario generation on both the extent of building collapse and the population in each area. To accurately represent this, we need a detailed and reliable population dataset for Istanbul.

Two prominent datasets for estimating the population distribution in Istanbul are WorldPop Project (2023) and Living Atlas Team (2023). Both datasets are using a combination of demographic information from census data, remote sensing, and geospatial analysis techniques to estimate population distribution at a high spatial resolution. The first dataset, provides population estimates in a 1km x 1km grid format, which offers a general view of population distribution but lacks the granularity needed for highly localized analysis. This coarser resolution limits its effectiveness for our study, as it does not capture smaller-scale population variations that can significantly impact demand in a disaster scenario. The second dataset, represents population estimates in 100m x 100m grids. This finer spatial resolution provides a much more detailed view of population distribution across the area. Granularity of the population data is crucial for our study, as population density—and therefore demand—can vary greatly even between neighboring streets. For our simulations, we require a dataset that captures these small-scale variations while maintaining reasonable accuracy, which the 100m x 100m grid dataset achieves effectively. The total sum of population estimates from this dataset is approximately 503463, closely aligning with the 2019 Kadıköy population figure of 482713 reported by İBB DEZİM Kadıköy (2020), indicating that our population data is quite realistic.

This dataset is available in raster format on ArcGIS, providing population estimates in the number of people per 100-meter square grid for multiple years. For our analysis, we are using the most recent available data from 2020. The population distribution for Kadıköy based on this dataset is shown in Figure 4.4. Each 100m grid has a separate entry in the table and the population estimate for the grid is given in the column `grid_code`. We convert the raster data into a point feature class, where each point represents the center of a raster grid cell. This transformation simplifies data processing and integration into the model and analysis.

However, this process generates 3,885 points as population data points, which poses a significant computational challenge. In the model, we create a decision variable $\nu_{i,j}^s$ for every POD and population point to indicate if the point is assigned to that POD. With 173 PODs and 3885 points, this would result in $173 \times (3885 + 173) = 702034 \nu_{i,j}^s$ variables. Including other parameters, the total number of decision variables would reach several million, making it computationally infeasible to solve within a reasonable time frame using our technical resources. To address this, we aggregate every 5 consecutive population points into a single point by averaging their longitude and latitude coordinates and summing their grid_code (population estimate) values. This aggregation reduces the number of points and results in the point feature class shown in Figure 4.5, which is now ready for use in our simulations.

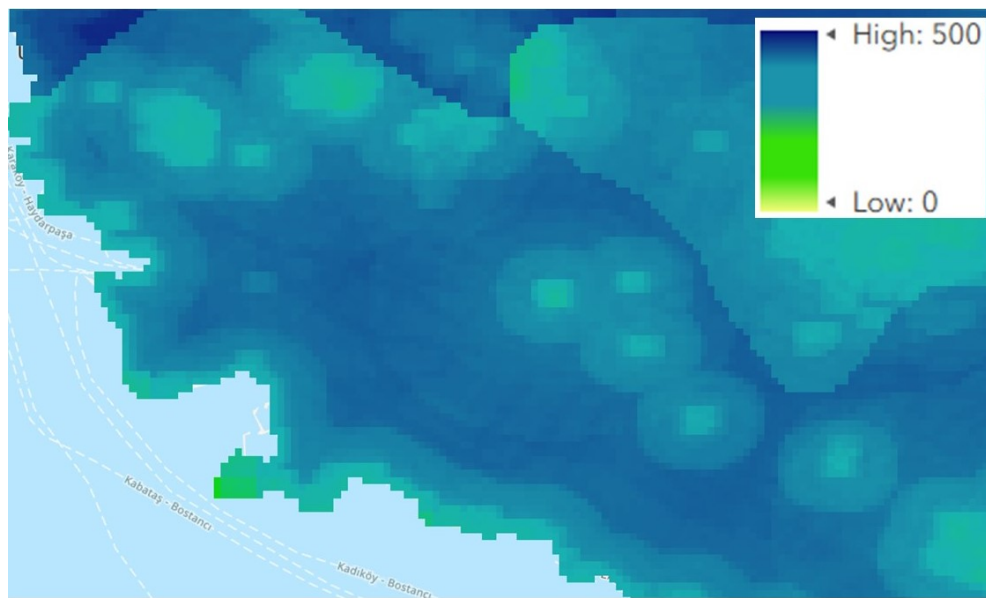


Figure 4.4: Population distribution in Kadıköy at a 100m x 100m grid resolution estimated by Living Atlas Team (2023)

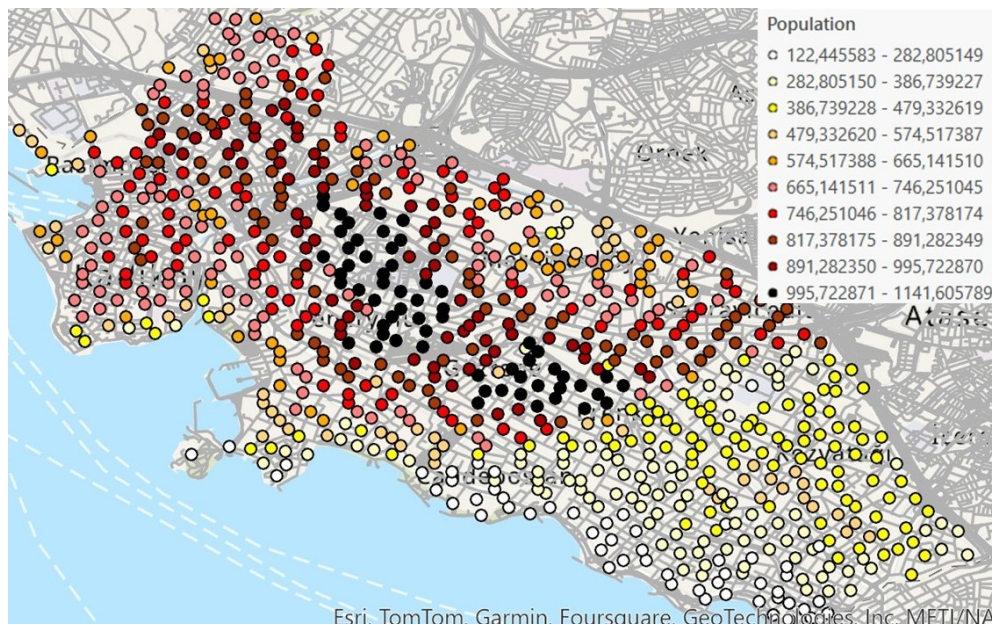


Figure 4.5: Population data aggregated from 100m x 100m grid cells, with every 5 consecutive cells represented by a single mean center point

4.5 Transportation Network Data for Istanbul

In our simulations, we rely on ArcGIS's OD Cost Matrix tool to calculate optimized travel times and distances between multiple origin and destination points. For accurate routing and time calculations across complex urban infrastructure, a well-structured network dataset is essential. This dataset is more than a collection of lines and points; it is a comprehensive model that captures connectivity, directionality, and travel restrictions (such as one-way streets or road closures) within the transportation network. The transportation network dataset used for these calculations is derived from the roads dataset in OSM Turkey (2024). Using ArcGIS's network dataset creation tool, we transform this raw data into a navigable network model. This tool organizes transportation data into a connected network of lines, representing road segments, and nodes, signifying intersections and entry/exit points. A small section of the network dataset created for Istanbul can be seen in Figure 4.6.

The data from the OD Cost Matrix is crucial for our scenario-based analysis, as it enables precise calculation of transportation times between the LDC and PODs, as well as between PODs and demand points. This allows us to evaluate and prioritize which PODs to activate based on accessibility metrics, ensuring that selected PODs are optimally located for efficient supply distribution. This approach minimizes travel times and enhances service delivery across various emergency response scenarios.

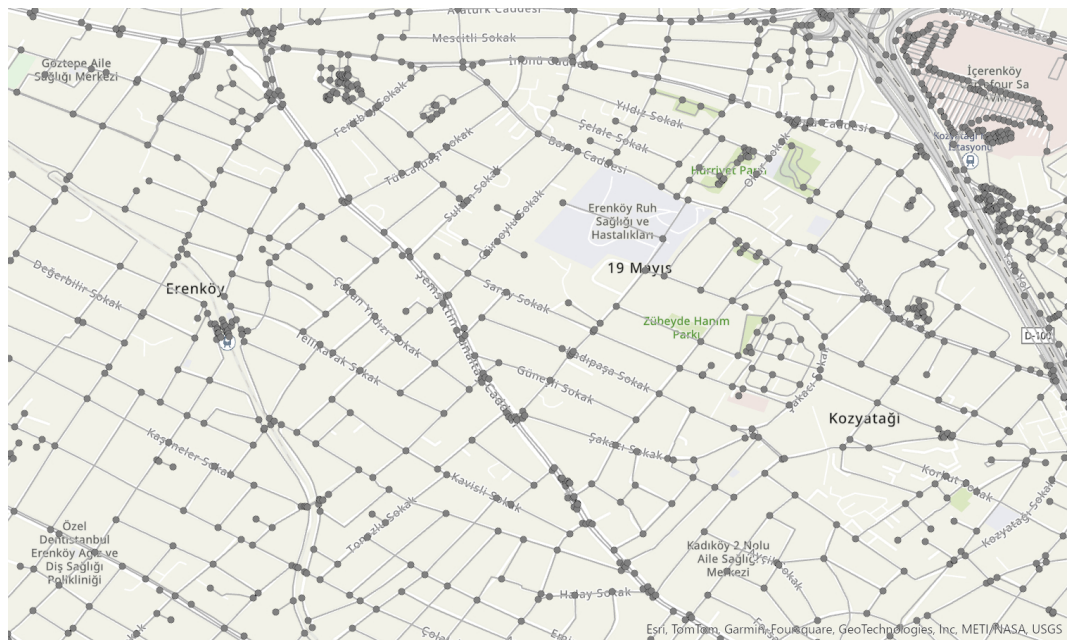


Figure 4.6: A segment of the transportation network dataset for Kadıköy

4.6 POD and LDC Selection for Kadıköy

In order to determine which PODs should be selected, we first need to create a set of candidate PODs. To achieve this, we require a reliable real-world dataset containing a variety of locations in Istanbul. The dataset provided by OSM Turkey (2024) offers extensive geospatial data for Turkey, which includes a wide range of features such as schools, parks, hospitals, and more. To identify the relevant dataset within this collection, we refer to the guide in Geofabrik GmbH (2022), which highlights the presence of a "Points of Interest (POI)" dataset. This dataset includes entries such as schools, restaurants, parks, and other facilities. Using geospatial mapping, we extract the POIs located within the boundaries of Kadıköy. After this extraction, we perform column filtering to isolate the relevant attributes and calculate the longitude and latitude of POI polygon centroids for spatial analysis. An example excerpt from the resulting table can be seen in Figure 4.7.

However, not all entries in the dataset are suitable for POD designation. For instance, it would not be logical to consider restaurants or post offices as PODs. Therefore, we filter the dataset to retain only relevant categories, such as parks, schools, universities, hospitals, and large malls. These locations are practical for PODs as they typically offer sufficient space and accessibility, which are essential for disaster relief distribution. In our simulations, we use the area of each location as a metric to estimate the maximum capacity of PODs. This approach is logical because larger areas can accommodate more people and supplies, making them more suitable for post-earthquake relief efforts. For example, a park with a vast open area can serve as an effective POD, whereas a small facility may lack sufficient space for

operations or gathering affected populations.

The area data provided in the original dataset is not in a readily processable format. To address this, we use a geospatial tool (DaftLogic, 2024) to manually calculate the areas of POI polygons, as shown in Figure 4.8. After calculating the areas, we implement a threshold to exclude locations smaller than 500 m², as they are impractical for POD purposes. Additionally, we filter out most seaside parks due to the risk of ground subsidence or collapse into the water following an earthquake, which would render them unsafe. In some cases, we manually add locations not included in the dataset but identified through Google Maps as large, open public spaces suitable for PODs.

A critical aspect of the disaster relief network is the selection of an LDC to serve as the primary hub for receiving and distributing supplies. For Kadıköy, Haydarpaşa Harbor is selected as the LDC (marked by the red square in Figure 4.9). Although its location at the edge of the Kadıköy area might lead to longer travel times between the LDC and PODs, it remains the most practical choice. The lack of another large harbor in southern Kadıköy, coupled with potential disruptions to main roads in post-earthquake conditions, makes Haydarpaşa Harbor ideal. Its size, facilities, and connectivity to main roads and railways position it as a likely LDC not just for Kadıköy but for other parts of İstanbul. Additionally, its accessibility by sea allows for efficient transportation of large supplies, which can then be distributed to PODs throughout Kadıköy. While Haydarpaşa Harbor is our chosen LDC, alternative locations could also have been considered. The final version of the LDC and PODs dataset, complete with filtered and manually adjusted entries, is shown in Figure 4.9. This dataset is now ready for use in our simulations.

Class	Name	Mahalle_Ad	Area	X	Y
school	Atatürk Fen Lisesi	EGITIM	0.0001	29.0523	40.9887
mall	Tepe Nautilus AVM	ACIBADEM	0.0002	29.0315	40.9996
park	Yoğurtçu Parkı	OSMANAGA	0.0001	29.0336	40.9853
pitch	Şükrü Saracoğlu Spor Kompleksi	ZUHTUPAŞA	0.0001	29.0369	40.9876
theme_park	Bostancı Lunapark	BOSTANCI	0.0002	29.1011	40.9565
police	Kadıköy Iskele Polis Merkezi	CAFERAGA	0.0001	29.0199	40.9905
hotel	Khalkedon Hotel	CAFERAGA	0.0001	29.0252	40.9894
bank	Halkbank	OSMANAGA	0.0001	29.0256	40.9913
theatre	Süreyya Operası	OSMANAGA	0.0001	29.029	40.988
arts_centre	Bostancı Gösteri Merkezi	BOSTANCI	0.0002	29.1023	40.9567
graveyard	Merdivenköy Mezarlığı	MERDIVENKOV	0.0002	29.0755	40.9894
post_office	PTT Haydarpaşa Gar Şubesi	RASIMPAŞA	0.0001	29.0194	40.9963
playground	Dumlupınar Parkı	MERDIVENKOV	0.0002	29.0609	40.9879
clinic	Kozyatağı Aile Sağlığı Merkezi	KOZYATAGI	0.0002	29.0951	40.9715
university	Istanbul Medeniyet Üniversitesi	DUMLUPINAR	0.0001	29.0619	40.9958

Figure 4.7: Example POIs in Kadıköy from OSM Turkey (2024)

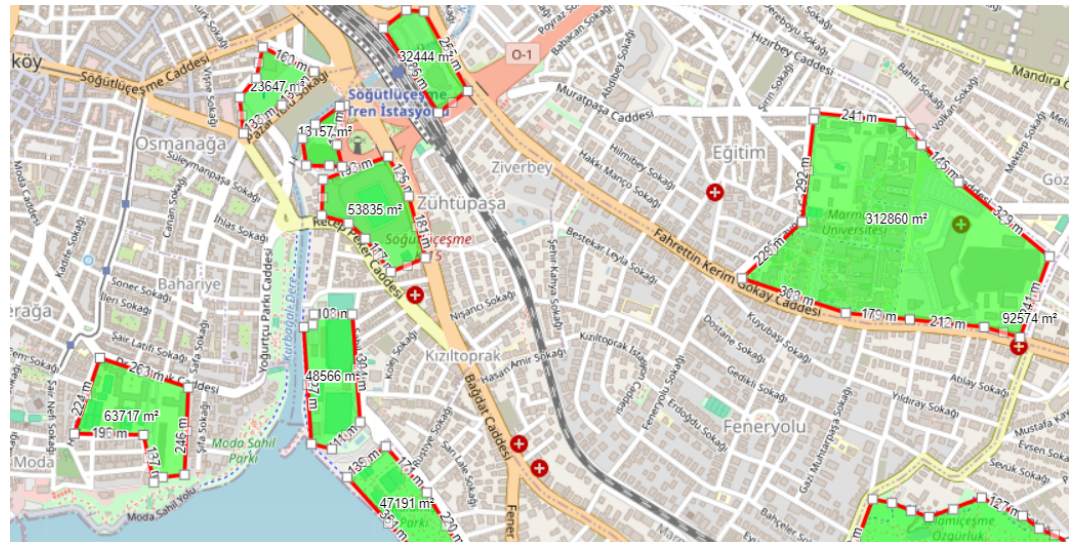


Figure 4.8: Example manual area calculation for PODs

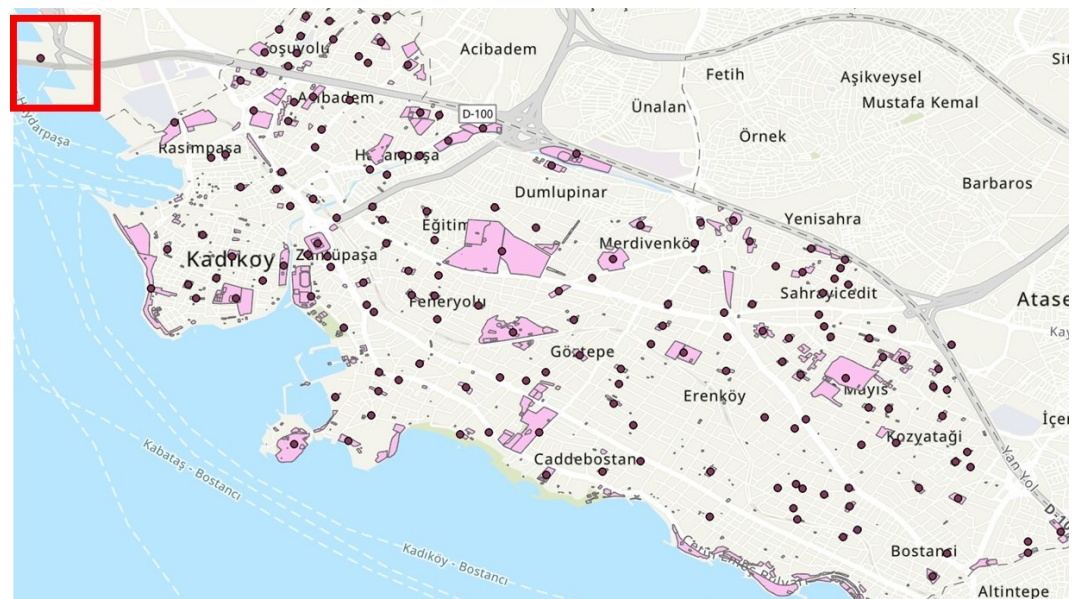


Figure 4.9: Selected LDC and PODs in Kadıköy

5 Simulation

In this section, we will provide a detailed explanation of how we conduct our simulations using the datasets gathered in Chapter 4, and how we introduce Latin Hypercube Sampling (LHS) to reduce bias in scenario generation.

5.1 Building Selection Algorithms

5.1.1 Monte Carlo Based Selection Algorithm

As the first step of the simulation, we implement a Python script that uses the tables shown at the end of the Section 4.3 and Figure 4.1 to do a Monte Carlo random sampling based selection of a specified number of buildings (likely collapsed) from each neighborhood in Istanbul. The selection process is based on the sum of the 'cok_agir_h' (very heavy damage) and 'agir_hasar' (heavy damage) columns, with neighborhoods identified by the combination of 'mahalle_ad' and 'ilce_adi' columns. The script generates a GeoJSON file that includes the selected buildings along with their geographic coordinates and damage information, to be used in ArcGIS environment. However, we filter the results to include only buildings in the neighborhoods of Kadıköy, as our simulations focus on this district. This process is repeated 10 times to create 10 different scenarios, each representing a distinct set of collapsed buildings for use in our simulations.

5.1.2 Monte Carlo Sampling and Its Bias

Monte Carlo sampling, as used in our basic building selection algorithm, selects points randomly without considering the overall distribution of the space. This means that some areas within the neighborhood might be sampled more frequently, while others might not be sampled at all. As a result, certain clusters of buildings may be overrepresented, leading to an inaccurate representation of the actual risk of collapse across the neighborhood. This bias can produce scenarios that do not adequately reflect real-world conditions, consequently the outputs generated by the stochastic optimization model may contain inaccuracies.

5.1.3 LHS and Its Reduction of Bias

Latin Hypercube Sampling (LHS) method addresses the bias inherent in Monte Carlo sampling by ensuring that each stratum (or sub-region) of the space is sampled at least once. This method helps avoid the overrepresentation and underrepresentation of certain regions within the parameter space. According to Löhndorf (2016), by dividing the space into strata and ensuring proportional sampling from each stratum, LHS generates more balanced and representative scenarios. Freimer and Linderoth (2012) further highlight that LHS improves sampling efficiency by reducing variance, leading to better coverage and more stable results. In the context of building selection, each neighborhood is stratified into segments, and buildings are selected so that each segment contributes to the sample in every scenario. We use a Python script that first applies K-means clustering to each neighborhood, and then uses LHS within each cluster to select a proportional number of buildings. The number of buildings selected from each cluster using LHS is determined by dividing the total number of collapsing buildings in the neighborhood by the number of clusters. This combined approach ensures a more even spread of selected buildings, minimizing clustering and gaps, and helps reduce bias by evenly distributing the buildings across the area.

5.1.4 Comparison of Thiessen Polygons in MC and LHS Building Selection

Thiessen (or Voronoi) polygons are used to visualize the influence of each sampled building by dividing the space so that each polygon contains the set of points closest to its corresponding selected building. In a well-distributed sample, the Thiessen polygons should be roughly uniform in shape and size, indicating that the selected buildings cover the area evenly. However, when buildings are selected randomly, the resulting polygons often exhibit significant variation in shape and size. Some areas may be oversampled, leading to smaller, more irregular polygons, while other areas are undersampled, creating large, sparsely populated polygons. These variations result in uneven coverage of the area and indicate clustering of selected buildings in certain regions. Figure 5.1 shows that the Monte Carlo-generated polygons are clustered and vary in shape, reflecting the uneven distribution of the sampled buildings, while the LHS-generated polygons display more uniform sizes, indicating a more evenly distributed sample. The polygons are generated using the ArcGIS tool for Thiessen polygon creation, which divides space based on proximity to selected points.

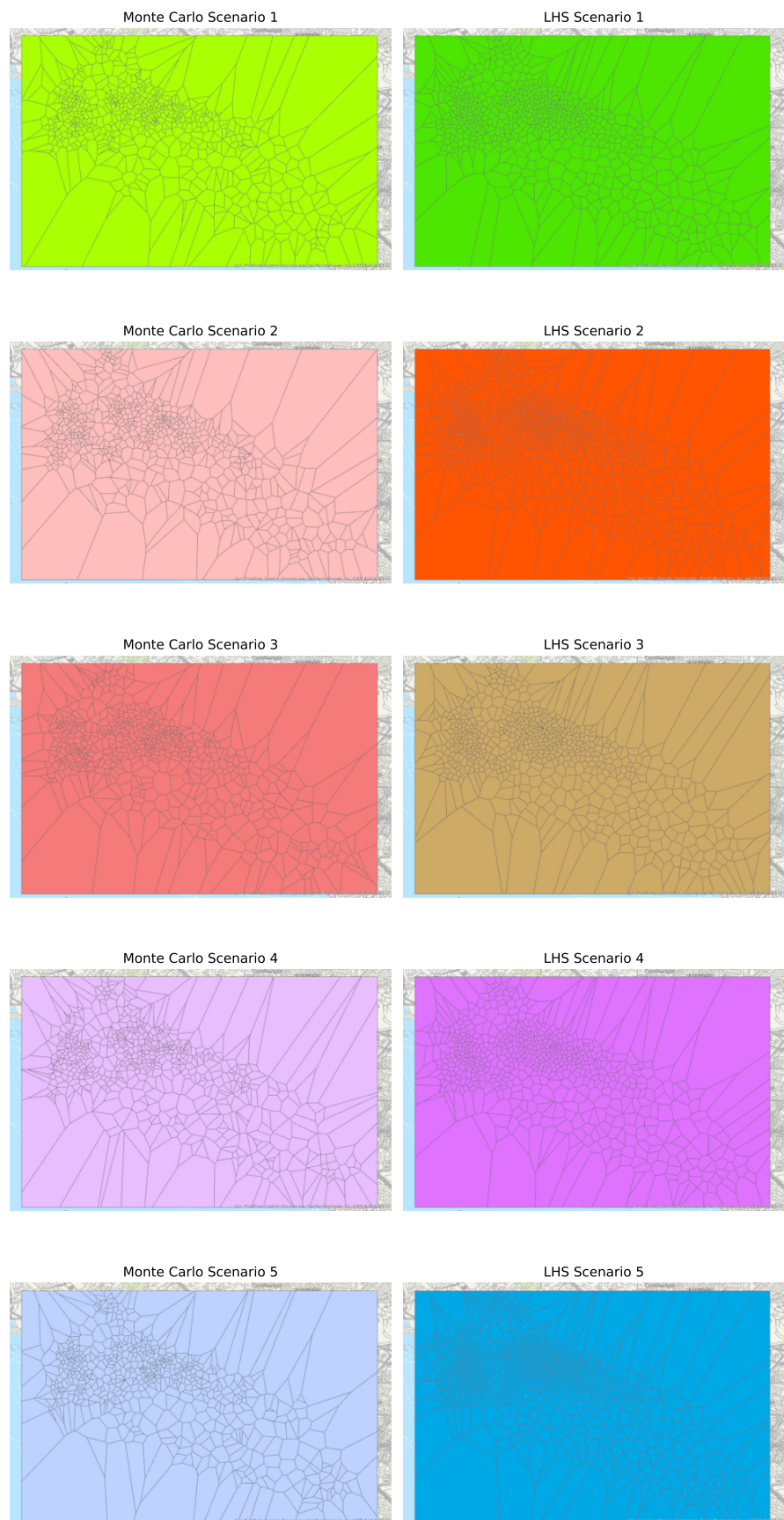


Figure 5.1: MC and LHS building selection: Thiessen polygon comparison

5.1.5 Further comparison of MC and LHS in building selection

We implement a python code to compare the number of buildings selected by LHS with the average number selected by MC simulations in each subregion of the neighborhood. For each subregion, we calculate the difference between the fixed sample size chosen by LHS and the average count from multiple MC simulations, highlighting if MC provides a similar sample size to LHS on average. In the Figure 5.2, we can observe significant deviations, indicating that the MC approach often produces varying sample counts across subregions, while LHS maintains a consistent selection size, providing a more uniform representation across the neighborhood. As illustrated by the wider spread of the boxplots in the figure, neighborhoods with higher building destruction, such as 'Hasanpaşa' and 'Fikirtepe' (which require more building selections), exhibit larger deviations for Monte Carlo (MC). This suggests that MC's purely random selection method may lead to biased distributions, particularly in densely sampled areas, potentially resulting in clustered or sparse building selections.

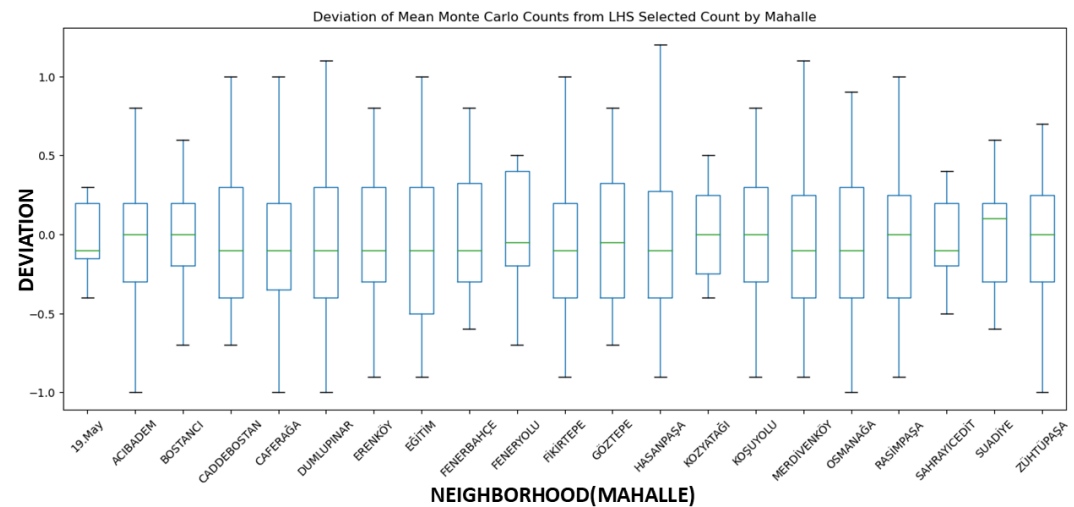


Figure 5.2: Comparison of Monte Carlo and LHS building selection: deviation across neighborhoods

5.1.6 Role of Sampling Methods in Our Study and Key Assumptions

It can be argued that, in a real-world scenario, the collapse of one building may increase the likelihood of collapse for surrounding buildings, which would necessitate the use of a Bayesian network in simulations. However, for the purposes of this research, we assume that the collapse of one building is independent of the collapse of others. Consequently, the use of LHS is justified within our framework, as it

indeed reduces bias in scenario generation by providing a more representative and balanced selection of buildings. However, this does not guarantee that the simulation outputs will be significantly more realistic or superior to those produced by Monte Carlo sampling. In Chapter 6, we will compare the outputs of simulations using LHS and Monte Carlo sampling algorithms by analyzing their selection of PODs and supply capacity allocation. This comparison will help evaluate whether LHS actually improves the realism of our simulations.

5.2 Simulation Construction

We have previously gathered all the simulation-relevant data, so we are now ready to set up our simulations in the ArcGIS environment. The first step is to create 10 scenarios using the Monte Carlo (MC) method and 10 using Latin Hypercube Sampling (LHS) for the selected buildings. Although the following steps are explained for one scenario, they are applied to all the scenarios generated.

We begin by creating 50-meter wide buffers around each selected building point using the "Create Buffer" tool in ArcGIS, and then dissolve these buffers to form continuous areas, as shown in Figure 5.3. Next, we calculate the demand at each demand point using two key parameters: local destruction and population. To assess local destruction, we create 150-meter buffers around each demand point. Using the "Spatial Join" tool, we count how many collapsed buildings fall within the 150-meter radius of each demand point, as shown in Figure 5.4. Demand for each demand point is then calculated using the following formula:

$$\text{Demand} = ([\text{Number of collapsed buildings within 150m}] \times 50) + \left(\frac{\text{Population}}{4} \right)$$

This formula takes into account both the extent of building collapse in the area and the population, providing an estimate of demand based on destruction and population density. The value of 50 is based on the assumption that an average building in Istanbul has 50 residents (5-6 stories with 8-10 people per floor), while dividing the population by 4 allows demand to be influenced by population density without overly emphasizing it, ensuring a balanced impact from both the scenario-based destruction and fixed population data. However, more detailed research and parameter analysis are needed to determine values that more accurately reflect reality. We define the demand in the LDC and PODs as 0 in our simulations.

We create a feature class containing all relevant points: LDC, PODs and demand points. Using the Network Analyst tool in ArcGIS, we generate Origin-Destination (OD) cost matrices. An OD cost matrix calculates the least-cost travel time or distance between multiple origins (e.g., LDCs or PODs) and destinations (e.g., demand points). For this analysis, we create two OD cost matrices: one for LDC-POD accessibility scores ($\nu_{0,j}^s$) and another for POD-all points accessibility scores ($\nu_{i,j}^s$).

Although we could choose walking mode for the POD-all points OD cost matrix, considering a real-world scenario where it is more likely that people needing relief aid would go to the distribution points on foot due to blocked roads and narrow streets, we use trucking mode for both cost matrices. This decision is made to maintain a consistent unit of measurement across all scenarios in our simulations; however, future research may explore this further and develop more realistic simulations. Using trucking mode reflects the movement of goods in a disaster relief scenario, which can be analogous to the movement of individuals accessing PODs.

To account for the effect of building collapse on accessibility, we use the buffers around collapsed buildings (Figure 5.3) as polygon barriers. These barriers are applied with scaled cost, where barrier type = 1 and the attribute “trucking duration” is set to 10. This means that if the routing passes through any of these polygon barriers, the travel time (or cost) will be multiplied by a factor of 10, representing the increased difficulty of reaching these areas due to the destruction.

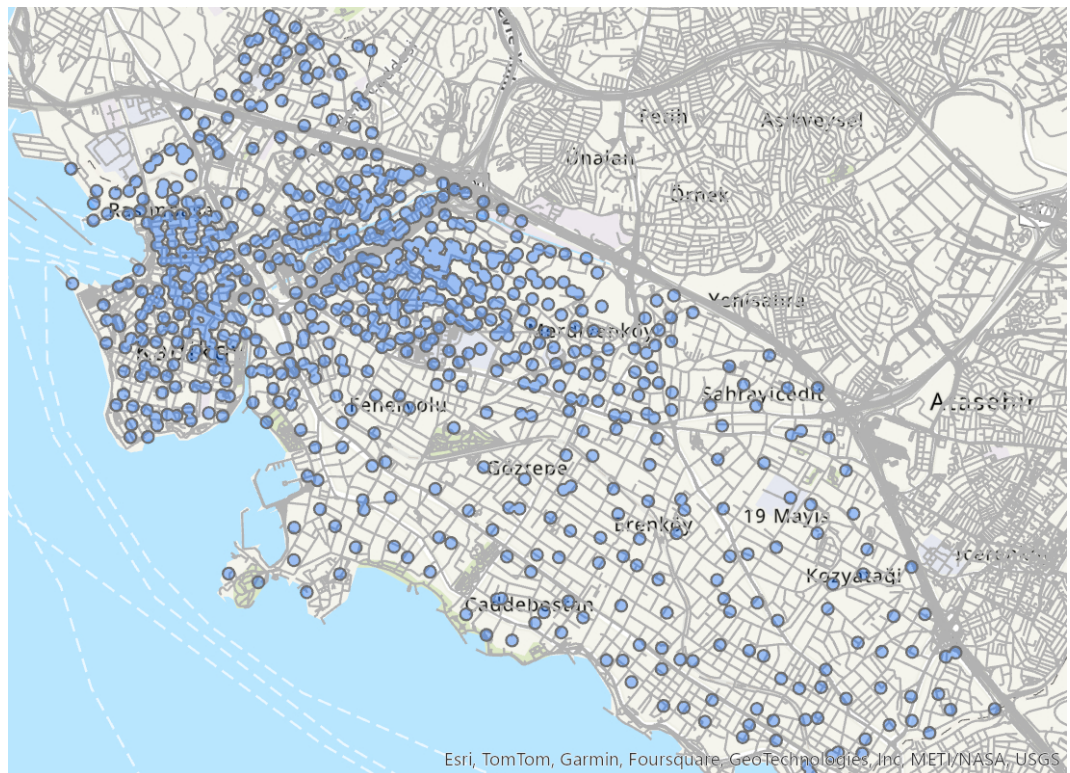


Figure 5.3: LHS Scenario 1: Buffer around destroyed buildings

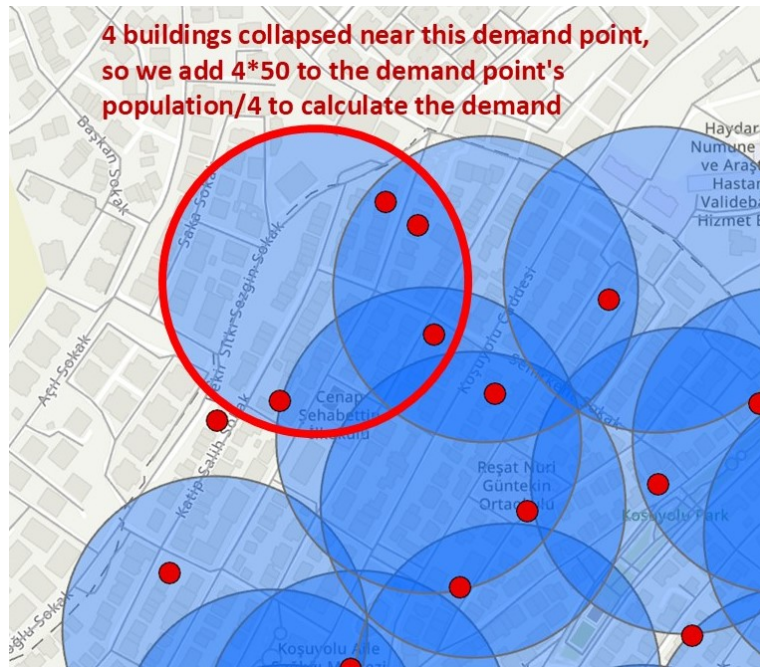


Figure 5.4: Example to show how demand is calculated for demand points

5.3 Simulation Model Overview

We implement the model presented in Chapter 3 in code and simulate it using the following input parameters and key elements.

5.3.1 Accessibility Scores

Accessibility scores $\nu_{0,j}^s$ and $\nu_{i,j}^s$ are normalized values derived from trucking durations between locations taken from the entries of OD cost matrices. Normalization ensures the scores range between 0 and 1, with shorter trucking durations corresponding to higher accessibility scores. The given example function calculates the normalized value for each trucking duration:

$$\text{Normalized Value} = \frac{\max - \text{value}}{\max - \min}$$

5.3.2 Maximum PODs Opened

There are 173 candidate PODs in our set (including the LDC to ensure matching IDs/indices between the OD cost matrix outputs), but only a maximum of 100 can be opened ($C = 100$). This limitation reflects the scale of the disaster, where a significant proportion of candidate PODs must remain operational to meet the needs of a densely populated district such as Kadıköy, with over 400,000 people. Opening fewer PODs would likely result in insufficient resource distribution.

5.3.3 POD Capacity Calculation

POD capacities are calculated using the formula:

$$\text{Capacity} = \frac{\text{POD Area} \times \text{Maximum Demand} \times 1.5}{\text{Total Sum of POD Area}}$$

The scalar "1.5" adjusts for the underestimation of demand when fewer PODs are opened than are available in the candidate set. Without this scalar, the available capacity often falls short, particularly when $C = 100$. We also conduct a series of simulations, varying the parameter C from 170 to 10, to observe the influence of the maximum number of PODs that can be selected on the simulation results. For simulations where $C \leq 80$, we increase the scalar to 4, as only 1-2 feasible solutions are generated out of 35 simulations with different scenario combinations. This requires increasing C and observing these subsets separately, as discussed in more detail in Section 6.

5.3.4 Scenario Handling and Probabilities

Since our scenario generation is based on LHS and Monte Carlo sampling, it is logical to assign equal probabilities (p_s) to all scenarios, representing uniform likelihood in stochastic modeling. Since the model supports the inclusion of multiple scenarios in a single optimization run, it is necessary to decide how many scenarios to combine in each simulation. Ideally, a stability analysis should be conducted to make a fully informed decision. However, stability testing is beyond the scope of this research. Instead, we adopt a similar approach by using 8 distinct Monte Carlo (MC) generated scenarios. We set the time limit for these simulations to 1200 seconds and evaluate combinations of scenarios ranging from 1 to 8 to assess their computational efficiency and solution quality. The results are as follows:

- **1 Scenario:** 4 optimal solutions; 3 solutions with an optimality gap of less than 0.1%.
- **2 Scenarios:** 15 solutions with an optimality gap of less than 0.1%.
- **3 Scenarios:** 19 solutions with an optimality gap of less than 0.1%; 5 feasible solutions with large optimality gaps (greater than 30%).
- **4 Scenarios:** 9 solutions with an optimality gap of less than 0.1%; 2 feasible solutions with large optimality gaps.
- **5 Scenarios:** 2 solutions with an optimality gap of less than 0.1%; 6 feasible solutions with large optimality gaps.
- **6 Scenarios:** 1 solution with an optimality gap of less than 0.1%; 2 feasible solutions with large optimality gaps.
- **7 Scenarios:** 1 feasible solution with a large optimality gap.

- **8 Scenarios:** No feasible solutions are obtained within the time limit.

Based on these results, we conclude that using 3 combinations of scenarios strikes a good balance between computational efficiency and solution quality. It is computationally much more efficient than including 4 or more scenarios, while still generating many near-optimal solutions and capturing scenario fluctuations better than using only 1 or 2 scenarios. Consequently, for our simulations, we incorporate 3 scenario combinations per optimization run.

5.3.5 Total Available Supplies

The variable O_{\max}^s represents the total supply available in scenario s , which is calculated by summing the demand values across all nodes in that scenario. This is based on our assumption that the total supply equals the total demand for each scenario:

$$O_{\max}^s = \sum_{i \in I} d_i^s$$

5.3.6 Other Parameters

We run our simulations by selecting all three scenario combinations from the LHS and Monte Carlo scenario sets, each containing 10 scenarios. These three scenario combinations are then used as inputs for a specific simulation run. To explore the impact of different scenario combinations, we set the maximum model run time to 600 seconds for all simulations, unless otherwise stated. This time constraint is due to the limitations in computational resources available for this study. Consequently, some simulation runs may fail to find a feasible or optimal solution within the time limit. In future research, with improved computational resources, the time limit can be extended, allowing for more extensive exploration and potentially more accurate results across a wider range of scenario combinations.

We set $\epsilon = 0.2$ and $\rho = 0.4$. The value $\epsilon = 0.2$ strikes a balance between accessibility and equity, avoiding imbalanced resource distribution. Smaller ρ values restrict the shortage, potentially causing infeasibility when demand exceeds POD capacity. In contrast larger ρ values increase flexibility but may lead to inefficiency by allowing large shortages and underutilization of PODs. Although our experiments on this parameter are not exhaustive, simulations varying ρ indicate that values of $\rho < 0.3$ result in significantly fewer feasible solutions for our simulations within the 600-second model runtime, while larger values cause inefficiencies. Therefore, we choose $\rho = 0.4$ to strike a balance, preventing infeasibility while maintaining effective resource allocation.

5.4 Optimization

For our optimization tasks, we utilize the Gurobi solver in Python due to its superior computational efficiency compared to alternatives like CPLEX. All calculations are performed in this environment to leverage Gurobi's robust performance and advanced capabilities.

The specific configuration of the optimization setup is as follows:

- **Gurobi Version:** 11.0.3 (build v11.0.3rc0)
- **Operating System:** Windows 10 (version 19045.2)
- **Processor:** AMD Ryzen 7 4700U with Radeon Graphics
- **Instruction Set:** [SSE2|AVX|AVX2]
- **Threads Utilized:** 8 physical cores, 8 logical processors, up to 8 threads

6 Simulation Results and Managerial Insights

In this chapter, we analyze the results from various simulations to derive meaningful managerial insights about the real-world applicability of the model. This includes evaluating the impact of different sampling techniques and variations in model parameters on simulation outcomes. By examining these factors, we aim to understand how the model performs under diverse conditions and its potential robustness in addressing complex disaster scenarios.

We also explore the implications of these findings for post-earthquake response planning in Kadıköy/Istanbul. This includes identifying patterns in POD selection and supply aid allocation decisions that appear to be the most optimal for ensuring effective and equitable disaster relief. These insights provide actionable recommendations for decision-makers to enhance preparedness and response strategies for future major earthquakes in urban environments.

An important observation from our simulations is that all β_j^s values are consistently 0. This occurs because we define the total aid supply o^s in each scenario to be equal to the total demand, $\sum_{i \in I} d_i^s$. As a result, the scalar becomes 1, leading to $PD_j^s = 1 \cdot TD_j^s$. Consequently, the only β_j^s values that satisfy constraint (9):

$$PD_j^s + \beta_j^s \leq TD_j^s \quad \forall j \in J, \forall s \in S,$$

are 0. Thus, the proportional demand is always consistent with the total demand in our model.

Another important consideration is that our model does not incorporate the threshold parameter τ , which is utilized in the SLMRND model in Noyan et al. (2016). Despite our attempts to include τ values ranging from 0 to 1 in increments of 0.1, the model consistently results in infeasibility across all scenarios. This highlights the need for further research to analyze the model's sensitivity to τ , the calculation of accessibility scores (ν_{ij}^s), and potentially other related parameters. The absence of τ prevents the definition of the coverage sets M_j^s and N_i^s , thereby making our model more flexible with respect to accessibility constraints. Nevertheless, our simulation results demonstrate that, even without an additional constraint enforcing a *minimum accessibility threshold*, the inclusion of accessibility values in the objective function is sufficient to generate solutions that account for accessibility. Consequently, our model effectively captures real-world fluctuations in the accessibility metric.

6.1 Monte Carlo Sampled Building Selection Simulation Results

In this section, we present the simulation results where collapsing buildings for scenario generation were selected using Monte Carlo sampling. As explained in Section 5, this approach utilizes random sampling at the neighborhood level to reflect the distribution of potential building collapses in a post-earthquake scenario. A total of 120 simulations were conducted, combining 10 different Monte Carlo-selected building scenarios in 3 combinations. Among these, 26 scenarios were feasible, 23 had solution gaps below 0.6%, and 3 had solution gaps ranging between 34–36%.

For more comprehensive research, increasing runtime or employing methods like Benders decomposition could enhance efficiency and reduce optimality gaps, resulting in better-optimized solutions. Nonetheless, the results provide sufficient insights, particularly in real-world contexts, to draw meaningful conclusions.

6.1.1 Results of POD Selection

As defined in the model, the y_j -values in this study are binary variables indicating whether a POD is selected (1) or not (0) in a given simulation scenario. These simulations are conducted using three scenario combinations of ten individual scenarios, providing a comprehensive view of potential conditions. By averaging the y_j -values across all feasible simulation runs, we calculate the mean y_j -value for each POD, which highlights the consistency of a POD's selection across scenarios and identifies key facilities in the network, offering valuable insights into selection trends. The selection process involves summing the y_j -values for each POD across all simulations and dividing by the number of feasible solutions (i.e., those simulation runs that resulted in a valid y -solution) to calculate the average selection probability. From these mean y_j -values, we then select the 100 PODs with the highest values, which aligns with the maximum number of PODs allowed in the individual simulations.

Additionally we identify the closest and furthest solutions from the previously defined aggregated solution. For this we first calculate the "distance" between each individual simulation solution and the aggregated mean y -solution. The distance is measured using the Euclidean distance formula, which compares the selection decisions (i.e., the y_j -values) for each POD in the solutions. Specifically, the distance is computed by summing the squared differences in y_j -values for each POD between the current solution and the aggregated solution, then taking the square root of this sum. This method quantifies to what extent each solution is similar or dissimilar to the aggregated mean solution. Once the distances for all simulation solutions are calculated, we identify the closest and furthest solutions by finding the smallest and largest distances, respectively.

These closest, furthest, and aggregated solutions are then mapped along with the aggregated mean y -solution on an ArcGIS map for spatial visualization. In Figure 6.1, the purple points represent PODs that are selected both in the aggregated y -solution and in the solution closest to the aggregated mean. The blue points denote the PODs selected in the aggregated solution but not in the closest solution, while the red points show the PODs selected in the closest solution but not in the aggregated one. As illustrated, only 3 POD selection decisions differ between the aggregated solution and the closest solution.

In a separate analysis, as shown in Figure 6.2, the green points represent the PODs selected in both the aggregated mean y -solution and the furthest solution from the mean. The blue points denote PODs selected only in the aggregated solution, while the yellow points represent those selected only in the furthest solution. In this case, 27 PODs are selected differently between the aggregated solution and the furthest simulation result, highlighting significant variability between the solutions.

This analysis defines the spectrum of variability in the selection of PODs across different simulation scenarios. The substantial difference of 27 PODs out of 100 selected between the aggregated and furthest solutions demonstrates how diverse the outcomes of different scenarios can be. Such variability underscores the importance of conducting extensive simulation studies and analyzing a range of possible outcomes. This approach is critical for optimizing last-mile relief logistics and enhancing disaster response preparedness, as it ensures that the decision-making process accounts for a wide variety of potential conditions and scenarios.

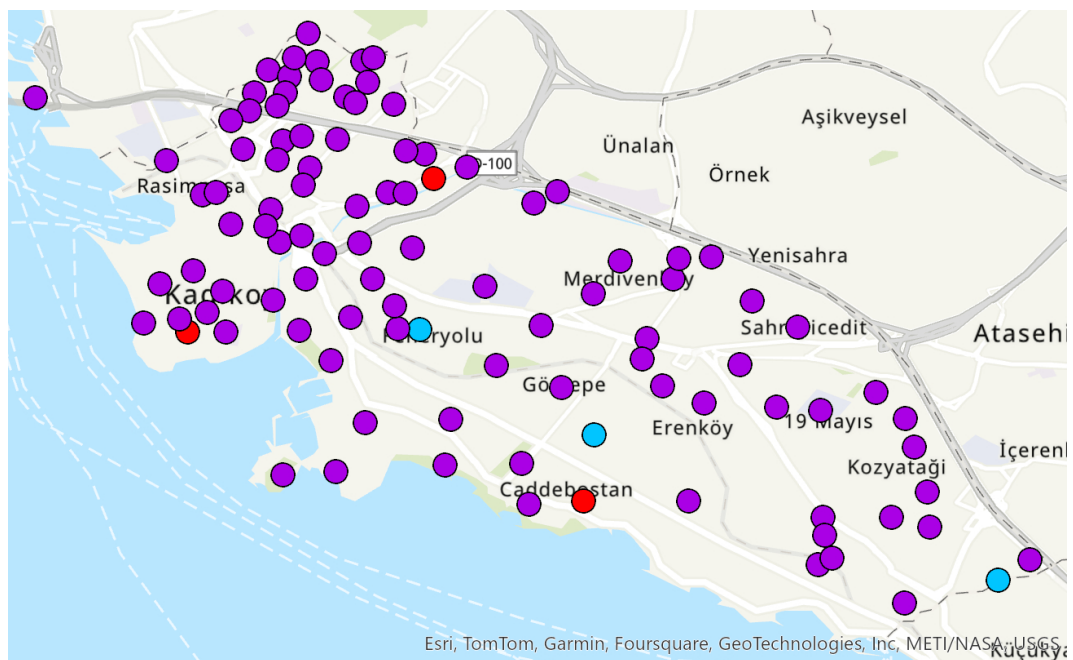


Figure 6.1: Comparison of Monte Carlo simulations: Mean y -solution and the closest y -solution to the aggregated result

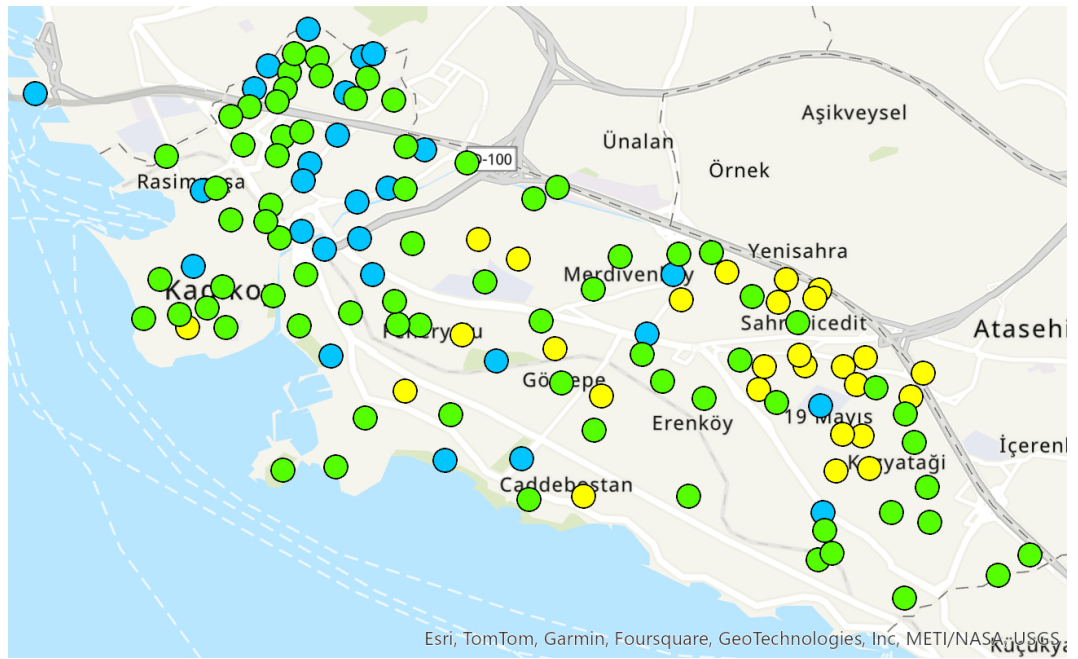


Figure 6.2: Comparison of Monte Carlo simulations: Mean y-solution and the furthest y-solution to the aggregated result

Now we analyze two key attributes of the PODs: POD area and POD location relative to the district centroid. The POD area directly influences its capacity, while the location helps us assess whether a POD is positioned near the center of Kadıköy or on its outskirts. To calculate the centroid of the district and the Euclidean distance from each POD to the centroid, we use this formula:

$$\text{Euclidean Distance} = \sqrt{(X - \text{mean}_x)^2 + (Y - \text{mean}_y)^2}$$

where X and Y are the geographic coordinates (longitude and latitude) of each POD, and mean_x and mean_y are the mean coordinates of all PODs. In this analysis, we ensure that coordinates are appropriately converted from degrees with decimal points to numerical values.

In the first graph (Figure 6.3), we observe a positive relationship between POD area and selection probability (mean y_j -value). This trend reflects the real world conditions, as larger areas typically provide more space for distribution, which increases their capacity to accommodate supplies and serve a larger population. For instance, large stadiums, hospitals, or parks, with their expansive open spaces, are more suitable for hosting distribution centers due to their ability to store and manage large volumes of goods. Thus, as the area of a POD increases, its suitability for disaster response and relief operations grows, making it more likely to be selected in the simulation.

In the figure 6.4, we do not observe a clear association between the location of a POD relative to the district POD centroid and its likelihood of being selected in the

simulation. Notably, some PODs that are close to the centroid are rarely selected throughout the simulation runs, while others located on the outskirts of Kadıköy are consistently selected in nearly all simulations. This result is intuitive, as the model does not prioritize accessibility based on the general proximity of a POD to the district center; instead, it prioritizes the accessibility of local demand points to the PODs that can best serve them.

For example, consider a POD located near the center of Kadıköy but surrounded by larger PODs with higher capacity or more suitable infrastructure (such as stadiums, hospitals, or parks). In a real-world scenario, demand points close to the central POD may be better served by these larger PODs, as they are capable of accommodating more people and supplies. As a result, the central POD would not be selected because there is no need for its services when a nearby, larger POD can cover the same demand points more efficiently. The model, therefore, may bypass the central POD in favor of the larger, more capable PODs, even though the central POD is geographically closer to the centroid of the district.

In an urban environment, such as Istanbul, where there are numerous potential distribution points for service, the capacity of a POD seems to be a more influential factor for its selection. As long as a POD is not too remote from demand points—since urban areas are densely populated and virtually every location becomes a potential demand point in a post-disaster scenario—the model may prioritize larger PODs with greater capacity. This suggests that in densely populated cities, models that focus on optimizing supply allocation across multiple points may be more effective. While this isn't universally true, the high population density and widespread demand in urban settings often make capacity a more critical factor than location when determining the selection of PODs.

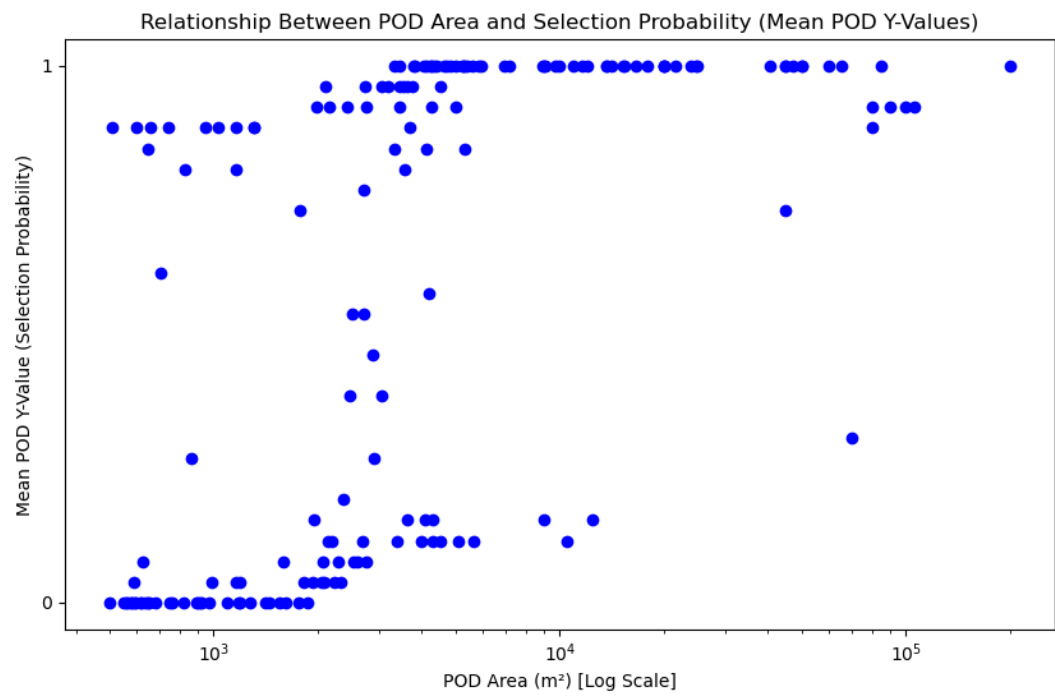


Figure 6.3: Relationship between POD area and selection probability (mean POD y-value)

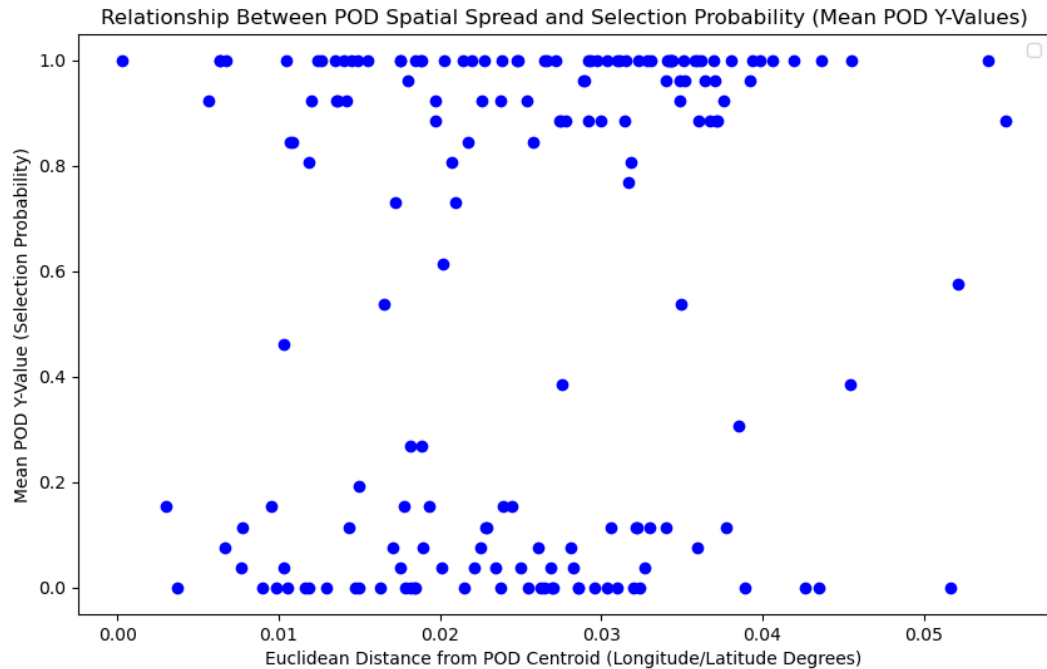


Figure 6.4: Relationship between POD location relative to the POD centroid and selection probability (mean POD y-value)

6.1.2 Supply Allocation Results for PODs

Another important decision variable in the model is R_j , which represents the supply capacity allocated to POD j . In Figure 6.5, we observe the mean supply allocation for the PODs across all Monte Carlo simulation results. As expected, PODs covering larger areas tend to receive higher mean supply allocations. Similar to the results for y_j , PODs with larger capacities are more frequently selected across simulations and consequently allocated substantial amounts of supplies. There is a clear relationship between POD size (measured by physical area) and the mean supply allocation to the POD across different scenarios, as shown in Figure 6.6. For instance, in Kadıköy, locations such as Göztepe Araştırma Hastanesi (hospital), Şükrü Saraçoğlu Stadyumu (stadium), and Erenköy Ruh ve Sinir Hastalıkları Hastanesi (hospital) are notable examples where large supply allocations correspond to public spaces with significant capacity.

However, there are some exceptions, as highlighted inside the red square in Figure 6.5, with Özgürlik Parkı serving as a notable real-world example. Despite being one of the candidate PODs with the largest available space, it is allocated fewer supplies on average compared to some smaller-capacity PODs. This discrepancy arises because Özgürlik Parkı is situated between two of the highest-capacity PODs, Göztepe Araştırma Hastanesi and Göztepe Parkı, which sufficiently fulfill the nearby demand. As a result, less supply allocation is necessary for Özgürlik Parkı.

This analysis highlights that while capacity is a primary determinant for POD selection in densely populated urban areas like Kadıköy, spatial distribution remains important. If a POD is surrounded by several other PODs—particularly those with substantial capacities—it is less likely to receive full supply allocation. In conclusion, while POD capacity serves as a strong indicator of the potential supply allocation, a detailed spatial analysis that considers the proximity of neighboring PODs and demand distribution is essential for optimal decision-making.

Another important metric is the standard deviation of POD supply allocations (R_j) across different Monte Carlo simulations relative to the mean supply allocation for all scenarios. Since PODs with larger areas or capacities naturally tend to have higher variations in their absolute supply allocations, we normalize these deviations by dividing the standard deviation of R_j by the respective POD area. This provides a relative deviation measure, allowing for a fair comparison across PODs of varying sizes. In Figure 6.7, this normalized deviation is plotted for each POD, providing insights into the consistency of supply allocations relative to the area of the POD.

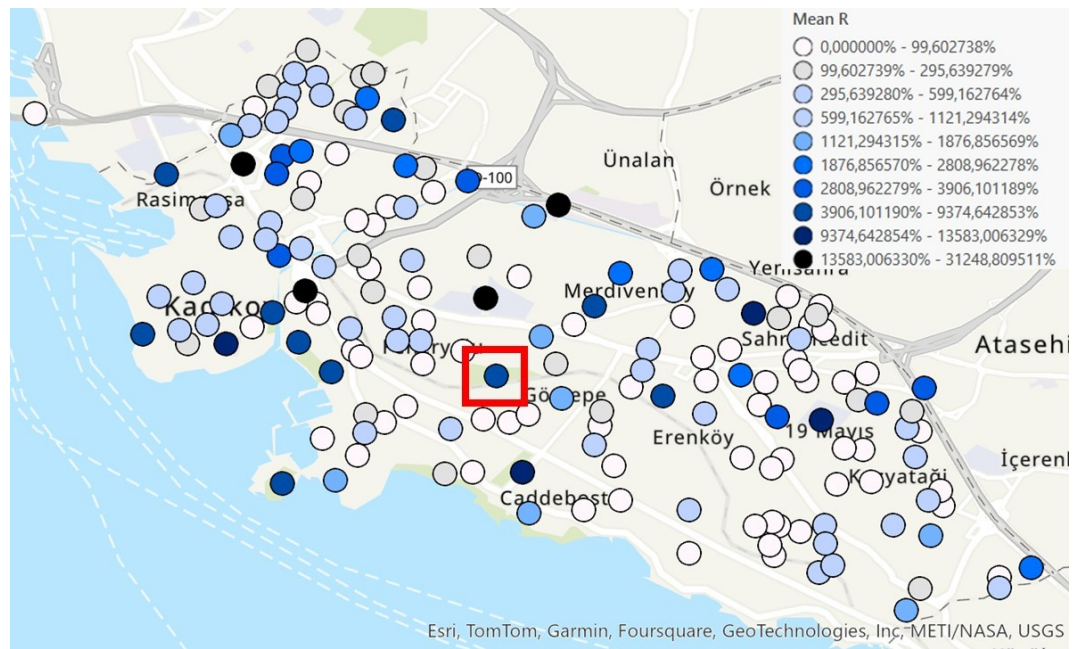


Figure 6.5: Monte Carlo Simulations: Mean supply allocation to PODs in Kadıköy

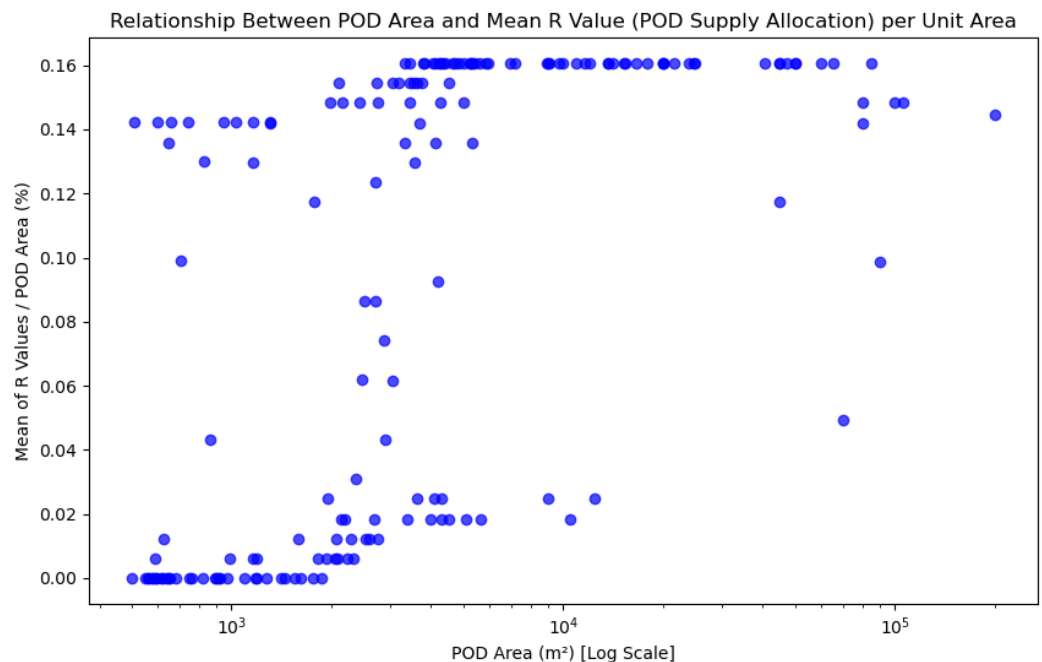


Figure 6.6: Relationship between POD area/capacity and mean supply allocation relative to the POD area

From the figure, it can be seen that there is no apparent straightforward correlation between POD area and the relative R_j deviation. Both the smallest and largest capacity PODs exhibit significant relative deviations, while many medium-to-large capacity PODs display minimal deviations relative to their areas. This observation suggests that while larger PODs are generally expected to experience higher absolute deviations, their relative consistency can vary significantly depending on their

role and spatial distribution within the network.

A closer analysis in Figure 6.8 highlights specific examples that underscore this phenomenon. For instance, PODs like Şükrü Saracoğlu Stadyumu and Göztepe Parkı show much higher deviations in supply allocation across scenarios compared to Göztepe Hastanesi, despite the latter having a significantly larger capacity than the combined capacities of the former two. This inconsistency in supply allocation for PODs with large capacities suggests that factors other than sheer capacity—such as location relative to demand hotspots or redundancy with neighboring PODs—play critical roles in supply distribution.

These findings carry important real-world implications for pre-earthquake planning and disaster response. By identifying PODs with consistently low deviations in supply allocation across different scenarios, such as Göztepe Hastanesi, we can prioritize these locations for pre-disaster supply stockpiling and logistical preparation. This would enable efficient and scenario-insensitive aid delivery, ensuring that certain high-priority PODs are preemptively equipped to handle demand without requiring significant real-time adjustments during disaster scenarios. Conversely, PODs with high supply allocation variability, like Göztepe Parkı, may require more flexible and adaptive supply strategies tailored to specific situational needs.

The results shown in Figure 6.9 suggest that there is no direct relationship between the proximity of a POD to the center of Kadıköy and its aid supply variability across scenarios. This indicates that, in a real-world context, factors other than mere geographic centrality play a significant role in determining the variability of supply allocations.

One might assume that proximity of the POD to the center would lead to more consistent supply allocations due to easier access to concentrated demand. However, our findings indicate that supply variability is primarily shaped by a combination of factors: surrounding demand density, the presence of nearby high-capacity PODs, and the overall layout of the relief network. For example, central PODs might show greater variability if they are surrounded by other large-capacity PODs competing for overlapping demand. On the other hand, PODs located on the periphery often exhibit more stable allocations when serving isolated demand areas with little competition. This underscores the need to account for the broader spatial dynamics of the network in planning, rather than focusing solely on centrality as a criterion.

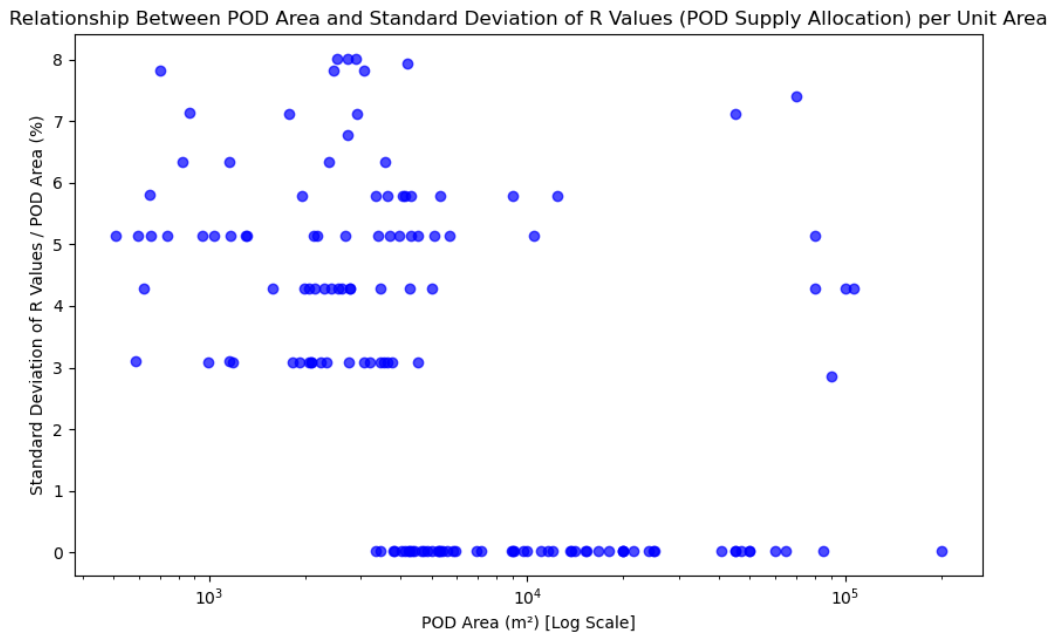


Figure 6.7: Relationship between POD area/capacity and deviation of supply allocation relative to the POD area

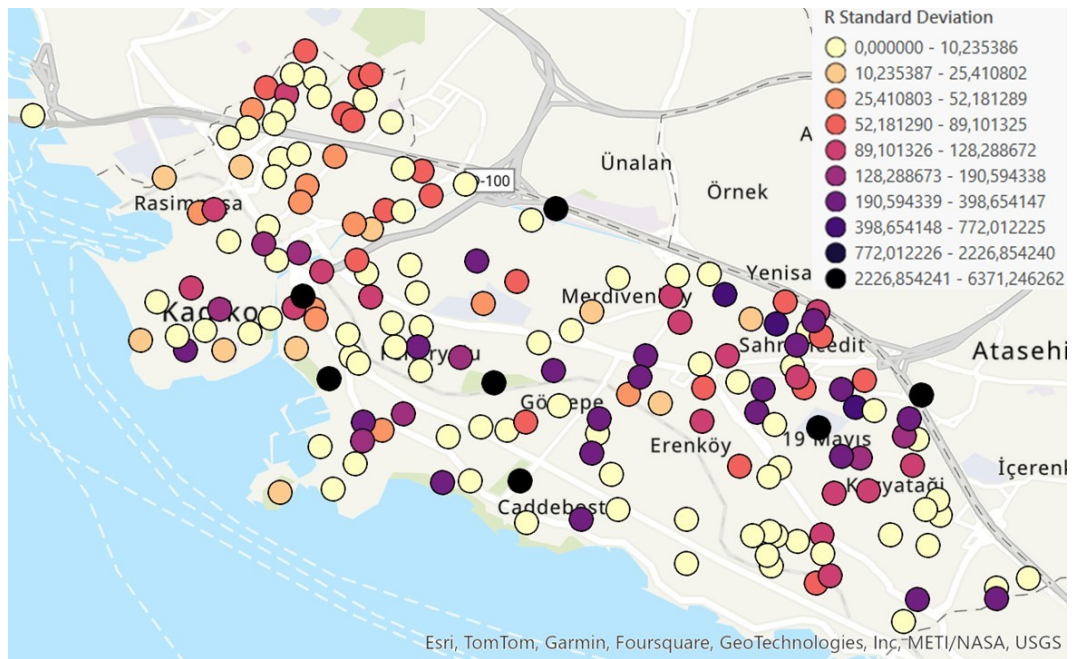


Figure 6.8: Monte Carlo Simulations: Deviation of supply allocations to PODs in Kadıköy

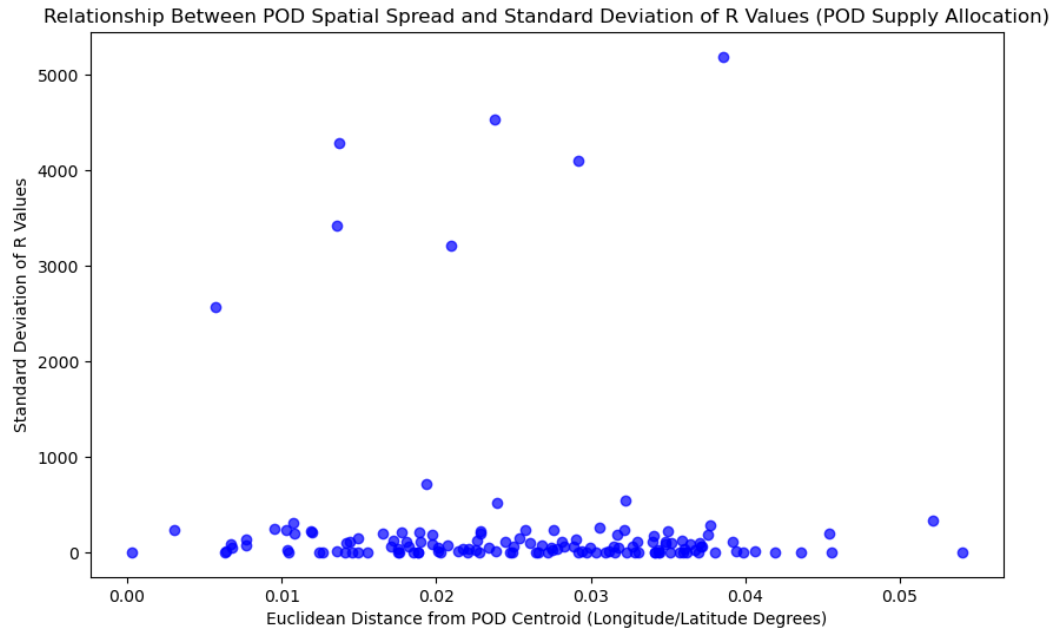


Figure 6.9: Relationship between POD location relative to the POD centroid and deviation of supply allocation

6.1.3 Demand Point Allocation Results for PODs

When planning last-mile relief networks, it is essential not only to select Points of Distribution (PODs) and allocate supplies but also to assign demand points (representing clusters of blocks or households) to their designated PODs. This assignment is captured by the decision variable $x_{i,j}^s$ in the model. This allocation ensures that affected individuals know in advance which nearby distribution points they should approach for relief aid in the aftermath of a disaster. Such planning is essential to avoid chaos and uncoordinated movements during the critical response period.

In the map provided (Figure 6.10), the allocation of demand points to PODs is represented through color coding. Each color group indicates the demand points that are assigned to the same POD, meaning people in those areas should go to the same distribution point for aid. It is worth noting that due to the limitation of using 100 distinctive colors, some colors are repeated in geographically distinct areas. These repetitions do not imply overlap in POD allocations but rather represent entirely separate POD assignments. In Figure 6.11, the clusters of demand points are shown in greater detail, with the PODs marked by white stars. It is evident that PODs with larger areas and capacities, such as Erenköy Hastanesi (highlighted in green), accommodate significantly more demand. This is due to their ability to supply a larger population compared to PODs with smaller capacities, such as the one assigned to cyan demand cluster. This allocation reflects the model's capacity-based approach, where demand is distributed proportionally to the supply capabilities of each POD.

The map illustrates the model's effectiveness in optimizing accessibility metrics for disaster relief operations. By prioritizing accessibility and geographic distribution, the relief network ensures that resources are allocated efficiently and equitably. Demand points are predominantly assigned to nearby PODs, reflecting the real-world necessity of minimizing travel time and enabling swift access to aid. This is visually represented by the clustering of same-colored points in geographically proximate areas. These clusters reflect a careful balance between relative location and the capacity of each POD to serve the assigned population.

From a real-world perspective, this allocation strategy ensures that no single POD is overwhelmed by excessive demand while others remain underutilized. In disaster scenarios, this approach is critical for preventing bottlenecks and ensuring that aid reaches all affected populations quickly. Additionally, by pre-defining these allocations and communicating them effectively to the public, authorities can further reduce confusion and panic in post-disaster situations.

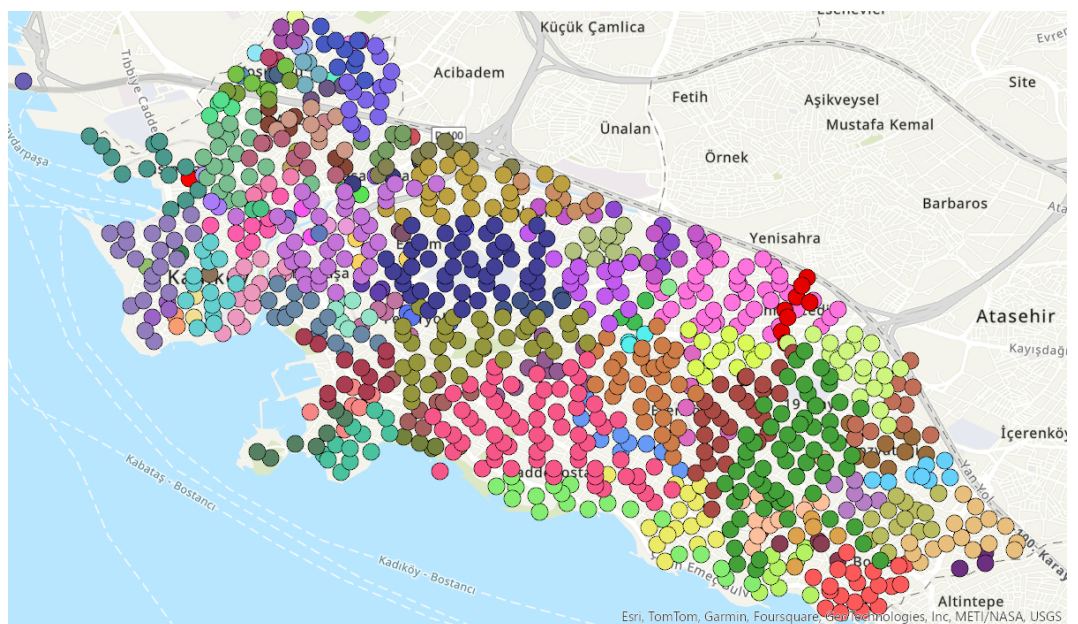


Figure 6.10: Monte Carlo Simulations: Demand point assignment to PODs

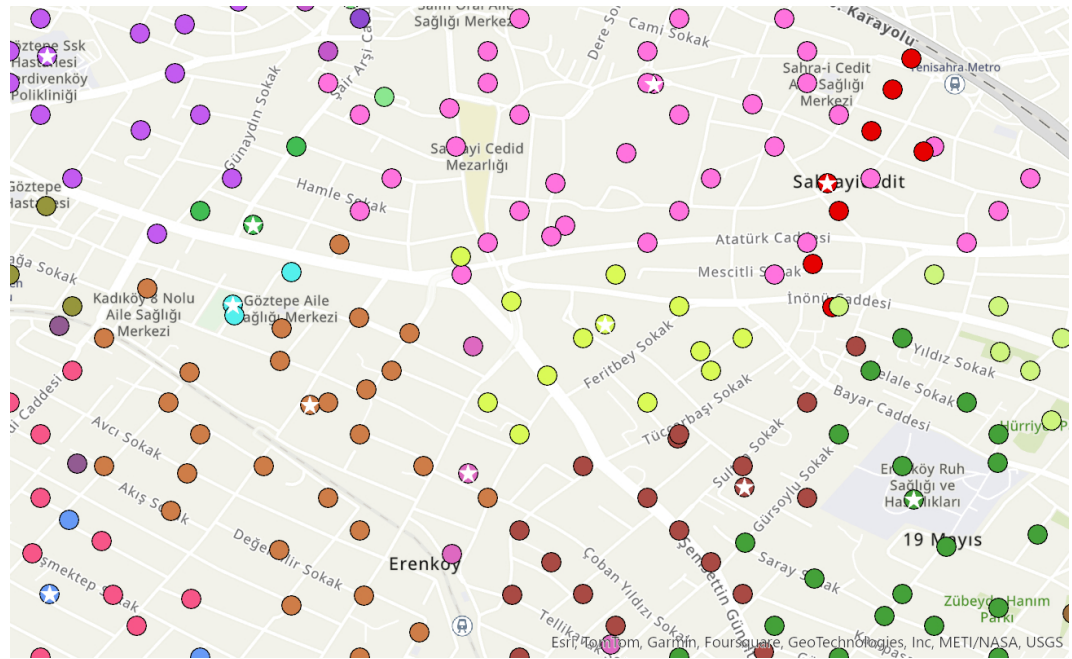


Figure 6.11: Monte Carlo Simulations: Demand point assignment to PODs - detailed map

6.2 Latin Hypercube Sampled Building Selection Simulation Results

In this section, we present the simulation results where collapsing buildings for scenario generation were selected using Latin Hypercube Sampling (LHS). As discussed in Section 5, this sampling approach offers reduced bias compared to Monte Carlo (MC) sampling, as it ensures a more uniform spatial distribution of selected buildings across the study area. Consequently, differences in various aspects of the results are expected when comparing LHS to MC scenarios due to the improved spatial spread of selected buildings.

A total of 120 simulations are conducted using LHS, encompassing 10 different LHS-selected building scenarios combined into 3 distinct combinations. Among these, 61 scenarios are deemed feasible, with 50 having solution gaps below 0.2% and 11 exhibiting solution gaps in the range of 25–40%. These results demonstrate that the number of feasible scenarios generated with LHS is more than double that of MC-based scenarios. This suggests that LHS scenarios exhibit a better balance in the distribution of demand and damage, enabling the optimization model to find feasible solutions more effectively.

The increased feasibility of LHS scenarios can be attributed to its ability to avoid overrepresentation of damage in certain areas, which is a common issue in MC sampling. In MC-generated scenarios, clustering of selected buildings may create imbalances in demand distribution and lead to exaggerated damage in specific

regions of the transportation network. These imbalances can make it more challenging for the model to allocate resources efficiently. In contrast, the spatially uniform distribution of damage in LHS scenarios ensures that each local area is impacted more evenly, reducing extreme disparities and making the optimization process more manageable.

However, it is important to note that these findings do not allow us to conclude which sampling method better reflects real-world conditions or is inherently more computationally efficient. The observed efficiency of LHS in this study is highly context-dependent, shaped by the specific manner in which simulations were constructed.

6.2.1 Results of POD Selection

In Figure 6.12, we compare the aggregated mean y solution with the scenario that has the closest y solution, following the same methodology used for the Monte Carlo (MC) y solutions in section 6.1.1. The purple points represent PODs that are selected both in the aggregated y -solution and in the solution closest to the aggregated mean. The blue points represent PODs that are selected in the aggregated solution but not in the closest solution, whereas red points denote PODs that are selected in the closest solution but not in the aggregated solution, highlighting PODs that are crucial to the closest solution but absent from the mean solution. From the map, we observe that the closest solution and the mean y solution differ by only 1 POD, which is a significant reduction compared to the 3 POD difference observed in the MC simulations. This suggests that some of the LHS scenarios capture the average more accurately, producing solutions that align more closely with the mean.

In Figure 6.13, we now compare the aggregated mean y solution with the scenario that has the furthest y solution. The green points represent PODs selected in both the aggregated mean y -solution and the furthest solution from the mean. The blue points represent PODs selected only in the aggregated solution, while the yellow points represent PODs selected only in the furthest solution, illustrating the extreme divergence between the two solutions. The map indicates that there are 27 PODs selected differently in the furthest LHS y solution, which is the same discrepancy observed in the furthest MC y solution. This suggests that LHS scenarios, despite their reduced bias compared to MC, are still capable of producing outlier solutions that diverge significantly from the aggregated mean. These outlier solutions, represented by the yellow points, can have a considerable impact on the overall results, just as extreme scenarios generated by MC can.

This variability reflects the inherent instability of the sampling process, where even with LHS's improved representation of the average, extreme or outlier scenarios may still arise. Such outliers can distort the optimization results, similar to the impact of extreme MC simulations, and may significantly affect decision-making,

especially in contexts like disaster relief logistics or network optimization. Therefore, while LHS offers improvements over MC in terms of bias reduction and better coverage of the parameter space, it still exhibits some instability that needs to be accounted for in the analysis.

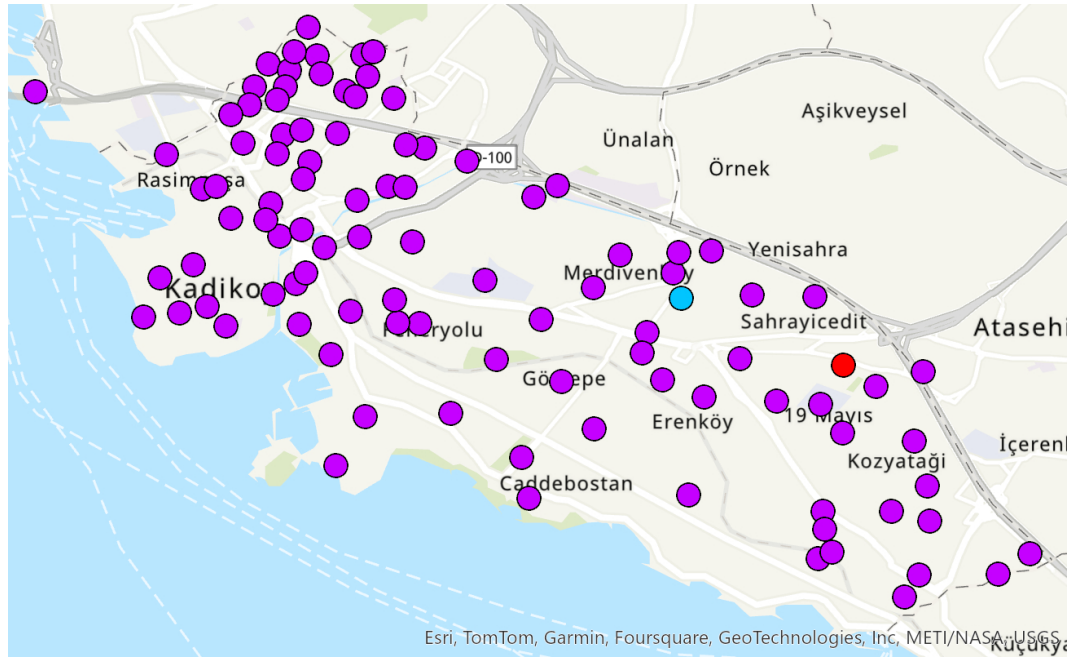


Figure 6.12: Comparison of LHS simulations: Mean y-solution and the closest y-solution to the aggregated result

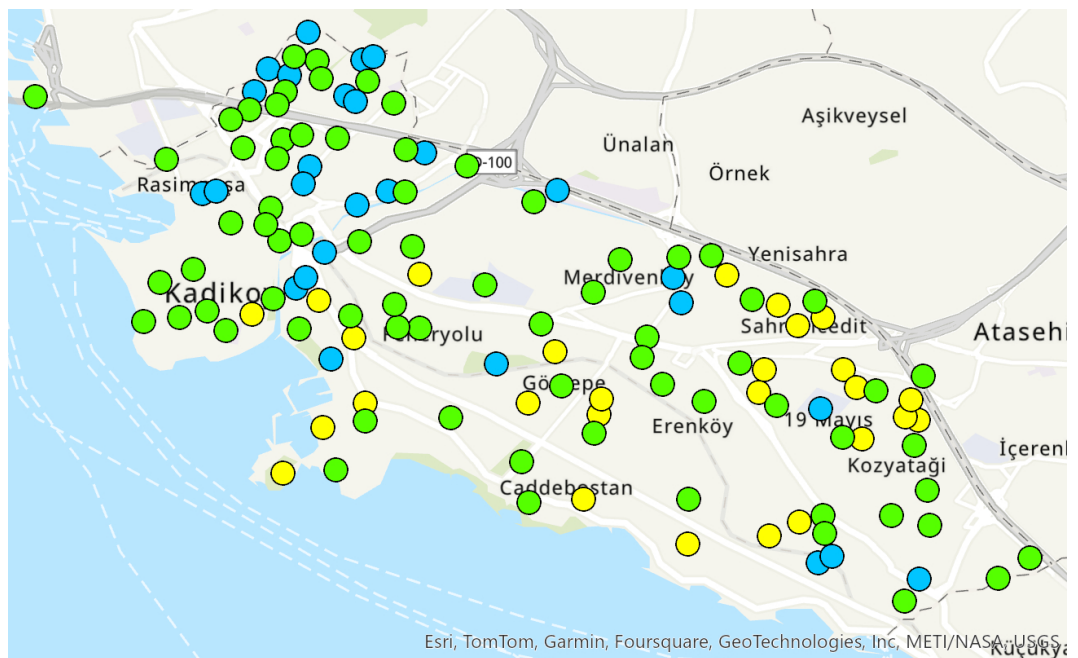


Figure 6.13: Comparison of LHS simulations: Mean y-solution and the furthest y-solution to the aggregated result

In Figure 6.14, we compare the PODs selected in the aggregated mean y solutions from the LHS and MC sampled simulations. The red dots represent the PODs that are selected only in the LHS simulations' mean y solution, whereas the blue dots denote the PODs that are selected only in the MC simulations' aggregated mean y solution. In total, there is a difference of 6 PODs out of 100, indicating that although there is a difference between the outputs of these two sampling methods for scenario generation, it is not a drastic one.

However, we observe that the PODs selected only in the LHS mean solution are more concentrated in inland areas, particularly near the neighborhoods Sahrayicedit, Kozyatağı and Bostancı. On the other hand, some of the PODs selected only by the MC mean solution are located along the coastline and in neighborhoods to the west of Kadıköy. An interesting observation is that the PODs selected by LHS tend to be located in areas with fewer large-capacity PODs. This could suggest that LHS outcomes are more aligned with real-world contexts, as the PODs with the largest capacities are already selected by both methods. By selecting additional locations in areas with fewer large PODs, the LHS simulations effectively address the unmet demand in these regions.

In a real-world context, the PODs selected exclusively through LHS might appear more appropriate, given that seaside areas are at higher risk of tsunamis or are generally unsafe in a post-earthquake scenario. However, the model does not account for such geographic risks. As a result, drawing universal conclusions about the suitability of LHS versus MC methods for real-world POD selection requires further analysis of these environmental and contextual factors.

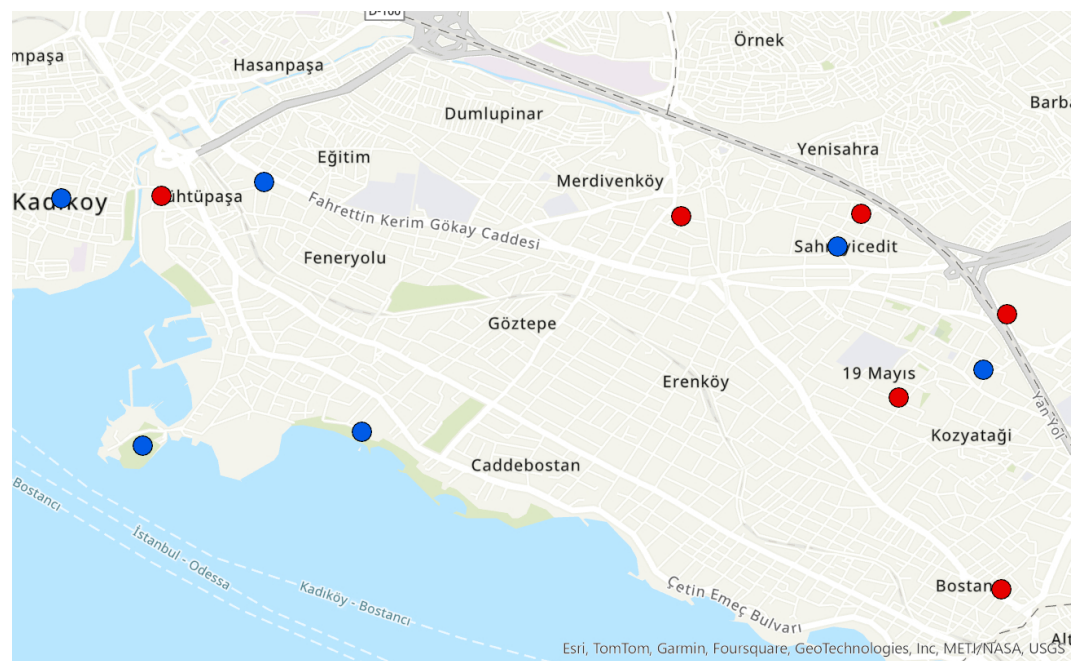


Figure 6.14: Comparison of mean y solutions of LHS and Monte Carlo simulations

As shown in Figure 6.15, the LHS simulations also exhibit an apparent correlation

between the POD area/capacity and its selection probability, similar to the MC simulations. Additionally, like the MC simulations, the LHS simulations reveal no clear association between the proximity of the POD to the district center and its selection probability (see Figure 6.16). The same explanations from the MC simulations in section 6.1.1 apply here as well.

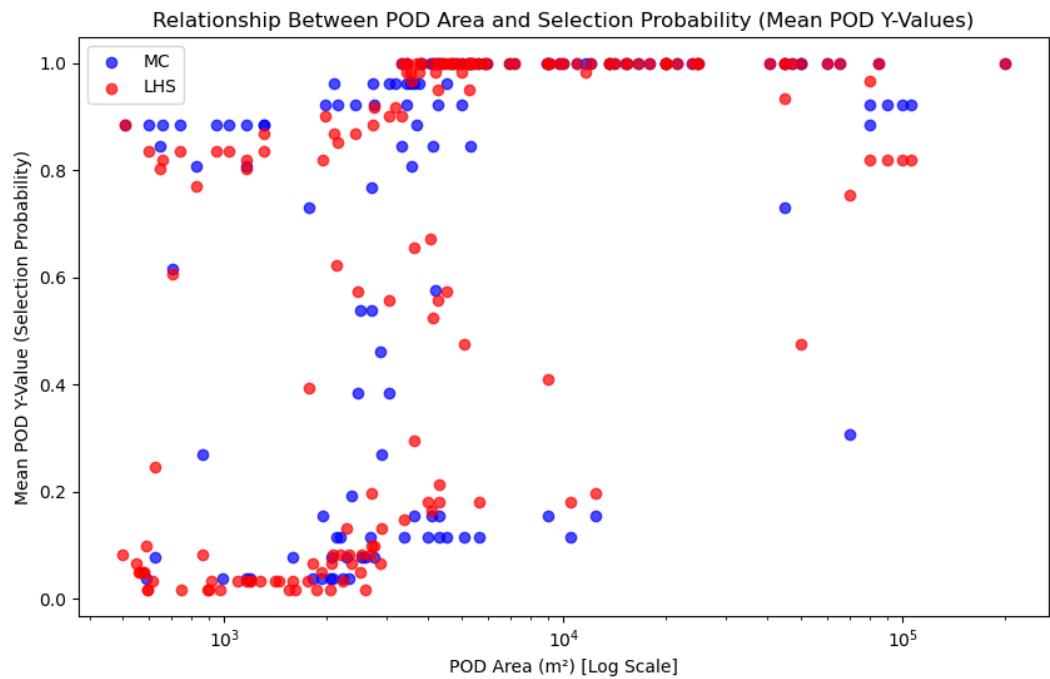


Figure 6.15: Relationship between POD area and selection probability (mean POD y-value)

6.2.2 Supply Allocation Results for PODs

As shown in Figure 6.17, the mean supply allocations to the PODs exhibit a distribution in the LHS simulations that mirrors that of the Monte Carlo simulations. Notably, PODs with substantial capacities, such as Göztepe Hastanesi and Şükrü Saracoğlu Stadyumu, once again emerge as critical supply distribution points to disaster-affected populations in the simulations.

Similar to the MC simulations, the LHS simulations reveal a potential relationship between the area-normalized POD capacity (calculated as the physical area of the POD in our simulations) and the mean supply allocation to the POD across different scenarios, as shown in Figure 6.18. Additionally, the distribution of relative mean R_j^s values with respect to area in the LHS simulations is consistent with that observed in the MC simulations. This consistency supports the conclusion that the scenario generation method, whether Monte Carlo or LHS, does not significantly affect the mean supply allocations to the PODs under the parameters used in this study.

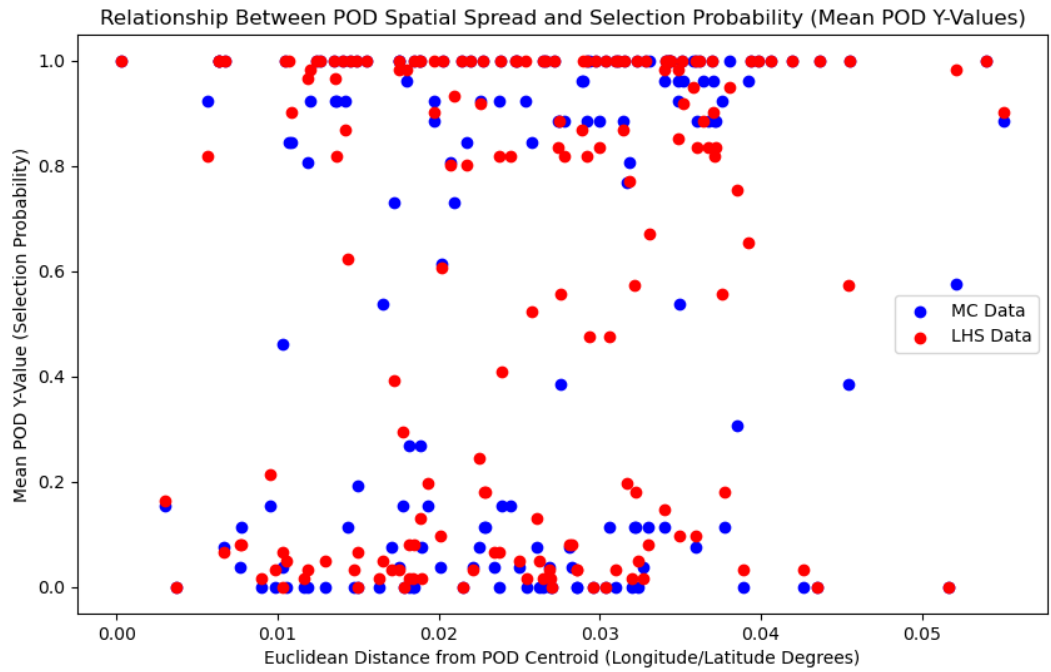


Figure 6.16: Relationship between POD location relative to the POD centroid and selection probability (mean POD y-value)

This finding highlights the robustness of the model and simulation design in accounting for fluctuations in external factors, such as demand variability and network disruptions, without being overly influenced by the scenario generation technique. From a practical perspective, this robustness ensures that the model delivers reliable and consistent outcomes across different methodological approaches, enhancing its utility for real-world disaster relief planning. The ability to maintain stable supply allocations across varying scenarios underscores the resilience of the framework, making it a critical tool for pre-disaster preparedness.

Figure 6.19 illustrates that the relationship between POD area (capacity) and the variation in supply allocation relative to the area (capacity) remains consistent across scenarios generated using both MC and Latin LHS methods. In both simulation series, PODs with very small or very large capacities exhibit greater relative variations in supply allocation. In contrast, PODs with medium-to-large capacities show minimal relative variation.

This pattern might be reasonably explained by the dynamics of supply distribution and capacity utilization. Smaller PODs may experience higher relative deviations due to their limited capacity, which amplifies the impact of fluctuations in demand and supply. Similarly, larger PODs often act as key distribution hubs, making them more sensitive to shifts in overall network demand and supply strategies, thereby resulting in larger relative deviations. On the other hand, PODs with medium-to-large capacities strike a balance between capacity utilization and supply stability, leading to lower relative variation in their allocations.

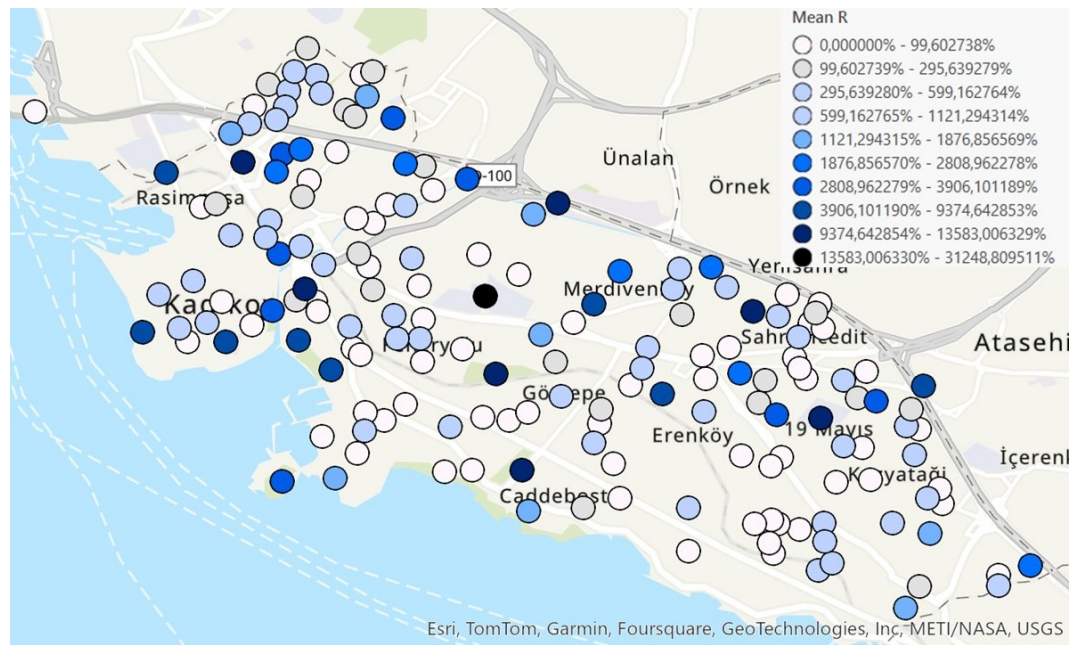


Figure 6.17: LHS Simulations: Mean supply allocation to PODs in Kadıköy

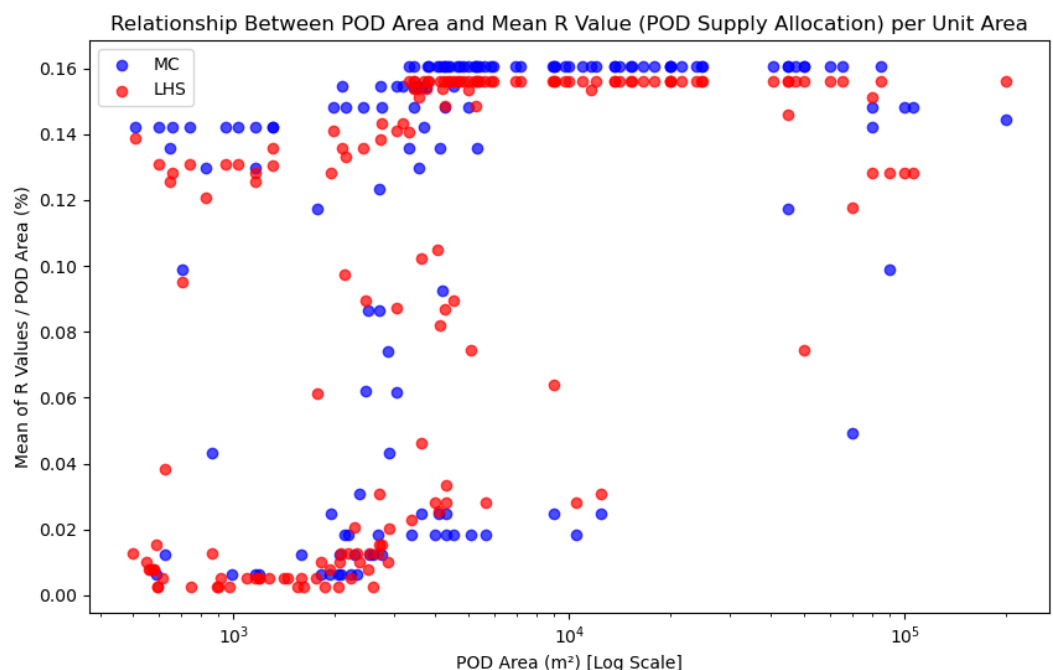


Figure 6.18: Relationship between POD area/capacity and mean supply allocation relative to the POD area

However, when comparing Figure 6.20 with Figure 6.8, we observe a slight increase in the overall deviation of supply allocations across different PODs in Kadıköy in the LHS simulations compared to the MC simulations. This difference can be attributed to the larger number of feasible solutions generated in the LHS simulations, which also tend to include more solutions with relatively larger optimality gaps compared to those generated in the MC approach. These larger gaps can result

in greater deviations, as the solver prioritizes identifying broadly feasible solutions over converging to a precise optimum within the computational time limits. Consequently, the increased deviations in LHS reflect a trade-off between the quantity of feasible solutions and the precision of the solution, highlighting the balance between computational efficiency and accuracy in the simulation process.

In Figure 6.21, we observe that, similar to the MC simulations, the LHS simulations do not exhibit a clear or direct correlation between a POD's proximity to the POD centroid (is near to the Kadıköy district center in our simulations) and the variation in supplies allocated to that POD.

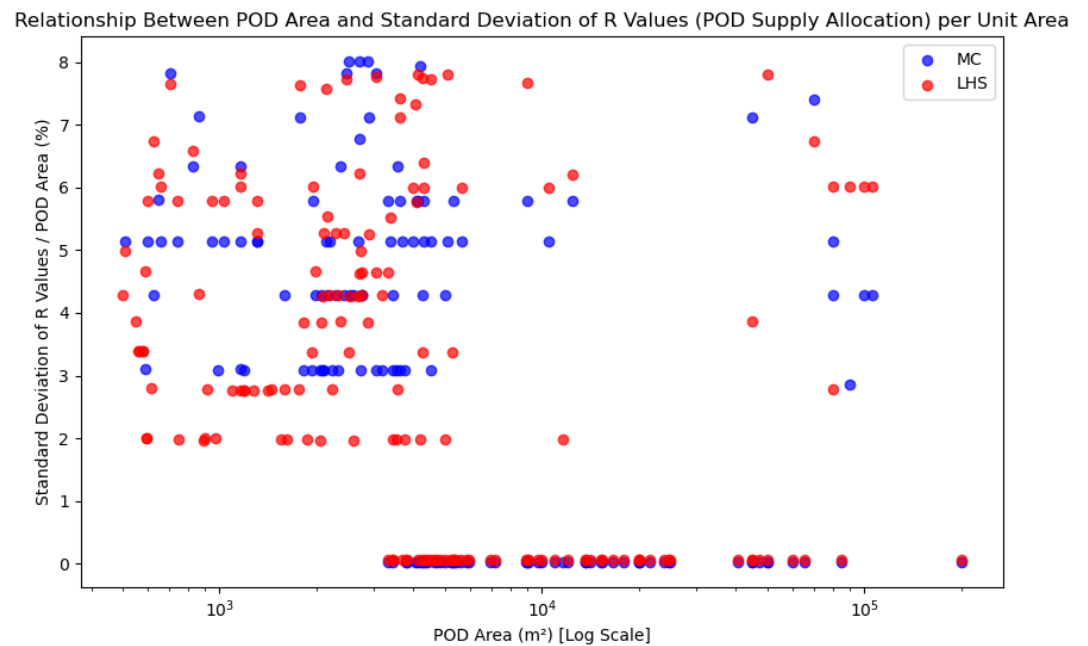


Figure 6.19: Relationship between POD area/capacity and deviation of supply allocation relative to the POD area

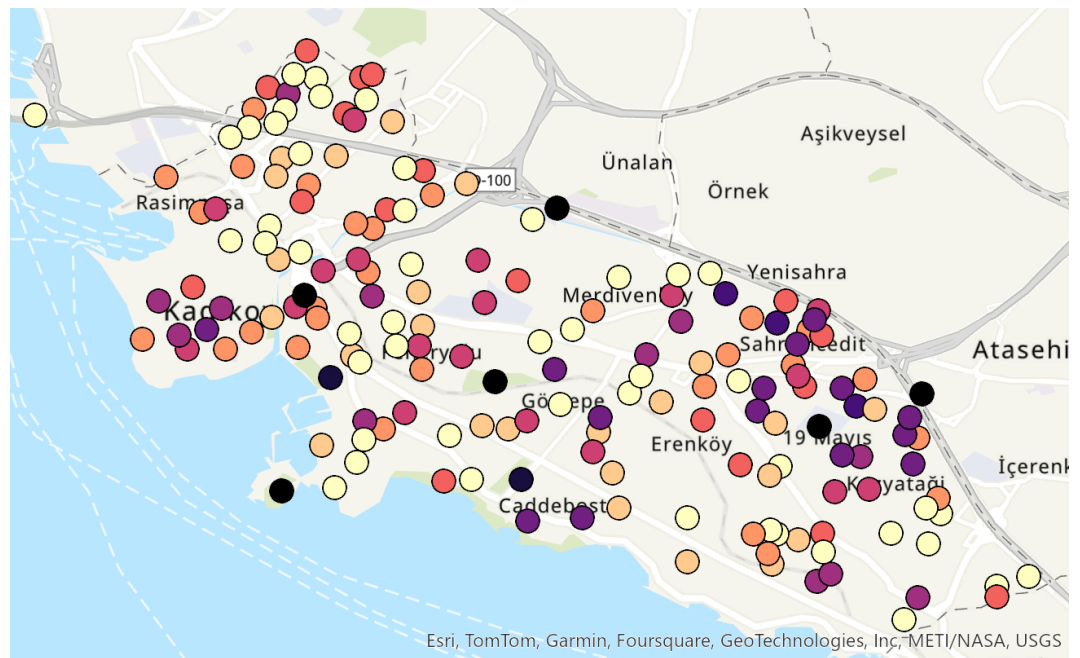


Figure 6.20: LHS Simulations: Deviation of supply allocations to PODs in Kadıköy

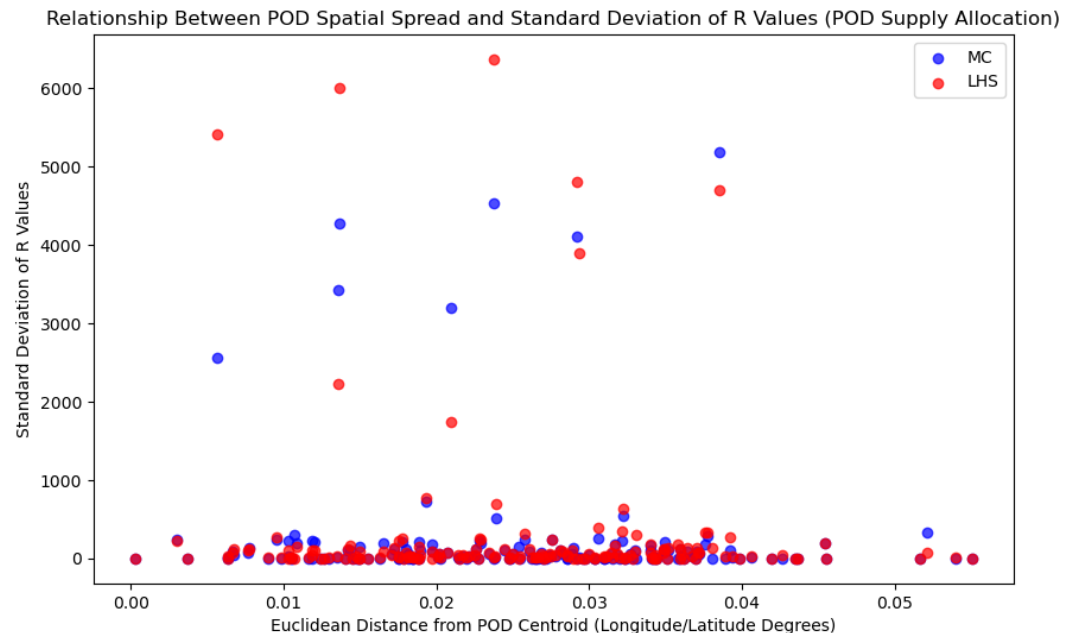


Figure 6.21: Relationship between POD location relative to the POD centroid and deviation of supply allocation

6.2.3 Demand Point Allocation Results for PODs

In Figure 6.22, each color group represents demand points assigned to the same POD, indicating that individuals in those areas would be directed to the same distribution point for aid. The similarity of these results to those shown in Figure 6.10

suggests that the LHS simulations also prioritize assigning demand points to nearby PODs. This reflects the real-world need to minimize travel time and ensure quick access to aid. These findings underscore the model's effectiveness in optimizing accessibility metrics for disaster relief, demonstrating its robustness and reliability in terms of maximizing accessibility regardless of the scenario generation method (LHS or MC).

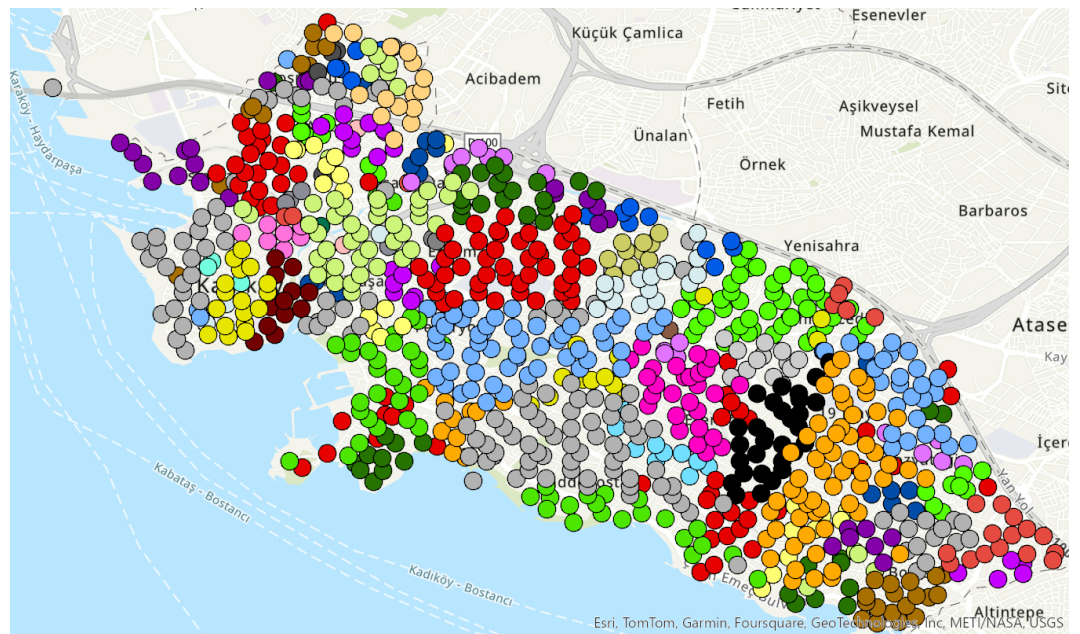


Figure 6.22: LHS Simulations: Demand point assignment to PODs

6.3 Effect of Maximum POD Number on Simulations

In our simulations comparing LHS and MC methods, we use $C = 100$ as the maximum number of PODs that can be opened. However, the variations in the results based on different values for this maximum number of PODs can provide valuable insights into real-world decision-making, specifically regarding how many PODs should be activated in a post-disaster environment. To explore this, we vary the C parameter from 170 to 20 in steps of 10 and observe the outcomes.

In contrast to the LHS/MC simulations, here we select 3 scenario combinations out of the 8 distinct scenarios and focus on MC scenarios. This allows us to isolate the effect of C on the simulation results, without the additional influences of factors like the sampling method. We use MC scenarios in this case because MC represents a simple random sampling approach, which minimizes the interaction effects between the sampling method and the maximum number of PODs. If we chose LHS instead, it might have introduced a higher interaction effect with the C parameter, which could potentially obscure the impact of the C value itself.

However, varying the parameter C introduces another challenge, as explained in Section 5.3.3. In the capacity calculation of our PODs, we use the POD area and the sum of all POD areas, regardless of the maximum number of PODs allowed in the simulation. Therefore, if we do not adjust the scalar in the formula for POD capacity calculation, our PODs become undersupplied when the C value is decreased, resulting in infeasible solutions. To address this, future research could focus on determining POD supply capacities independently, though this would likely require physical measurements and calculations specific to each POD.

In our simulations, we initially use a scalar of 1.5 while varying C from 170 to 60. We observe that for values below 90, it becomes increasingly difficult for the model to find feasible solutions, prompting us to conduct another experiment for C values between 20 and 60, using a scalar of 2.5 instead. This adjustment allows us to examine scenarios with a low maximum number of PODs in more detail. However, due to this parameter variation, we do not compare the results of these two experiments within the same calculations or context. Despite this, the findings follow a similar pattern and can be considered generalizable. For a clearer overview, Figure 6.23 shows the number of solutions with a low feasibility gap (below 1%) and the number of feasible solutions with high feasibility gap (above 1%) for different C values.

Number of feasible solutions for different C from 70 to 170 when scalar 1.5 is used for POD capacity calculation			Number of feasible solutions for different C from 20 to 60 when scalar 2.5 is used for POD capacity calculation		
C (max POD)	Number of Feasibility Gap > 1%	Number of Feasibility Gap < 1%	C (max POD)	Number of Feasibility Gap > 1%	Number of Feasibility Gap < 1%
70	0	2	20	13	71
80	0	1	30	5	34
90	3	5	40	0	0
100	0	8	50	0	6
110	2	9	60	0	6
120	2	9			
130	0	9			
140	0	7			
150	1	7			
160	0	8			
170	0	7			

Figure 6.23: Feasibility gap numbers of simulations with varying C (max POD) values

6.3.1 The POD Consistency Principle: Bigger Capacities Stick Around

Reducing the maximum allowed PODs in simulations helps to highlight the key PODs for the last mile relief network. In Figure 6.24, the mean y solutions of sim-

ulations with varied C values are represented. Red dots indicate the mean y values for $C = 20$, blue dots show the mean y values that differ in $C = 30$ from $C = 20$, and green dots represent the mean y values for $C = 50$, selected differently from $C = 30$. By particularly examining the PODs selected on average for $C = 20$ and $C = 30$, we can identify the most critical PODs in Kadıköy. It is evident that these PODs are typically the ones with the largest areas (and thus capacities), which underscores the importance of POD capacity in densely populated urban environments in the aftermath of a disaster.

Another key observation is that there are only 10 blue dots, which represent PODs that are only selected in $C = 30$ but not in $C = 20$. This shows that the additional 10 PODs allowed by increasing C from 20 to 30 correspond to new PODs, separate from those selected in $C = 20$. Additionally, there are only 22 green dots, indicating that only 2 PODs, selected on average by both $C = 20$ and $C = 30$, are not selected when $C = 50$. This finding demonstrates the robustness of POD selection across different C values, as most critical PODs remain selected even as C increases.

These results suggest that the capacity-based selection of PODs is not highly sensitive to the maximum number of PODs allowed. In other words, increasing the maximum number of PODs does not significantly alter the selection of key PODs for the relief network, implying that the identified critical PODs can be considered reliable and resilient to variations in C . This robustness is particularly important for ensuring that the network remains effective and responsive in post-disaster scenarios, even when the number of PODs available fluctuates due to factors such as understaffing or the inability to predict the exact number of available staff. These uncertainties can affect the operational capacity of the PODs, but the consistency in selecting the most critical PODs ensures that the network can still function optimally, even under changing conditions.

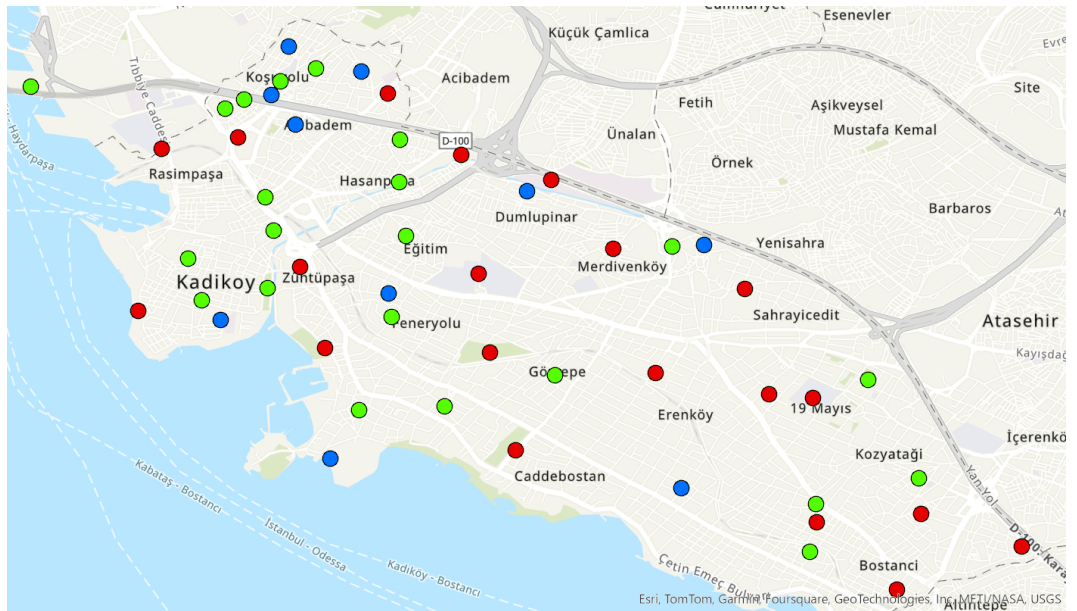


Figure 6.24: Comparison of PODs selected on average between $C = 20, 30$ and 50

6.3.2 Short on PODs, High on Deviation: The Effects of Limited Availability of PODs

The figures 6.25, 6.26 and 6.27 represent the deviations in POD supply allocation when the maximum number of PODs (C) is chosen as 170, 90, and 20, respectively. These figures illustrate how supply allocations change as the allowed number of PODs decreases.

When C is set to 170, meaning that almost all available PODs can be opened, the deviations in supply allocation are relatively small. This is especially true for PODs with smaller capacities, whose supply allocations may be influenced heavily by the selected scenario. However, these deviations are still limited as there is enough flexibility to adjust supply distribution across multiple PODs.

As C is reduced to 90, we start to observe larger deviations in supply allocation, particularly in PODs with larger capacities. At this point, the PODs are not always selected or fully supplied, depending on the scenario. This happens because the number of PODs that can be chosen is now more limited, resulting in a higher likelihood that some larger capacity PODs will not be utilized to their full extent or may be excluded altogether in favor of smaller ones, based on scenario-specific demands.

For $C = 20$, the deviations in supply allocation become even more pronounced, with many PODs experiencing no significant change in supply. This is because when the maximum number of PODs that can be selected is so low, only the PODs with the largest capacities can be chosen. Smaller PODs are no longer viable for

supplying the demand, leading to a more rigid network configuration. In this scenario, the supply amounts fluctuate drastically within the large capacity PODs. With such a low maximum POD limit, localized disruptions or changes in demand near these large PODs can cause significant shifts in supply allocation. This may result in the selection of another POD with a similarly large capacity or a drastic change in the supply amount to meet demand effectively.

In summary, as the C value (maximum number of PODs to be opened) decreases, the system's flexibility to allocate supply across multiple PODs diminishes, leading to larger fluctuations in POD selection and supply allocation, especially for large capacity PODs.

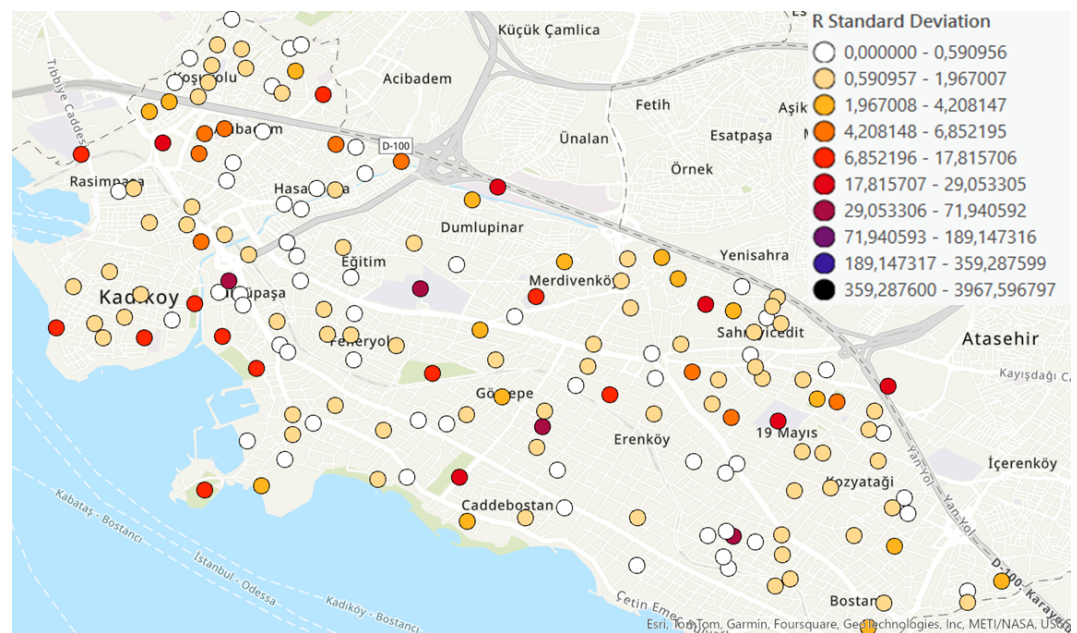


Figure 6.25: Deviation of supply allocation to PODs when $C = 170$

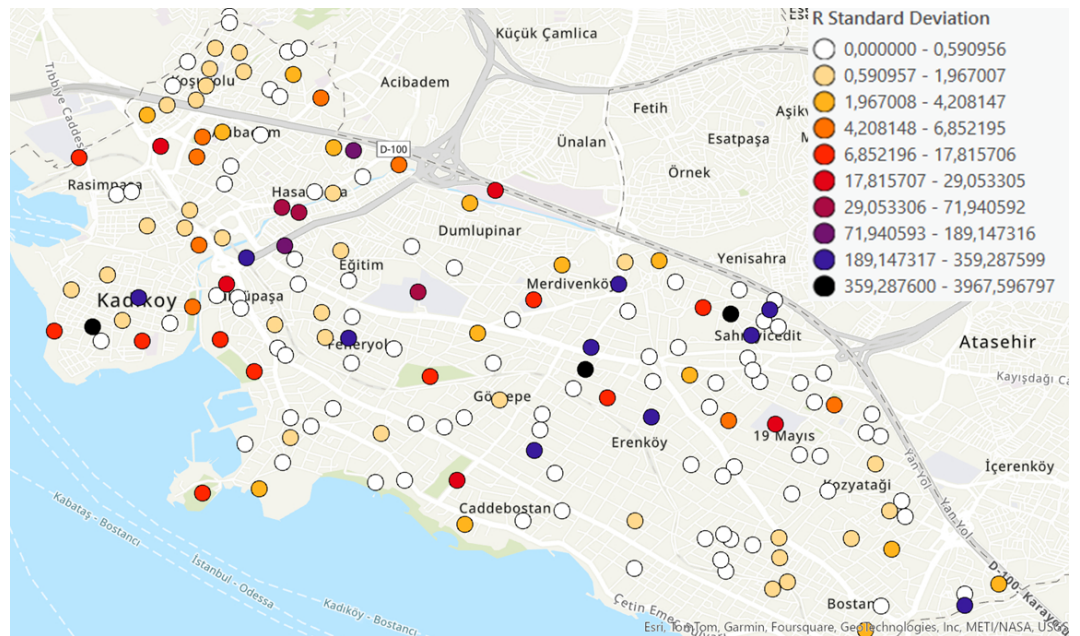


Figure 6.26: Deviation of supply allocation to PODs when $C = 90$

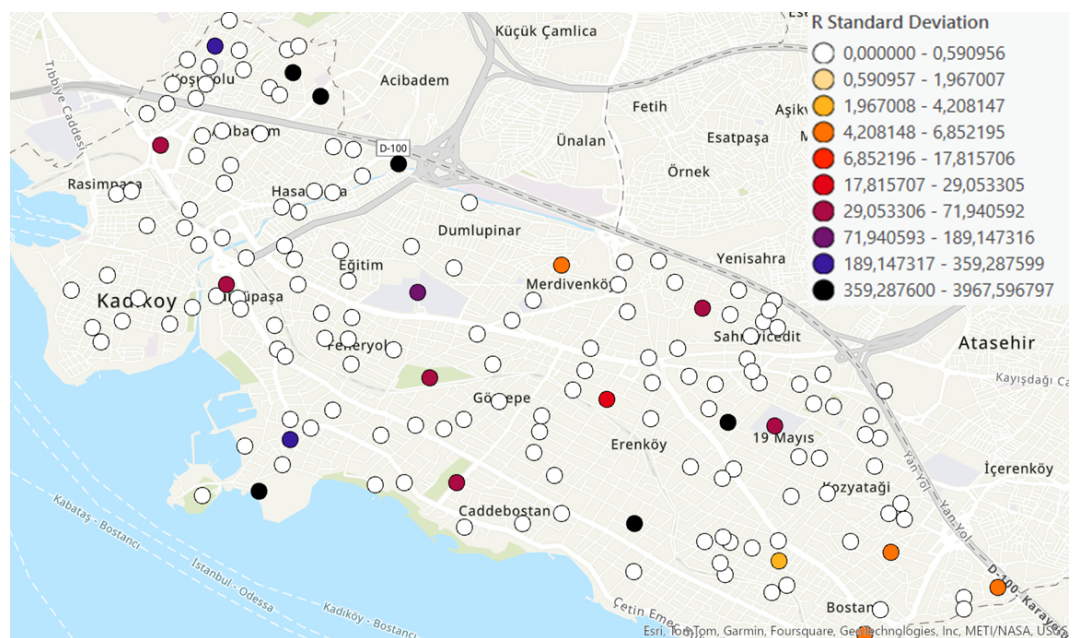


Figure 6.27: Deviation of supply allocation to PODs when $C = 20$

6.3.3 Fewer PODs, More Chaos: Demand Point Allocation Results for PODs

Decreasing the maximum number of PODs that can be selected also leads to the formation of larger demand clusters, as seen in Figures 6.28 and 6.29. In these figures, the selected PODs are marked with black stars, and the color-coded points represent demand points assigned to the same POD. This highlights a critical issue

in disaster relief planning, as these larger clusters may represent populations of tens of thousands of people needing aid. In this scenario, even the largest PODs can face significant bottlenecks in delivering assistance, putting significant pressure on the available resources and logistics.

From a real-world perspective, this is problematic because a reduced number of PODs can severely limit the system's capacity to distribute aid efficiently. As observed in the figures, increasing the maximum number of PODs (C) to 60 helps to reduce overcrowding at critical PODs. This allows the affected populations to be more evenly and locally distributed across PODs, significantly improving accessibility and reducing response times. In contrast, when the number of PODs is constrained, people may be required to travel long distances to receive help, which is especially dangerous in a post-earthquake scenario where time is of the essence and mobility can be severely impaired.

Another important insight is the spatial variation in demand clusters. Specifically, the eastern neighborhoods of Kadıköy exhibit larger demand clusters compared to the west. This can be attributed to two factors. First, there are more vulnerable buildings in the western neighborhoods, resulting in higher demand for PODs in that region. Second, the eastern neighborhoods have fewer smaller PODs available, leading to a reliance on larger PODs to serve a relatively less affected population. This distribution strategy may seem appropriate in normal circumstances, but it introduces significant risks. Figures 6.32, 6.31, and 6.30 provide a clearer view of eastern neighborhoods in Kadıköy as the maximum number of PODs that can be selected is decreased from 170 to 120 and then to 90. Even when nearly all PODs are open, we observe that demand points (represented by purple dots) in the Suadiye area are assigned to the POD at Erenköy Ruh Sağlığı Hastanesi. This assignment implies a walking distance of nearly 30 minutes even under normal conditions, highlighting the scarcity of smaller, more local candidate PODs in these areas.

In the event that the eastern part of Kadıköy is impacted more severely than expected, the large PODs in that area may not be able to meet the underestimated demand. This could result in a chaotic situation where people have to travel long distances to reach help, further complicating the logistics and potentially leading to loss of life. This underscores the importance of spreading earthquake assembly areas and candidate PODs more evenly across a district. By ensuring that both large and small PODs are distributed equitably, the system can respond more flexibly to varying levels of demand across different areas, reducing the likelihood of critical shortages and improving overall disaster response effectiveness.

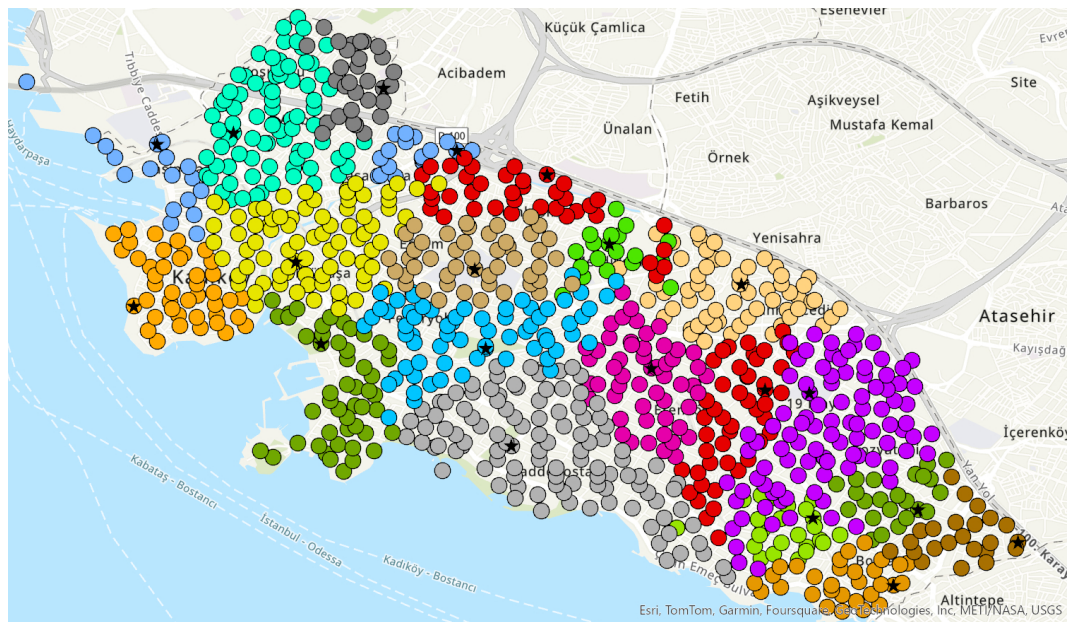


Figure 6.28: Demand point assignments to PODs in Kadıköy when $C = 20$

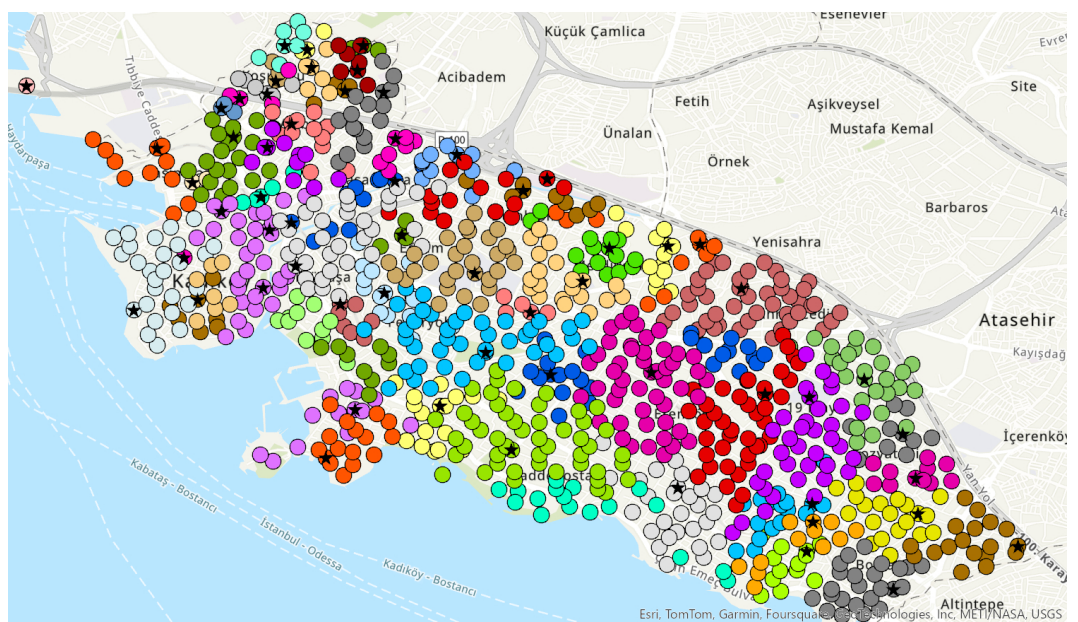


Figure 6.29: Demand point assignments to PODs in Kadıköy when $C = 60$

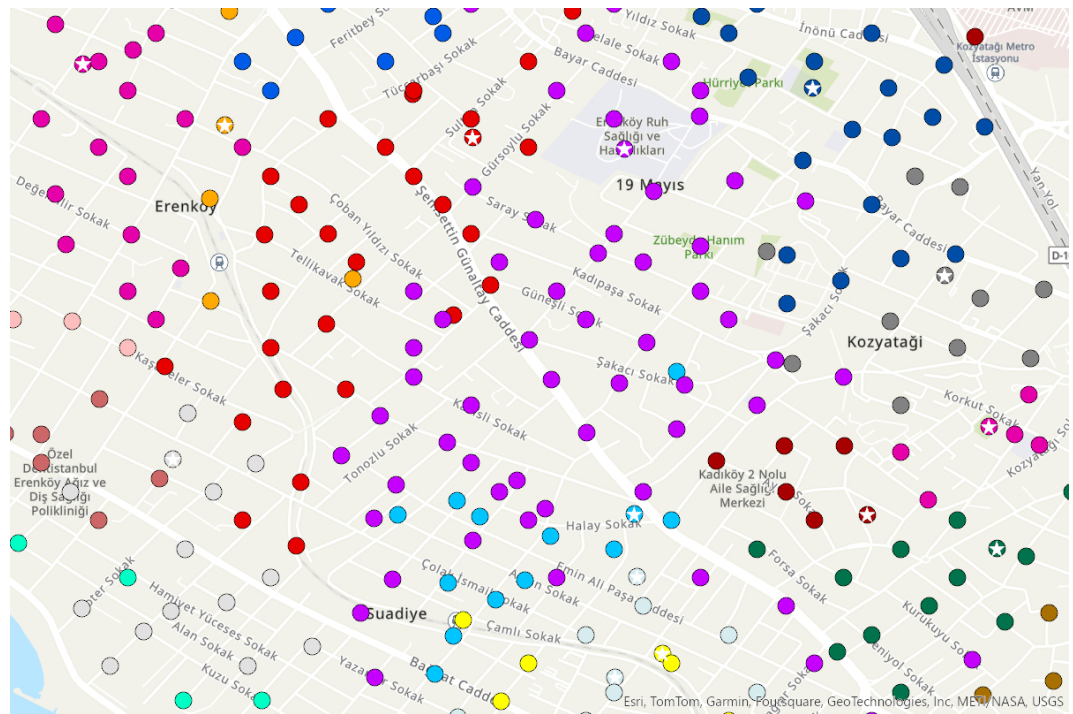


Figure 6.30: Overview on demand point assignments to PODs in Eastern Kadıköy when $C = 90$

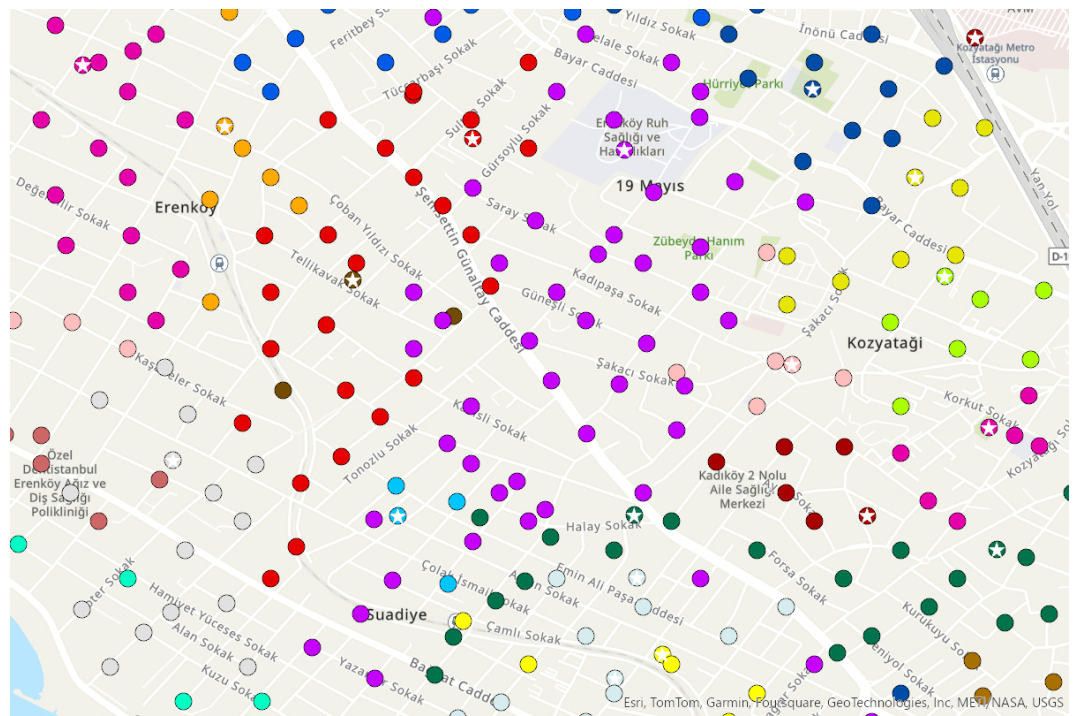


Figure 6.31: Overview on demand point assignments to PODs in Eastern Kadıköy when $C = 120$

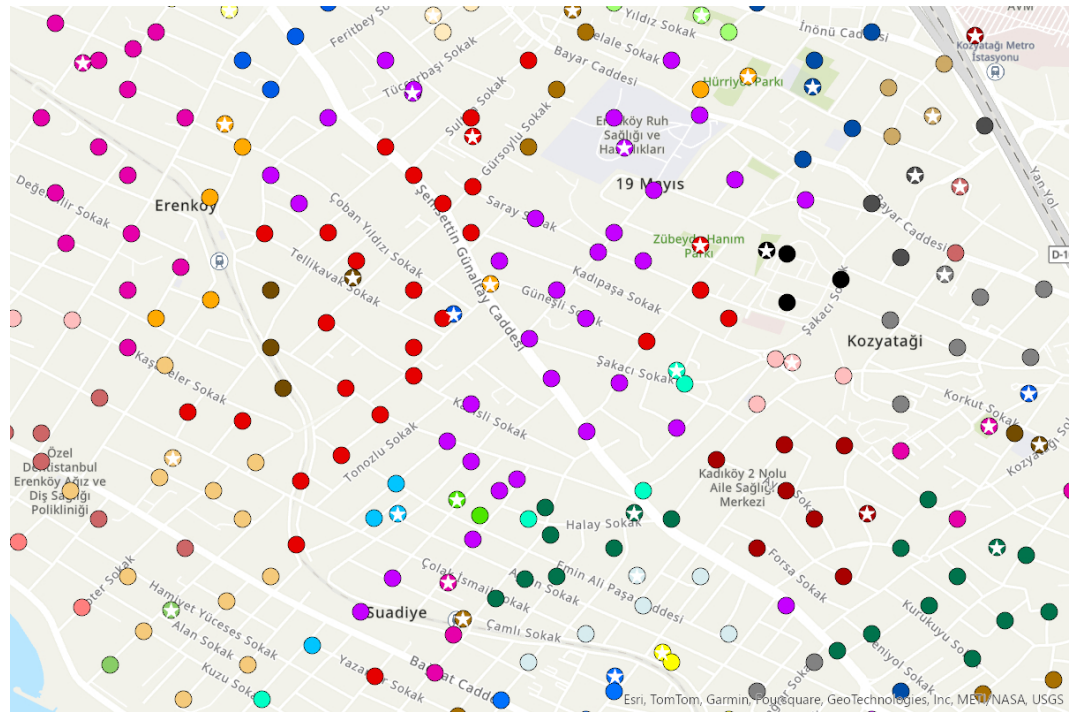


Figure 6.32: Overview on demand point assignments to PODs in Eastern Kadıköy when $C = 170$

To quantitatively assess the performance of demand point assignments to PODs ($x_{i,j}^s$) for different C values, we calculate two key metrics: *Total Trucking Duration* and *Total Shape Length*. These metrics are computed by summing the products of the $x_{i,j}^s$ entries with the corresponding values from the OD cost matrices, on which the $v_{i,j}^s$ values are based. The *Trucking Duration* represents the time required to transport supplies between PODs and demand points, measured in minutes, and incorporates the variability of network disruptions (varies across scenarios). The *Shape Length* refers to the physical length of the network paths (e.g., road segments) used for supply delivery, measured in meters, and remains constant across different scenarios.

Using these two metrics, we conduct a quantitative comparison of the demand point assignments to PODs for the two sets of simulation scenarios. The results for the experiment using a scalar value of 1.5 in the POD capacity calculations are presented in Table 6.33 and Graph 6.34. The results for the experiment with a scalar value of 2.5 in the POD capacity calculations are shown in Figure 6.35.

In both experiments, we observe a consistent pattern: as C increases, the total Trucking Duration and Shape Length sums decrease. This can be explained by the fact that lower C values, which correspond to fewer PODs available for assignment, force the system to cover longer distances. Consequently, trucking durations increase, and network path lengths become greater. With fewer PODs, the system is forced to rely on a smaller number of routes, which may not be as efficient or optimal in meeting demand, leading to suboptimal performance. These results highlight

the importance of having an adequate number of PODs to ensure efficient resource distribution and reduce network congestion.

However, it is also important to note that increasing C from 50 to 60, for instance, does not significantly alter the total accessibility. This suggests that after a certain point, the marginal benefit of adding more PODs diminishes. Further experimentation with different C values could help identify an optimal balance, maximizing total accessibility while minimizing the number of PODs required.

maxPOD	total_trucking_duration	total_shape_length
70	1306,17231634838	599492,870542426
80	1247,14487079223	576076,526292293
90	1238,32838302774	555559,189689850
100	1194,26556597694	538888,930388753
110	1157,15801128434	521770,631981435
120	1148,73611224532	508954,329763141
130	1095,25315451610	486319,291357233
140	1080,32855350963	476498,955482211
150	1068,21187004911	468037,442657902
160	1066,02600976903	467345,449184999
170	1052,20294383736	460538,471606983

Figure 6.33: Total accessibility for $C = 70$ to 170 for POD capacity scalar 1.5

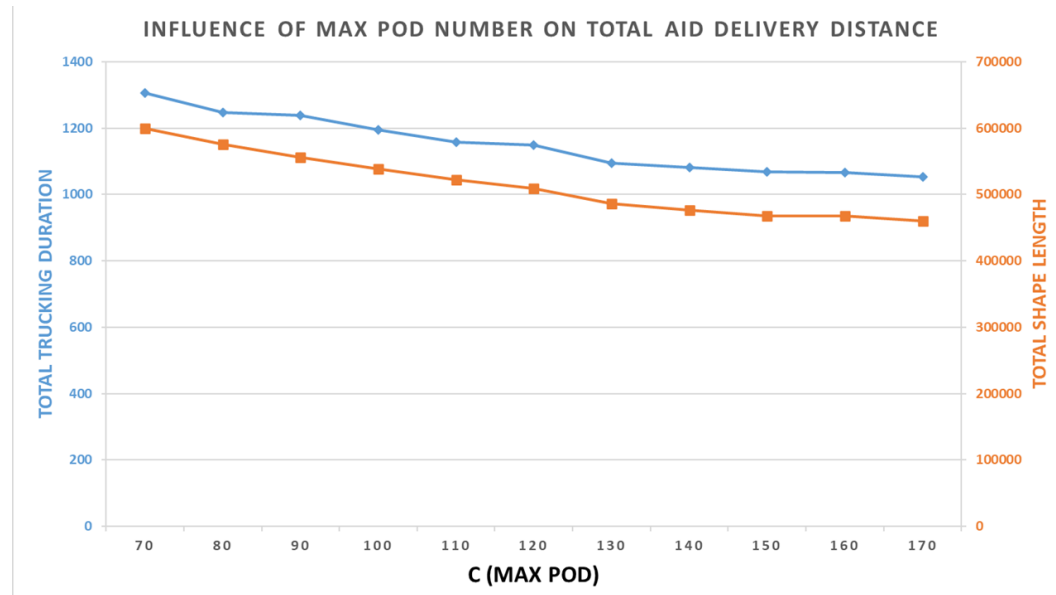


Figure 6.34: Total accessibility for $C = 70$ to 170 for POD capacity scalar 1.5

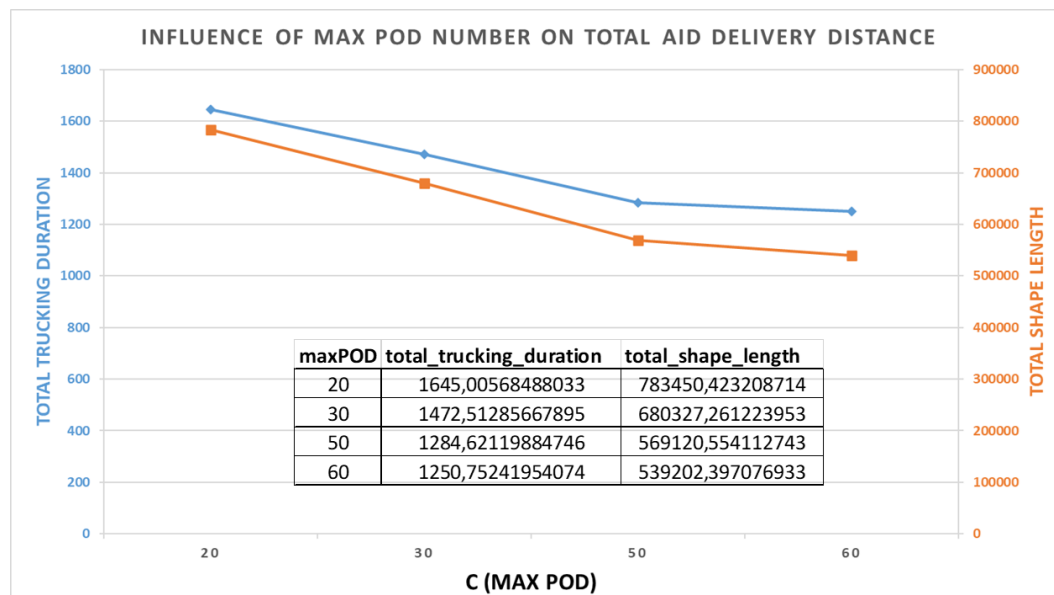


Figure 6.35: Total accessibility for $C = 20$ to 60 for POD capacity scalar 2.5

7 Conclusion

In this study, we address the challenge of selecting relief distribution points and determining their supply capacities in an urban area following a major earthquake. We focus on Istanbul, specifically the Kadıköy district, where a significant earthquake is anticipated in the near future. To support this analysis, we gather various datasets for Istanbul and create a simulation framework in a GIS environment, integrating the data to establish a geospatial basis for our logistics network. Our approach is built upon a two-stage stochastic optimization model, adapted from the SLMRND model in Noyan et al. (2016), which emphasizes two key metrics: accessibility and equity. Our scenario generation method involves informed random selection of buildings in each neighborhood of Kadıköy. In addition to using real-world data, we incorporate Latin Hypercube Sampling (LHS) into the simulations and compare the results of building selection using Monte Carlo versus LHS.

Our simulation results indicate that in post-disaster urban settings with dense demand points and numerous candidate PODs, capacity plays a more decisive role than location in determining POD selection outcomes. However, it is also important to note that the location of a POD becomes a critical factor when the maximum number of PODs that can be selected is limited (i.e., when the POD-to-demand ratio decreases) or when a POD is situated near other PODs with larger capacities that can already fulfill local demand.

Our results indicate that, despite the variability in demand and network disruptions across different scenarios, certain PODs are consistently selected and supplied with aid. This suggests that through comprehensive pre-disaster research and planning—particularly by leveraging extensive simulations of relief network models and optimizations based on real-world data—preparedness efforts can be significantly enhanced. For instance, identifying these consistently selected PODs enables proactive strategies such as pre-positioning critical supplies and stockpiling resources at these locations. These findings highlight the potential for stable and detailed planning, even in the face of uncertainty, which remains resilient to fluctuations. Ultimately, this demonstrates that disaster preparedness and organization can be significantly strengthened before an earthquake, reinforcing the idea that it is never too late to take action to mitigate the impact of such events.

7.1 Future Research

Our study demonstrates that incorporating LHS in the building selection algorithm reduces selection bias and improves feasible solution generation under time constraints, though it does not significantly alter POD selection and capacity outcomes compared to Monte Carlo sampling. Future research could further test this approach across other neighborhoods and with additional simulation runs to assess whether LHS yields a more significant impact, highlighting it as a valuable tool for enhancing realism in disaster response planning. Additionally, future research could explore alternative techniques to reduce scenario bias beyond LHS. Examples include "Importance Sampling", which determines and focuses on scenarios with higher probabilities or greater impact or "Bayesian Updating", which incorporates prior knowledge or real-time data to refine scenario generation. These methods could provide further insights into scenario-based planning for disaster response.

While our data support city-wide relief network design for whole Istanbul, computational constraints limit our experiments to Kadıköy. However, our datasets and simulation framework allow future researchers with greater computational resources to potentially scale the model to a city-wide network.

Another direction of for future research is to conduct a detailed stability analysis by testing a broader set of scenarios to determine the effect of scenario count on model output consistency. Increasing the number and variety of scenarios could reveal a point of stability beyond which additional scenarios have minimal impact, optimizing computational demands while preserving result reliability.

Bibliography

- AFAD. 2023. Kahramanmaraş depremi raporu. URL https://deprem.afad.gov.tr/assets/pdf/Kahramanmara%C5%9F%20Depremi%20%20Raporu_02.06.2023.pdf. Last viewed on 30/10/2024.
- Afshar, A., A. Haghani. 2012. Modeling integrated supply chain logistics in real-time large-scale disaster relief operations. *Socio-Economic Planning Sciences* **46** 327–338.
- Aghababaei, Mohammad, Seosamh B. Costello, Prakash Ranjitkar. 2020. Transportation impact assessment following a potential alpine fault earthquake in new zealand. *Transportation Research Part D: Transport and Environment* **87** 102511. doi:<https://doi.org/10.1016/j.trd.2020.102511>.
- Anadolu Agency. 2023. Countries, organizations rush to provide aid to quake-hit türkiye. URL <https://shorturl.at/4p6o9>. Last viewed on 30/10/2024.
- Anaya-Arenas, A. M., J. Renaud, A. Ruiz. 2014. Relief distribution networks: a systematic review. *Annals of Operations Research* **223**(1) 53–79. doi:[10.1007/s10479-014-1581-y](https://doi.org/10.1007/s10479-014-1581-y).
- Ansal, Atilla, Aybige Akinci, Giovanna Cultrera, M. Erdik, Vera Pessina, G. Tönük, Gabriele Ameri. 2009. Loss estimation in istanbul based on deterministic earthquake scenarios of the marmara sea region (turkey). *Soil Dynamics and Earthquake Engineering* **29** 699–709. doi:[10.1016/j.soildyn.2008.07.006](https://doi.org/10.1016/j.soildyn.2008.07.006).
- Balcik, B., B. M. Beamon, K. Smilowitz. 2008. Last mile distribution for humanitarian relief chains. *Journal of Intelligent Transportation Systems* **12**(2) 51–63.
- Balcik, Burcu, Cem Deniz Caglar Bozkir, O. Erhun Kundakcioglu. 2016. A literature review on inventory management in humanitarian supply chains. *Surveys in Operations Research and Management Science* **21**(2) 101–116. doi:<https://doi.org/10.1016/j.sorms.2016.10.002>. URL <https://www.sciencedirect.com/science/article/pii/S1876735416300204>.
- Bing Maps Quadkey Locator. 2024. Quadkey locator for geospatial indexing. URL <https://samples.bingmapsportal.com/spatial-math/quadkey-locator>. Last viewed on 20/10/2024.
- Bing Maps Team. 2023. make-gis-friendly.py. URL <https://github.com/microsoft/GlobalMLBuildingFootprints/blob/main/scripts/make-gis-friendly.py>. Last viewed on 25/10/2024.

- Choukolaei, Hassan Ahmadi, Mustafa Jahangoshai Rezaee, Samuel Yousefi, Morteza Saberi. 2022. A simulation-based approach for decision making in earthquake crisis management. Muhammet Gul, Melih Yucesan, Melike Erdogan, eds., *Multi-Criteria Decision Analysis: Case Studies in Disaster Management*. CRC Press, 281–302. doi:10.1201/9781003212904-19.
- DaftLogic. 2024. Google maps area calculator tool. <https://www.daftlogic.com/projects-google-maps-area-calculator-tool.htm>. Last viewed on 15/11/2024.
- Daneshvar, Mohammad, Sanjay Dominik Jena, Walter Rei. 2023. A two-stage stochastic post-disaster humanitarian supply chain network design problem. *Computers Industrial Engineering* **183** 109459. doi:<https://doi.org/10.1016/j.cie.2023.109459>.
- Day, Jamison. 2014. Fostering emergent resilience: The complex adaptive supply network of disaster relief. *International Journal of Production Research* **52**. doi: 10.1080/00207543.2013.787496.
- Disasters Emergency Committee. 2013. 2010 haiti earthquake: Facts and figures. URL <https://dec.org.uk/article/2010-haiti-earthquake-facts-and-figures>. Last viewed on 30/10/2024.
- Disasters Emergency Committee (DEC). 2023. Fact file: One year on from the turkey-syria earthquakes — the full impact of the disaster and the response. URL <https://shorturl.at/AOO4I>. Last viewed on 30/10/2024.
- Dukkanci, Okan, Achim Koberstein, Bahar Y. Kara. 2023. Drones for relief logistics under uncertainty after an earthquake. *European Journal of Operational Research* **310**(1) 117–132. doi:<https://doi.org/10.1016/j.ejor.2023.02.038>.
- Ece Sanci and Mark S. Daskin. 2021. An integer l-shaped algorithm for the integrated location and network restoration problem in disaster relief. *Transportation Research Part B: Methodological* **145** 152–184. doi:<https://doi.org/10.1016/j.trb.2021.01.005>.
- Erdik, M., K. Eren. 1983. Attenuation of intensities for earthquake associated with the north anatolian fault. *Middle East Technical University Earthquake Engineering Research Center, Ankara* .
- Erdik, M., Y. Fahjan, Oguz Ozel, Hakan Alcik, Aydin Mert, M. Gul. 2003. Istanbul earthquake rapid response and the early warning system. *Bulletin of Earthquake Engineering* **1** 157–163. doi:10.1023/A:1024813612271.
- Feizizadeh, Bakhtiar, Seyed Javad Adabikhosh, Soodabe Panahi. 2023. A scenario-based and game-based geographical information system (gis) approach for earthquake disaster simulation and crisis mitigation. *Sustainability* **15**(14). doi: 10.3390/su151411131.

- Freimer, Michael, Jeffrey Linderoth. 2012. The impact of sampling methods on bias and variance in stochastic linear programs. *Computational Optimization and Applications* **51** 51–75. doi:10.1007/s10589-010-9322-x.
- Geofabrik GmbH. 2022. Openstreetmap data in gis formats. <https://download.geofabrik.de/osm-data-in-gis-formats-free.pdf>. Last viewed on 15/11/2024.
- Holguín-Veras, José, Noel Pérez, Satish Ukkusuri, Tricia Wachtendorf, Bethany Brown. 2007. Emergency logistics issues affecting the response to katrina: A synthesis and preliminary suggestions for improvement. *Transportation Research Record* **2022**(1) 76–82. doi:10.3141/2022-09.
- Hooshangi, Navid, Ali Asghar Alesheikh. 2018. Developing an agent-based simulation system for post-earthquake operations in uncertainty conditions: A proposed method for collaboration among agents. *ISPRS International Journal of Geo-Information* **7**(1). doi:10.3390/ijgi7010027.
- Horner, M., J. Downs. 2010. Optimizing hurricane disaster relief goods distribution: model development and application with respect to planning strategies. *Disasters* **34**(3) 821–844.
- Horner, Mark W, Joni A Downs. 2008. Analysis of effects of socioeconomic status on hurricane disaster relief plans. *Transportation Research Record* **2067**(1) 1–10.
- Humanitarian OpenStreetMap. 2024. Hotosm turkey buildings (openstreetmap export). URL https://data.humdata.org/dataset/hotosm_tur_buildings. Last viewed on 25/10/2024.
- IBB Muhtarlık. 2024. Muhtarlık adres bilgileri. URL <https://data.ibb.gov.tr/dataset/muhtarlik-adres-bilgileri>. Last viewed on 5/11/2024.
- IHH. 2023. Kahramanmaraş depremi afet yönetimi raporu. URL <https://ihh.org.tr/public/publish/0/172/kahramanmaras-depremi-afet-yonetimi-raporu--w.pdf>. Last viewed on 30/10/2024.
- Kandilli Observatory. 2023. Deprem hasar tahmin raporu. URL <https://shorturl.at/dBwNk>. Last viewed on 30/10/2024.
- Kaut, Michal, Stein Wallace. 2003. Evaluation of scenario-generation methods for stochastic programming. *Pacific Journal of Optimization* **3**.
- Kovacs, G., K. Spens. 2007. Humanitarian logistics in disaster relief operations. *International Journal of Physical Distribution and Logistics Management* **37**(2) 99–114.
- Kovács, Gyöngyi, Karen Spens, Mohammad Moshtari, eds. 2017. *The Palgrave Handbook of Humanitarian Logistics and Supply Chain Management*. 1st ed.

- Palgrave Macmillan London. doi:10.1057/978-1-137-59099-2. EBook ISBN: 978-1-137-59099-2.
- Living Atlas Team. 2023. 100 m Grid Population Data. URL <https://www.arcgis.com/home/item.html?id=8c2db10c952e45b68efdfc78f64267b0>. Last viewed on 5/11/2024.
- Löhndorf, Nils. 2016. An empirical analysis of scenario generation methods for stochastic optimization. *European Journal of Operational Research* **255**. doi: 10.1016/j.ejor.2016.05.021.
- Mahdi Mostajabdeh, Walter J. Gutjahr, F. Sibel Salman. 2019. Inequity-averse shelter location for disaster preparedness. *IIE Transactions* **51**(8) 809–829. doi: 10.1080/24725854.2018.1496372.
- Microsoft Bing Maps. 2023. Bing global ml building footprints. URL <https://github.com/microsoft/GlobalMLBuildingFootprints>. Last viewed on 25/10/2024.
- Noyan, N. 2012. Risk-averse two-stage stochastic programming with an application to disaster management. *Computers and Operations Research* **39**(3) 541–559.
- Noyan, Nilay, B. Balcik, S. Atakan. 2016. A stochastic optimization model for designing last mile relief networks. *Transportation Science* **50**(3) 1092–1113. doi:10.1287/trsc.2016.0702.
- OSM Turkey. 2024. OpenStreetMap Data for the Turkey Region. URL <https://download.geofabrik.de/europe/turkey.html>. Last viewed on 5/11/2024.
- Puca Huachi Vaz Penna, Andréa Cynthia Santos, Christian Prins. 2018. Vehicle routing problems for last mile distribution after major disaster. *Journal of the Operational Research Society* **69**(8) 1254–1268. doi:10.1080/01605682.2017.1390534.
- Sphere Project. 2011. Sphere project: Humanitarian charter and minimum standards in humanitarian response. Tech. rep. URL <http://www.spheredproject.org/resources/?search=1&keywords=&language=English&category=22&subcat-22=23&subcat-29=0&subcat-31=0&subcat-35=0&subcat-49=0>. Last viewed on 20/10/2024.
- (TUIK), Turkish Statistical Institute. 2012. URL <http://tuikapp.tuik.gov.tr/adnksdagitapp/adnks.zul>. Last viewed on 30/10/2024.
- World Health Organization. 2014. A decade after the 2004 asian tsunami: Recalling the turning point for disaster management. URL <https://shorturl.at/aCU6n>. Last viewed on 30/10/2024.
- WorldPop Project. 2023. 1 km Grid Population Data. URL

- <https://www.arcgis.com/home/item.html?id=38b7672a1977426caa6cf4c62e37b777>. Last viewed on 5/11/2024.
- Zhang, Pei-Yu, Yan-Kui Liu, Guo-Qing Yang, Guo-Qing Zhang. 2020. A robust optimization model for a last mile relief network design problem. Xiang Li, Xiaofeng Xu, eds., *Proceedings of the Seventh International Forum on Decision Sciences*. Springer Singapore, Singapore, 99–106.
- Özgün Elçi and Nilay Noyan. 2018. A chance-constrained two-stage stochastic programming model for humanitarian relief network design. *Transportation Research Part B: Methodological* **108** 55–83. doi:10.1016/j.trb.2017.12.002.
- İBB DEZİM. 2019. Olası deprem kayıp tahminleri İlçe kitapçıkları. URL <https://depremzemin.ibb.istanbul/tr/olasi-deprem-kayip-tahminleri-ilce-kitapciklari>. Last viewed on 30/10/2024.
- İBB DEZİM Kadıköy. 2020. Olası deprem kayıp tahminleri kadıköy kitabı. URL <https://8luvomezzsk.merlincdn.net/wp-content/uploads/2021/01/Kadikoy.pdf>. Last viewed on 30/10/2024.
- İzzet Kılıç. 2020. Istanbul admin level 8 geojson. URL <https://github.com/izzetkalic/geojsons-of-turkey/blob/master/geojsons/istanbul-admin-level-8.geojson>. Last viewed on 20/10/2024.